

1 **Acetylcholine is released in the basolateral amygdala in response to predictors of**
2 **reward and enhances learning of cue-reward contingency**

3 Richard B. Crouse^{1,2}, Kristen Kim^{1,2}, Hannah M. Batchelor^{1,2}, Eric M. Girardi¹, Rufina
4 Kamaletdinova^{1,3}, Justin Chan¹, Prithviraj Rajebhosale^{4,5}, Steven T. Pittenger¹, Lorna
5 W. Role⁵, David A. Talmage⁶, Miao Jing⁷, Yulong Li⁸⁻¹⁰, Xiao-Bing Gao¹¹, Yann S.
6 Mineur¹, Marina R. Picciotto^{1,2,*}

7 ¹Department of Psychiatry,

8 Yale University, 34 Park Street, 3rd Floor Research, New Haven, CT 06508, USA

9 ²Yale Interdepartmental Neuroscience Program, New Haven, CT

10 ³City University of New York, Hunter College, New York, NY

11 ⁴Program in Neuroscience, Stony Brook University, NY

12 ⁵National Institute of Neurological Disorders & Stroke (NINDS), Bethesda MD

13 ⁶National Institute of Mental Health (NIMH), Bethesda MD

14 ⁷Chinese Institute for Brain Research (CIBR), Beijing, China

15 ⁸State Key Laboratory of Membrane Biology, Peking University School of Life Sciences,
16 Beijing, China.

17 ⁹PKU-IDG/McGovern Institute for Brain Research, Beijing, China.

18 ¹⁰Peking-Tsinghua Center for Life Sciences, Academy for Advanced Interdisciplinary
19 Studies,

20 Peking University, Beijing, China.

21 ¹¹Section of Comparative Medicine, Yale University School of Medicine New Haven, CT

22

23 * To whom correspondence should be addressed

24 Marina R. Picciotto

25 Dept. of Psychiatry, Yale University School of Medicine

26 34 Park Street – 3rd floor research

27 New Haven, CT 06508

28 Phone: 203-737-2041; Fax: 203-737-2043; email: marina.picciotto@yale.edu

29

30 **Running title:** BLA ACh enhances reward learning

31 **Keywords:** cholinergic, reward learning, basolateral amygdala, optogenetics, fiber

32 photometry, GRAB_{ACh3.0}, GCaMP

33 **Abstract**

34 The basolateral amygdala (BLA) is critical for associating initially neutral cues
35 with appetitive and aversive stimuli and receives dense neuromodulatory acetylcholine
36 (ACh) projections. We measured BLA ACh signaling and activity of neurons expressing
37 CaMKII α (a marker for glutamatergic principal cells) in mice during cue-reward learning
38 using a fluorescent ACh sensor and calcium indicators. We found that ACh levels and
39 nucleus basalis of Meynert (NBM) cholinergic terminal activity in the BLA (NBM-BLA)
40 increased sharply in response to reward-related events and shifted as mice learned the
41 cue-reward contingency. BLA CaMKII α neuron activity followed reward retrieval and
42 moved to the reward-predictive cue after task acquisition. Optical stimulation of
43 cholinergic NBM-BLA terminal fibers led to quicker acquisition of the cue-reward
44 contingency. These results indicate BLA ACh signaling carries important information
45 about salient events in cue-reward learning and provides a framework for understanding
46 how ACh signaling contributes to shaping BLA responses to emotional stimuli.

47

48 **Introduction**

49 Learning how environmental stimuli predict the availability of food and other
50 natural rewards is critical for survival. The basolateral amygdala (BLA) is a brain area
51 necessary for associating cues with both positive and negative valence outcomes
52 (Baxter & Murray, 2002; Janak & Tye, 2015; LeDoux et al., 1990). Recent work has
53 shown that genetically distinct subsets of BLA principal neurons encode the appetitive
54 and aversive value of stimuli (J. Kim et al., 2016). This encoding involves the interplay
55 between principal neurons, interneurons, and incoming terminal fibers, all of which need
56 to be tightly regulated to function efficiently.

57 The neuromodulator acetylcholine (ACh) is released throughout the brain and
58 can control neuronal activity via a wide range of mechanisms. ACh signals through two
59 families of receptors (nicotinic, nAChRs and muscarinic, mAChRs) that are differentially
60 expressed on BLA neurons as well as their afferents (Picciotto et al., 2012). ACh signals
61 through these receptors to increase signal-to-noise ratios and modify synaptic
62 transmission and plasticity in circuits involved in learning new contingencies (Picciotto et
63 al., 2012), especially in areas that receive dense cholinergic input, like the BLA (Woolf,
64 1991; Zaborszky et al., 2012). The effect of ACh signaling can differ depending on the
65 receptor, as metabotropic mAChRs work on a slower timescale than the rapid,
66 ionotropic nAChRs (Gu & Yakel, 2011; Picciotto et al., 2012). The overall impact of ACh
67 signaling on the BLA is likely quite heterogeneous since mAChRs are coupled to both
68 inhibitory and excitatory signaling cascades and nAChRs are found on both
69 glutamatergic and GABAergic BLA neurons (Picciotto et al., 2012).

70 The basal forebrain complex is a primary source of ACh input to the BLA. In
71 particular, the nucleus basalis of Meynert (NBM) sends dense cholinergic projections to
72 the BLA (Woolf, 1991; Zaborszky et al., 2012). Optical stimulation of BLA-projecting
73 cholinergic terminal fibers (NBM-BLA) during fear conditioning is sufficient to strengthen
74 fear memories (Jiang et al., 2016) and may support appetitive behavior (Aitta-aho et al.,
75 2018). Cholinergic NBM neurons increase their firing in response to both rewarding and
76 aversive unconditioned stimuli (Hangya et al., 2015). Cholinergic signaling in the medial
77 prefrontal cortex and visual cortex has been linked to cue detection (Parikh et al., 2007)
78 and reward timing (Chubykin et al., 2013; Liu et al., 2015), respectively. A recent study
79 has also demonstrated that NBM cells fire in response to a conditioned stimulus during
80 trace fear conditioning, indicating that ACh signaling may be involved in learning about
81 cues that predict salient outcomes (Guo et al., 2019).

82 We hypothesized that ACh signaling in the BLA is a critical neuromodulatory
83 signal that responds to both unconditioned stimuli and cues that gain salience, thereby
84 coordinating activity in circuits necessary for learning cue-reward contingencies. To test
85 this hypothesis, we measured relative levels of BLA ACh (ACh signaling), cholinergic
86 NBM-BLA terminal fiber activity (BLA ACh signal origin), and the activity of BLA
87 principal neurons (BLA output) across all phases of learning in an appetitive operant
88 learning task to evaluate how BLA output and ACh signaling are related to behavioral
89 performance in this paradigm. We then optically stimulated cholinergic NBM fibers
90 locally in the BLA while mice learned to nose poke in response to an auditory cue to
91 receive a food reward to determine if accelerating the increase in ACh signaling that
92 occurs as mice learn the task would enhance performance. We also pharmacologically

93 blocked different ACh receptors during the learning task to determine the subtypes
94 involved, and varied the timing of optical stimulation of cholinergic NBM-BLA terminal
95 fibers to determine whether time-locked ACh release with the reward-predictive cue is
96 necessary for the improvement of the task performance. These studies provide a novel
97 framework for understanding how NBM ACh signaling in the BLA is recruited during
98 perception of novel stimuli and how it contributes to linking previously neutral cues to
99 predictions about future salient outcomes.

100

101 **Results**

102 **Acetylcholine release in the BLA occurs at salient points in the cue-reward** 103 **learning task and shifts as mice learn the cue-reward contingency**

104 The BLA is critical for learning that previously neutral cues can predict future
105 punishments or rewards and for assigning valence to those cues (Baxter & Murray,
106 2002; Janak & Tye, 2015). The BLA receives dense cholinergic input (Woolf, 1991;
107 Zaborszky et al., 2012) and we speculated that, since ACh signaling is involved in both
108 attention and several types of learning (Picciotto et al., 2012), it could be essential for
109 learning about cues that predict salient events, such as reward delivery. Based on data
110 showing that ACh neurons fire in response to unexpected or salient events (Hangya et
111 al., 2015), we also hypothesized that ACh release might vary as mice learn a cue-
112 reward contingency. Therefore, we designed a cue-reward learning task in which food-
113 restricted mice were trained to perform a nose poke when signaled by a cue (tone) to
114 receive a palatable reward (Ensure) on a 30 sec variable intertrial interval (ITI) (**Figure**
115 **1A-D**). We injected adeno-associated virus (AAV) carrying an improved version of the

116 fluorescent ACh sensor GRAB_{ACh3.0} (ACh3.0; (Jing et al., 2018, 2019) construct into the
117 BLA of mice and implanted an optical fiber above the BLA to record ACh signaling
118 during the cue-reward learning task (**Figure 2A + Figure 2-figure supplement 1A**).

119 During the Pre-Training phase of the task, mice received reward and cue light
120 presentation for performing a nose poke in the active port during tone presentation
121 (**Figure 1C**, purple active nose poke coincident with tone) but there was no
122 consequence for an incorrect nose poke (**Figure 1C**, red active nose poke not
123 coincident with tone). Animals quickly learned to make a high number of responses over
124 the course of each Pre-Training session. In this paradigm, mice obtained most available
125 rewards by day 5 of Pre-Training (**Figure 2B**, blue shaded region). However, this phase
126 of training did not promote learning of the cue-reward contingency, (i.e. that they should
127 only nose poke during tone presentation) seen by the high number of incorrect nose
128 pokes (**Figure 2-figure supplement 2A**, blue shaded region). Mice performed roughly
129 8-fold more incorrect nose pokes than correct nose pokes, suggesting that mice were
130 not attending to the task contingency. The Training phase of the task was identical to
131 Pre-Training except incorrect nose pokes resulted in a 5 sec timeout, during which the
132 house light was illuminated, that concluded with a restarting of the ITI timer (**Figure 1D**,
133 red active nose poke not coincident with tone). On day 1 of the Training phase, all
134 animals earned fewer rewards (**Figure 2B**, pink shading) and, while still high, incorrect
135 nose pokes dropped (**Figure 2-figure supplement 2A**, pink shading). Animals that did
136 not meet acquisition criterion by day 9 (defined as consistently earning 20 or more
137 rewards per session, **Figure 2B**, white horizontal line) were moved to a 20 sec variable
138 ITI to promote responding (**Figure 2B**, pink shading day 10). Following the change in

139 ITI, mice acquired the cue-reward behavior at different rates. After acquisition, animals
140 were switched to Extinction training in which correct nose pokes did not result in reward
141 delivery, and all mice decreased nose poke responding (**Figure 2B + Figure 2-figure**
142 **supplement 2A**, orange shading).

143 During Pre-Training, when there were high numbers of both correct and incorrect
144 nose pokes, there was a large increase in ACh release following correct nose pokes,
145 which were followed by reward delivery and cue light, but not incorrect nose pokes
146 (**Figure 2C + Figure 2-figure supplement 1 B-C**). We used bootstrapped confidence
147 intervals (bCI) to determine when transients were statistically significant (bCI did not
148 contain the null of 0 (Jean-Richard-dit-Bressel et al., 2020)). Correct, but not incorrect,
149 nose poke trials consistently showed a sustained, significant increase in fluorescence
150 close to the time of nose poke onset (**Figure 2C**). We also observed a significant
151 decrease in fluorescence for most mice around 2-4 sec after correct nose poke, which
152 corresponds to the time of reward retrieval.

153 ACh release occurred in response to different events as mice learned the task
154 (data for individual mice are shown in **Figure 2D + Figure 2-figure supplement 1D-G**
155 and averaged data across all mice at key time points in the task is shown in **Figure 2E**
156 **+ Figure 2-figure supplement 1H**). During Pre-Training rewarded trials, the highest
157 levels of ACh release occurred close to the time of correct nose pokes (NP), with a
158 smaller peak at the time of reward retrieval (entry into the reward receptacle, Rec). As
159 Training began, the ACh release during reward trials shifted dramatically toward the
160 time of reward retrieval, likely because the animals were learning that many nose pokes
161 did not result in reward delivery. Incorrect nose pokes that triggered a timeout were also

162 followed by a modest but non-significant increase in BLA ACh levels (**Figure 2-figure**
163 **supplement 2B-H**). As mice began to learn the contingency (**Figure 2E + Figure 2-**
164 **figure supplement 1H**, 10 rewards), the peak ACh release during rewarded trials
165 shifted back to the time of the correct nose poke response. As animals approached the
166 acquisition criterion (**Figure 2E + Figure 2-figure supplement 1H**, Acq.), ACh level
167 significantly increased at the time of the tone, suggesting that as animals learned the
168 cue-reward contingency, the tone became a more salient event. At this time point, there
169 was still a peak at the time of reward, but its magnitude was diminished. After task
170 acquisition, the increase in ACh following correct nose pokes remained but was
171 diminished, and incorrect nose pokes did not elicit apparent ACh release (**Figure 2-**
172 **figure supplement 2C-H**, Acq.). During Extinction, ACh release to tone onset
173 diminished. We replicated this experiment in an independent cohort of mice and found
174 similar results (**Figure 2-figure supplement 3-4**). Mice in this replicate cohort learned
175 in a similar fashion (**Figure 2-figure supplement 3B + 4A**) but met the acquisition
176 criteria faster than initial mice because aspects of the behavioral setup were optimized
177 (3D printed wall extensions) to allow the imaging apparatus to be used inside sound
178 attenuating chambers (see Methods section). One difference observed in this group that
179 learned the task more rapidly, was small magnitude, but significant, increases in BLA
180 ACh release following tone onset late in Pre-Training (**Figure 2-figure supplement 3C-**
181 **I**). As behavioral performance during the Training phase increased, ACh release to tone
182 onset became more pronounced, as in the initial cohort.

183 In order to determine the source of the ACh released in the BLA during cue-
184 reward learning, we recorded calcium dynamics as a measure of cell activity of ChAT⁺

185 NBM terminal fibers in the BLA (NBM-BLA), since the NBM is a major source of
186 cholinergic input to the BLA (Jiang et al., 2016; Woolf, 1991; Zaborszky et al., 2012).
187 We injected AAV carrying a Cre-recombinase-dependent, genetically-encoded calcium
188 indicator (DIO-GCaMP7s) into the NBM of ChAT-IRES-Cre mice and implanted an
189 optical fiber above the ipsilateral BLA (**Figure 2F + Figure 2-figure supplement 5A-C**).
190 As with the ACh3.0 sensor, there was a significant increase in NBM-BLA cholinergic
191 terminal activity following correct, but not incorrect, nose pokes (**Figure 2H + Figure 2-**
192 **figure supplement 5D-E**). NBM-BLA cholinergic terminal activity evolved across
193 phases of the reward learning task as was seen for ACh levels in the BLA (data for each
194 mouse shown in **Figure 2I + Figure 2-figure supplement 5F-G**, averaged across all
195 mice at key time points in the task shown in **Figure 2J + Figure 2-figure supplement**
196 **7G**). Strikingly, NBM-BLA cholinergic terminal activity most closely followed correct
197 nose pokes in Pre-Training and shifted primarily to tone onset as mice learned the
198 contingency during Training. As in the replication cohort for the ACh sensor, small
199 magnitude, but significant, increases in terminal activity were observed following tone
200 onset late in Pre-Training (**Figure 2J + Figure 2-figure supplement 7G**). Incorrect
201 nose pokes that resulted in a timeout in Training sessions were followed by a modest
202 increase in NBM-BLA cholinergic terminal activity before task acquisition (**Figure 2-**
203 **figure supplement 6B-E**). During Extinction, activity of NBM-BLA terminals following
204 tone onset diminished. These findings were replicated in an independent cohort of mice,
205 which we combined for across-mouse statistical analyses (**Figure 2-figure supplement**
206 **7-8**).

207 In order to record NBM-BLA cholinergic terminal activity and BLA ACh levels
208 simultaneously in the same mouse, we injected AAV carrying a construct for Cre-
209 recombinase dependent red-shifted genetically-encoded calcium indicator (DIO-
210 jRCaMP1b) into the NBM of ChAT-IRES-Cre mice, ACh3.0 sensor into the ipsilateral
211 BLA, and implanted a fiber above the BLA (**Figure 2-figure supplement 9A-E**, mouse
212 1). DIO-jRCaMP1b was also injected into the NBM of a wild type littermate so Cre-
213 mediated recombination would not occur to control for any crosstalk between the
214 ACh3.0 and jRCaMP1b channels. While this was only a single animal and proof of
215 principle for future studies, we found that NBM-BLA cholinergic terminal activity
216 coincided with ACh levels (**Figure 2-figure supplement 9F-G**). Importantly, this
217 relationship between ACh release and NBM-BLA terminal fiber activity was not
218 explained by signal crosstalk (**Figure 2-figure supplement 9H-I**), further indicating that
219 the BLA ACh measured comes at least in part from the NBM.

220

221 **BLA principal neurons respond to reward availability and follows cue-reward**
222 **learning**

223 Glutamatergic principal cells are the primary output neurons of the BLA (Janak &
224 Tye, 2015), and their firing is modulated by NBM-BLA cholinergic signaling (Jiang et al.,
225 2016; Unal et al., 2015). BLA principal neurons can increase their firing in response to
226 cues as animals learn cue-reward contingencies (Sanghera et al., 1979; Schoenbaum
227 et al., 1998; Tye & Janak, 2007). Calcium/calmodulin-dependent protein kinase
228 (CaMKII) has been shown to be a marker for glutamatergic BLA principal cells (Butler et
229 al., 2011; Felix-Ortiz & Tye, 2014; McDonald, 1992; Tye et al., 2011). To determine

230 whether ACh modulates principal neuron activity during cue-reward learning, we
231 injected AAV carrying a Cre-recombinase dependent genetically encoded calcium
232 indicator (DIO-GCaMP6s) into the BLA of CaMKII α -Cre mice to record BLA principal cell
233 activity during the learning task (**Figure 3A + Figure 3-figure supplement 1A**). As was
234 seen for BLA ACh levels, there was a significant increase in BLA CaMKII α cell activity
235 following correct and a modest, but not significant, decrease in activity following
236 incorrect nose pokes on the last day of Pre-Training (**Figure 3B**). However, the activity
237 peaked later after the correct nose poke response (~2.5 sec) compared to the ACh3.0
238 signal (~0.5 sec) and appeared to align more tightly with reward retrieval (**Figure 3-**
239 **figure supplement 1B**). As mice learned the task (**Figure 3C + Figure 3-figure**
240 **supplement 2A**), BLA CaMKII α cell activity increased first in response to reward and,
241 after acquisition of the task, to the reward-predictive cue (individual data for each mouse
242 shown in **Figure 3D + Figure 3-figure supplement 1E-F**, and averaged data across all
243 mice at key time points in task is shown in **Figure 3E + Figure 3-figure supplement**
244 **1G-H**).

245 During Pre-Training, the highest levels of BLA CaMKII α cell activity followed
246 reward retrieval. In addition, during the first few days of Training, BLA CaMKII α cell
247 activity after reward retrieval was higher than it was during Pre-Training, and the
248 magnitude of response decreased as mice learned the contingency and earned more
249 rewards, ultimately reaching similar intensity to that observed during Pre-Training.
250 Concurrently, as mice approached acquisition of the task (**Figure 3C**, white horizontal
251 line), BLA CaMKII α cell activity significantly increased in response to tone onset (**Figure**
252 **3D-E + Figure 3-figure supplement 1E-H, Acq.**), suggesting that the recruitment of

253 BLA CaMKII α cell activity likely reflects the association of the cue with a salient outcome
254 (Lutas et al., 2019; Sengupta et al., 2018). Incorrect nose pokes that triggered a timeout
255 did not elicit a different response in CaMKII α cell activity compared to before timeouts
256 were incorporated (**Figure 3-figure supplement 2B-G**). In an independent cohort of
257 mice, those with more posterior fiber tip placements (mice 4 + 7) replicated the primary
258 findings (**Figure 3-figure supplement 3-4**).

259

260 **Stimulation of cholinergic terminals in BLA improves cue-reward learning**

261 Since ACh released by NBM-BLA terminals during Training shifted to tone onset
262 during acquisition of cue-reward learning (**Figure 2E, J**), we hypothesized that ACh may
263 potentiate learning the cue-reward contingency. We therefore tested whether increasing
264 ACh release in BLA during learning could alter cue-reward learning by injecting AAV
265 carrying a Cre-recombinase-dependent channelrhodopsin-EYFP (AAV-DIO-ChR2-
266 EYFP) construct bilaterally into the NBM of ChAT-IRES-Cre transgenic mice and
267 placing fibers over the BLAs to optically stimulate cholinergic terminals originating from
268 the NBM selectively (**Figure 4A + Figure 4-figure supplement 1**). Optical control over
269 ChAT⁺ NBM cells was verified by *ex vivo* slice recordings, depolarizations followed light
270 flashes and clear action potentials were observed *ex vivo* (**Figure 4B + Figure 4-figure**
271 **supplement 2**). After operant familiarization, ChAT⁺ NBM-BLA terminals were
272 stimulated via bilateral optical fibers (2 sec, 20 Hz, 25 ms pulses) triggered by a correct
273 nose poke throughout both Pre-Training (**Figure 4C**) and Training (**Figure 4D**).
274 Stimulation usually occurred during at least a portion of all three components of a

275 rewarded trial: tone, correct nose poke, and reward retrieval, since these events were
276 often separated by short latencies.

277 As seen in previous experiments, during the Pre-Training phase animals made a
278 high number of nose poke responses over the course of each session, obtained most
279 available rewards by the last day (**Figure 4E + Figure 4-figure supplement 3A**, blue
280 shading), and committed a very high number of incorrect nose pokes (**Figure 4F +**
281 **Figure 4-figure supplement 3B**, blue shading). There were no differences in rewards
282 earned (main effect of group (EYFP vs. ChR2) in a two-way repeated-measures
283 ANOVA, $F(1, 9) = 1.733$, $p = 0.2205$) or incorrect nose pokes (main effect of group
284 (EYFP vs. ChR2) in a two-way repeated-measures ANOVA, $F(1, 9) = 0.002433$, $p =$
285 0.9617) between the EYFP control ($n = 5$) and ChR2 ($n = 6$) groups during the Pre-
286 Training phase (**Figure 4E-F + Figure 4-figure supplement 3A-B**, blue shading),
287 suggesting that increasing BLA ACh signaling was not sufficient to modify behavior
288 during the Pre-Training phase of the task.

289 On Day 1 of the Training phase, all animals earned fewer rewards (**Figure 4E +**
290 **Figure 4-figure supplement 3A**, pink shading) and incorrect nose pokes remained
291 high (**Figure 4F + Figure 4-figure supplement 3B**, pink shading). As the animals
292 learned that a nose poke occurring outside of the cued period resulted in a timeout, both
293 control EYFP and ChR2 groups learned the contingency and improved their
294 performance, resulting in acquisition of the cue-reward task (20 rewards earned).
295 However, significant group differences emerged, such that ChR2 mice earned
296 significantly more rewards than EYFP controls (**Figure 4E + Figure 4-figure**
297 **supplement 3A**, pink shaded; main effect of group (EYFP vs. ChR2) in a two-way

298 repeated-measures ANOVA, $F(1, 9) = 9.434$, $p = 0.0133$), and there was a significant
299 Day x Group (EYFP vs. ChR2) interaction (two-way repeated-measures ANOVA, $F(11,$
300 $99) = 3.210$, $p = 0.0009$). ChR2 mice also made significantly fewer incorrect nose pokes
301 than control mice (**Figure 4F + Figure 4-figure supplement 3B**, pink shaded; two-way
302 repeated-measures ANOVA, $F(1, 9) = 12.67$, $p = 0.0061$), suggesting that the ChR2
303 group learned the tone-reward contingency more quickly than the EYFP group. EYFP
304 mice were able to reach the same peak cue-reward performance as the ChR2 group
305 only after 4-6 additional days of training. Once peak performance was achieved, there
306 was no difference in extinction learning between the groups (main effect of group (EYFP
307 vs. ChR2) in a two-way repeated-measures ANOVA, $F(1, 9) = 2.293$, $p = 0.1643$).

308 While sex differences in the behavior were not formally tested side by side, an
309 independent cohort of male mice (EYFP $n = 7$, ChR2 $n = 7$, **Figure 4-figure**
310 **supplement 4**) was tested to determine whether both male and female mice would
311 respond to ACh stimulation, revealing similar trends during Training for rewards earned
312 (**Figure 4-figure supplement 3C,E**, pink shaded; two-way repeated-measures ANOVA,
313 Group main effect (EYFP vs. ChR2): $F(1, 12) = 3.636$, $p = 0.0808$, Day x Group
314 interaction: $F(11, 132) = 3.033$, $p = 0.0012$) and incorrect nose pokes (**Figure 4-figure**
315 **supplement 3D,F**, red shaded; two-way repeated-measures ANOVA, Group main
316 effect (EYFP vs. ChR2): $F(1, 12) = 4.925$, $p = 0.0465$).

317 In order to determine if optical stimulation of NBM-BLA cholinergic terminals
318 improved performance in the task by increasing the rewarding value of the outcome,
319 rather than enhancing cue-reward learning by some other means, we allowed mice to
320 nose poke for optical stimulation rather than for Ensure (**Figure 4-figure supplement**

321 **5A**). There were no differences between the EYFP control and ChR2 groups (two-way
322 repeated-measures ANOVA, $F(1, 9) = 0.6653$, $p = 0.4357$). We also tested whether
323 NBM-BLA cholinergic terminal activation was reinforcing on its own by stimulating these
324 terminals in a real-time place preference test. Mice were allowed to explore two similar
325 compartments to determine baseline preference, and NBM-BLA cholinergic terminals
326 were then stimulated in one of the two chambers to determine whether it increased time
327 spent in the stimulation-paired chamber. There was no difference between groups
328 (**Figure 4-figure supplement 5B**, main effect of group (EYFP vs. ChR2) in a two-way
329 repeated-measures ANOVA, $F(1, 9) = 0.1311$, $p = 0.7257$) in place preference,
330 confirming that optical activation of NBM-BLA cholinergic terminals is not innately
331 rewarding. Stimulation of NBM-BLA cholinergic terminals also did not lead to changes in
332 nose poke behavior in an uncued progressive ratio task (**Figure 4-figure supplement**
333 **5C**, main effect of group (EYFP vs. ChR2) in a two-way repeated-measures ANOVA, F
334 $(1, 12) = 0.0009814$, $p = 0.975$). Locomotor behavior was also not significantly affected
335 by NBM-BLA cholinergic terminal activation (**Figure 4-figure supplement 5D**, two-way
336 repeated-measures ANOVA, $F(1, 9) = 0.05804$, $p = 0.8150$.) Finally, to determine
337 whether there was any effect of NBM-BLA cholinergic terminal stimulation on
338 preference for, or avoidance of, a stressful environment, mice were tested for changes
339 in time spent in the dark or light side due to laser stimulation in the Light/Dark Box test,
340 and there were no differences between the groups (**Figure 4-figure supplement 5E-F**,
341 unpaired t-tests, number of crosses: $p = 0.3223$; time in light side: $p = 0.1565$).
342

343 **Muscarinic, but not nicotinic, receptors are required for acquisition of the cue-**
344 **reward contingency**

345 ACh signals through multiple receptor subtypes, with rapid, ionotropic signaling
346 mediated through stimulation of nAChRs, and metabotropic signaling mediated through
347 stimulation of mAChRs (Picciotto et al., 2012). To determine which ACh receptors were
348 involved in this cue-reward learning task, mice were injected intraperitoneally with saline
349 (n = 8), mecamylamine (non-competitive nicotinic antagonist, Mec, n = 9), scopolamine
350 (competitive muscarinic antagonist, Scop, n = 8), or a combination of both antagonists
351 (Mec+Scop, n = 9) 30 min prior to Pre-Training and Training, during the same epochs of
352 the task in which optical stimulation was administered (**Figure 5A**). Like optical
353 stimulation, blockade of ACh receptors during the Pre-Training phase of the task had no
354 effect on rewards earned (**Figure 5B + Figure 5-figure supplement 1A**, blue shading,
355 main effect of Group (antagonist) in a two-way repeated-measures ANOVA, $F(3, 30) =$
356 1.285 , $P=0.2973$) or on the large number of incorrect nose pokes (**Figure 5C + Figure**
357 **5-figure supplement 1B**, blue shading, main effect of Group (antagonist) in a two-way
358 repeated-measures ANOVA, $F(3, 30) = 1.496$, $p = 0.2356$). In contrast, blockade of
359 muscarinic signaling abolished the ability of mice to learn the correct cue-reward
360 contingency during the Training period (**Figure 5B + Figure 5-figure supplement 1A**,
361 pink shading, two-way repeated-measures ANOVA, Antagonist main effect: $F(3, 30) =$
362 23.13 , $p < 0.0001$, Day x Antagonist interaction: $F(33, 330) = 10.79$, $p < 0.0001$), with
363 these mice maintaining high levels of incorrect nose pokes for the duration of Training
364 compared to Saline and Mec treated mice (**Figure 5C + Figure 5-figure supplement**
365 **1B**, pink shading, main effect of Group (antagonist) in a two-way repeated-measures

366 ANOVA, $F(3, 30) = 25.64$, $p < 0.0001$). Saline and Mec groups were not significantly
367 different in any phase of the task, including across Extinction (**Figure 5B-C + Figure 5-**
368 **figure supplement 1A-B**, orange shading, main effect of Group (antagonist) in a two-
369 way repeated-measures ANOVA, $F(1, 15) = 1.201$, $p = 0.2903$). We have shown that
370 this dose of mecamylamine delivered i.p. has significant effects in tests of anxiety-like
371 behavior and responses to inescapable stress. In addition, chronic treatment with
372 mecamylamine at this dose is sufficient to decrease BLA c-fos immunoreactivity (Mineur
373 et al., 2007). Consistent with the inability to acquire the cue-reward contingency, mice
374 treated with Scop or Mec+Scop also obtained very few rewards during Extinction
375 (**Figure 5B + Figure 5-figure supplement 1A**, orange shading). The antagonists had
376 no effect on locomotion as measured by beam breaks (**Figure 5-figure supplement**
377 **1C**) one-way ANOVA, $F(3, 30) = 0.5074$, $p = 0.6802$.

378

379 **ACh-mediated accelerated cue-reward learning does not require contingent**
380 **stimulation of ChAT⁺ NBM terminals in the BLA**

381 Acetylcholine is often thought of as a neuromodulator (Picciotto et al., 2012), and
382 the window for cholinergic effects on synaptic plasticity varies across ACh receptor
383 subtypes (Gu & Yakel, 2011). It is therefore possible that ACh signaling may result in
384 intracellular signaling changes that outlast the cue presentation window. In order to
385 determine if the effect of NBM-BLA stimulation is dependent upon the timing of correct
386 nose poke and laser stimulation contingency, we repeated the experiment in an
387 independent cohort of mice with an additional non-contingent ChR2 group that received
388 the same number of stimulation trains as the contingent ChR2 group, but in which light

389 stimulation was explicitly unpaired with task events (**Figure 6A + Figure 6-figure**
390 **supplement 1**). As in the previous experiment, there were no differences between the
391 EYFP control (n = 6) and stimulation groups (contingent-ChR2 n = 5 and non-contingent
392 ChR2 n = 5) during Pre-Training (**Figure 6B-C + Figure 6-figure supplement 2A-B**,
393 blue shading; main effect of group (EYFP vs. contingent-ChR2 vs. non-contingent
394 ChR2) two-way repeated-measures ANOVAs; rewards earned: $F(2, 13) = 0.7008$, $p =$
395 0.5140 ; incorrect nose pokes: $F(2, 13) = 0.3906$, $p = 0.6843$). However, the non-
396 contingent ChR2 group was not significantly different from the contingent ChR2 group
397 during the Training period with respect to number of rewards earned (two-way repeated-
398 measures ANOVA, $F(1, 8) = 0.09147$, $p = 0.7700$) or incorrect nose pokes (two-way
399 repeated-measures ANOVA, $F(1, 8) = 0.3681$, $p = 0.5609$), but both ChR2 groups were
400 significantly better than the EYFP control group (**Figure 6B-C + Figure 6-figure**
401 **supplement 2A-B**, pink shading; two-way repeated-measures ANOVAs; rewards
402 earned: Group (EYFP vs. contingent-ChR2 vs. non-contingent-ChR2) main effect: $F(2,$
403 $13) = 7.254$, $p = 0.0077$; Day x Group interaction: $F(22, 143) = 1.861$, $p = 0.0164$.
404 Incorrect nose pokes: Group main effect: $F(2, 13) = 4.884$, $p = 0.0262$). These results
405 demonstrate that ChR2-mediated ACh release does not have to be time-locked to the
406 cue, nose poke, or reward retrieval to improve performance of the task, suggesting that
407 ACh may alter the threshold for neuronal plasticity for cue-reward pairing over a much
408 longer timescale than might be expected based on results from the ACh3.0 recording
409 and NBM-BLA recordings, which could be consistent with the involvement of mAChR
410 signaling in this effect. As in the previous experiment, once all groups reached criterion
411 for acquisition of the cue-reward contingency, there were no differences between any of

412 the groups during Extinction (**Figure 6B-C + Figure 6-figure supplement 2A-B**, orange
413 shaded; two-way repeated-measures ANOVA, $F(2, 13) = 0.04229$, $p = 0.9587$).

414

415 **Discussion**

416 It is increasingly recognized that the BLA is involved in learning to predict both
417 positive and negative outcomes from previously neutral cues (Cador et al., 1989; Janak
418 & Tye, 2015; LeDoux et al., 1990). Cholinergic cells in the basal forebrain complex fire
419 in response to both positive and negative reinforcement (Hangya et al., 2015). The
420 results shown here indicate that ACh signaling in the BLA is intimately involved in cue-
421 reward learning. Endogenous ACh is released in the BLA in response to salient events
422 in the task, and ACh dynamics evolved as the subject formed associations between
423 stimuli and reward. While the pattern of ACh signaling in the BLA may seem reminiscent
424 of how dopamine neurons encode reward prediction errors as measured in other brain
425 areas (Schultz et al., 1997), the current results suggest that ACh release in the BLA
426 may instead be involved in signaling a combination of salience and novelty. ACh
427 release and NBM-BLA activity increased following correct nose poke and, around the
428 time that animals acquired the cue-reward task, following tone onset. However, earlier
429 in Training, incorrect nose pokes that resulted in a timeout were also followed by ACh
430 release, although this was smaller in magnitude. Further, stimulating NBM-BLA
431 cholinergic terminals during learning enhanced behavioral performance, but was not
432 intrinsically rewarding on its own and did not support responding for the tone alone.
433 Although ACh was released in the BLA at discrete points during the task, the effects of
434 heightened BLA ACh signaling were relatively long lasting, since it was not necessary

435 for stimulation to be time-locked to cue presentation or reward retrieval to enhance
436 behavioral performance. Thus, cholinergic inputs from the basal forebrain complex to
437 the BLA are a key component of the circuitry that links salient events to previously
438 neutral stimuli in the environment and uses those neutral cues to predict future
439 rewarded outcomes.

440

441 **BLA ACh signaling and CaMKII α cell activity are related to cue-reward learning**

442 We have shown that ACh release in the BLA is coincident with the stimulus that
443 was most salient to the animal at each phase of the task. Use of the fluorescent ACh
444 sensor was essential in determining these dynamics (Jing et al., 2018, 2019). Previous
445 microdialysis studies have shown that ACh is released in response to positive, negative,
446 or surprising stimuli, but this technique is limited by relatively long timescales (minutes)
447 and cannot be used to determine when cholinergic transients align to given events in an
448 appetitive learning task and how they evolve over time (Sarter & Lustig, 2020). In this
449 cue-reward learning paradigm, when there was no consequence for incorrect nose-
450 poking (Pre-Training phase), animals learned to perform a very high number of nose
451 pokes and received a large number of rewards, and BLA ACh signaling peaked
452 following correct nose pokes. Both the behavioral response (nose poking that was not
453 contingent with the tone) and the ACh response (linked to the correct nose poke)
454 suggest that the animals were not attending to the tone during most of the Pre-Training
455 phase of the task, but rather were attending to the cues associated with reward delivery,
456 such as the reward light or the sound of the pump that delivered the reward. Consistent
457 with this possibility, in the next phase of the task when mice received a timeout for

458 responding if the tone was not presented, performance of all groups dropped
459 dramatically. Interestingly, in animals that had difficulty learning the cue-reward
460 contingency, during early Training sessions ACh release shifted to reward retrieval,
461 likely because this was the most salient aspect of the task when the majority of nose
462 pokes performed did not result in reward. Finally, as mice acquired the contingency
463 between tone and reward availability, the tone also began to elicit ACh release in the
464 BLA, suggesting that mice learned that the tone is a salient event predicting reward
465 availability. Since there are multiple sources of ACh input to the BLA, it was important to
466 determine whether NBM cholinergic neurons were active during the periods when ACh
467 levels were high (Woolf, 1991). Recordings from cholinergic NBM-BLA terminal fibers
468 showed similar dynamics to ACh measurements, suggesting that the NBM is a primary
469 source of ACh across the phases of cue-reward learning.

470 Perhaps the most well-known example of dynamic responding related to learning
471 cue-reward contingencies and encoding of reward prediction errors is the firing of
472 dopaminergic neurons of the ventral tegmental area (VTA; Schultz, 1998). After
473 sufficient pairings, dopaminergic neurons will fire in response to the cue that predicts
474 the reward, and no longer to the rewarding outcome, which corresponds with behavioral
475 changes that indicate an association has been formed between conditioned stimuli (CS)
476 and unconditioned stimuli (US). It should be noted that dopamine signaling is not unique
477 in this learning-related dynamic response profile. Serotonergic neuronal responses also
478 evolve during reward learning in a manner distinct from dopaminergic neurons (Zhong
479 et al., 2017). Plasticity related to learning has also been observed in cholinergic neurons
480 in the basal forebrain complex during aversive trace conditioning, such that after several

481 training days, neuronal activity spans the delay between CS and US (Guo et al., 2019).
482 Additionally, a recent study suggested that ACh may signal a valence-free
483 reinforcement prediction error (Sturgill et al., 2020). Future studies on the selective
484 inputs to NBM to BLA cholinergic neurons would be of interest to identify the links
485 between brain areas involved in prediction error coding.

486 We found that BLA CaMKII α cells were most reliably activated following reward
487 retrieval before contingency acquisition (both when they were receiving several rewards
488 but no timeouts in Pre-Training and few rewards early in Training). Similar to the
489 recording of ACh levels, after acquisition, the tone began to elicit an increase in BLA
490 CaMKII α cell population activity. However, activity of CaMKII α neurons differed from
491 ACh signaling in the BLA in important ways. ACh was released in response to the
492 salient events in the task that were best able to predict reward delivery or availability. In
493 contrast, the activity of BLA CaMKII α neurons was not tightly time-locked to correct
494 nose poking, and instead followed reward retrieval until acquisition, when activity
495 increased in response to tone onset. The divergent dynamics of ACh release and
496 CaMKII α neuron activity underscores that ACh's role in the BLA is to modulate, rather
497 than drive, the activity of CaMKII α neurons, and therefore may alter dynamics of the
498 network through selective engagement of different populations of GABA interneurons
499 (Unal et al., 2015).

500

501 **Increasing BLA acetylcholine levels enhances cue-reward learning**

502 Neuronal activity and plasticity in the BLA is required for both acquisition of
503 appetitive learning (conditioned reinforcement) and fear conditioning, however the

504 inputs that increase activity in the structure during salient events likely come from many
505 brain areas (McKernan & Shinnick-Gallagher, 1997; Rogan et al., 1997; Tye et al.,
506 2008). In particular, dopaminergic inputs to the BLA are important for acquisition of
507 conditioned reinforcement and for linking the rewarding properties of addictive drugs to
508 cues that predict their availability (Cador et al., 1989). Our results indicate that ACh is a
509 critical neuromodulator upstream of the BLA that is responsive to salient events, such
510 as reward availability, motor actions that elicit reward, and cues that predict reward. We
511 show here that increasing endogenous ACh signaling in the BLA caused mice to
512 perform significantly better than controls in an appetitive cued-learning task. Heightened
513 ACh release during learning of a cue-action-reward contingency led to fewer incorrect
514 responses and increased acquisition rate in both female and male mice. The optical
515 stimulation was triggered by correct nose poke, thus the cholinergic NBM-BLA terminal
516 fiber stimulation overlapped with all three salient events: tone, nose poke, and reward
517 retrieval, since the tone terminated 2 sec after correct nose poke. We chose this
518 stimulation pattern, as opposed to linking optical stimulation to tone onset, to ensure
519 stimulation was dependent on behavioral responses. Therefore, stimulation did not
520 precisely recapitulate the ACh release profile observed in mice that had already
521 acquired the task (when ACh increases following tone onset). This suggests that
522 behaviorally-contingent increases in BLA ACh are sufficient to enhance task acquisition
523 (but see below). It is also possible that optogenetic-mediated ACh release may last
524 longer than endogenous, tone-evoked release. A simultaneous stimulation and
525 recording approach would be required to compare ACh release under both conditions
526 (Pisansky et al., 2019). It is important to note that basal forebrain neurons have been

527 demonstrated to co-release ACh and GABA (Ma et al., 2018; Saunders et al., 2015),
528 and cholinergic basal forebrain neurons that project to the BLA have been shown to co-
529 express a glutamate transporter (Ma et al., 2018; Poulin et al., 2006). Thus, it is
530 possible that both fiber photometry and optogenetic results could be influenced, in part,
531 by co-release of other neurotransmitters from ChAT-positive neurons. Future studies
532 employing additional fluorescent neurotransmitter sensors (Marvin et al., 2013, 2018,
533 2019) could help understand the interaction between the different signals employed by
534 basal forebrain neurons.

535 It is possible that ACh improved learning by increasing the intensity of the
536 reward, potentiating the learned association, improving discrimination, or a combination
537 of these phenomena. However, increasing ACh release in the BLA was not inherently
538 rewarding, because it did not support self-stimulation or real-time place preference. This
539 is at odds with a recent study that found stimulation of NBM-BLA cholinergic terminals
540 could induce a type of place-preference and modest self-stimulation (Aitta-aho et al.,
541 2018). Perhaps slight differences in targeting of ChR2 infusion or differences in the
542 behavioral paradigm could be responsible for the lack of direct rewarding effects of
543 optical ChAT terminal stimulation in the current study. Other recent work (Jiang et al.,
544 2016) has demonstrated that stimulating this NBM-BLA cholinergic pathway is sufficient
545 to strengthen cued aversive memory, suggesting that the effect of ACh in the BLA may
546 not be inherently rewarding or punishing, but instead potentiates plasticity in the BLA,
547 allowing learning of cue-outcome contingencies. Similarly, it is possible that ACh alters
548 motor activity. However, there were no effects of optical stimulation on locomotion or
549 responding in the inactive nose poke port. In addition, during the Pre-Training phase

550 when there was no consequence for incorrect nose pokes, all groups earned the same
551 number of rewards, regardless of optical stimulation or pharmacological blockade of
552 ACh receptors, suggesting that ACh is not involved in the motor aspects of the task or
553 the value of the reward. Indeed, differences emerged only during the Training phase,
554 when attention to the tone was critical to earn rewards. Further, incorrect nose poking
555 remained high for mice administered scopolamine. This suggests that scopolamine-
556 treated animals were seeking the reward, as in the operant familiarization and Pre-
557 Training phases of training, but were unable to learn that they should only nose poke in
558 response to the tone.

559 Cell-type-specific expression of AChRs and activity-dependent effects place
560 cholinergic signaling at a prime position to shape BLA activity during learning. For
561 instance, late-firing interneurons in the BLA exhibit nAChR-dependent EPSP's when no
562 effect is seen on fast-spiking interneurons, while principal neurons can be either excited
563 or inhibited through mAChRs, depending on activity level of the neuron at the time of
564 cholinergic stimulation (Unal et al., 2015). BLA mAChRs can support persistent firing in
565 principal neurons and can be important for the expression of conditioned place
566 preference behavior, as well as trace fear conditioning (Baysinger et al., 2012; Egorov
567 et al., 2006; McIntyre et al., 1998). Similar to studies of trace fear conditioning, in which
568 activity of the network over a delay period must be maintained, we found that
569 metabotropic (mAChRs) but not ionotropic (nAChRs) ACh receptors were required for
570 learning the contingency of this cue-reward task. The timing of cholinergic signaling can
571 be a critical factor in the induction of synaptic plasticity in other brain regions, so we
572 hypothesized that the enhancement of cue-reward learning observed might be

573 dependent upon when NBM-BLA terminal fibers were stimulated with respect to tone
574 presentation and/or behavioral responses (Gu & Yakel, 2011). However, we found that
575 heightened ACh signaling in the BLA improved behavioral performance even when
576 stimulations were explicitly unpaired with the cue or correct nose poking. This suggests
577 that the effect of increased cholinergic signaling in the BLA is long lasting, and that
578 stimulation during a learning session is sufficient to potentiate synaptic events linking
579 the cue to a salient outcome—even if CS and/or reward delivery are presented tens of
580 seconds later. Given the findings from fiber photometry recordings, which showed
581 endogenous ACh release was time-locked to salient stimuli during the task and evolved
582 with learning, it is surprising that time-locking of exogenous ACh release was not
583 necessary for enhancement of cue-reward learning. Coupled with pharmacological
584 evidence demonstrating that muscarinic signaling is necessary for reward learning in
585 this task, these results suggest the involvement of metabotropic signaling downstream
586 of muscarinic receptors that outlasts the initial cholinergic stimulation.

587 To conclude, the abundant ACh input to the BLA results in ACh release in
588 response to stimuli that predict reward in a learned cue-reward task. Increasing
589 cholinergic signaling results in accelerated learning of the cue-reward contingency.
590 These findings are consistent with the hypothesis that ACh is a neuromodulator that is
591 released in response to salient stimuli and suggests that ACh signaling may enhance
592 neuronal plasticity in the BLA network, leading to accelerated cue-reward learning.

Key Resources Table				
Reagent type (species) or resource	Designation	Source or reference	Identifiers	Additional information
genetic reagent (<i>M. musculus</i>)	B6;129S6- <i>Chat</i> ^{tm2(cre)Lowl/J}	Jackson Laboratory	Stock #: 006410 RRID:IMSR_JAX:006410	
genetic reagent (<i>M. musculus</i>)	C57BL/6J	Jackson Laboratory	Stock #: 000664 RRID:IMSR_JAX:000664	
genetic reagent (<i>M. musculus</i>)	Tg(<i>Camk2a-cre</i>)2Gsc	Günter Schütz, German Cancer Research Center	RRID:MGI:4457404	(Casanova et al., 2001; Wohleb et al., 2016)
antibody	anti-ChAT (goat polyclonal)	Millipore Sigma	Cat #: AB144P RRID:AB_2079751	(1:1000)
antibody	anti-GFP (chicken, polyclonal)	Thermo Fisher Scientific	Cat #: A10262, RRID:AB_2534023	(1:1000)
antibody	anti-DsRed (rabbit, monoclonal)	Takara Bio	Cat #: 632392, RRID:AB_2801258	(1:1000)
antibody	donkey anti-chicken 488 (secondary)	Jackson ImmunoResearch	Cat #: 703-545-155, RRID:AB_2340375	(1:1000)
antibody	donkey anti-rabbit 555 (secondary)	Thermo Fisher Scientific	Cat #: A-31572, RRID:AB_162543	(1:1000)
antibody	donkey anti-goat 555 (secondary)	Thermo Fisher Scientific	Cat #: A-21432, RRID:AB_141788	(1:1000)

antibody	donkey anti-goat 647 (secondary)	Thermo Fisher Scientific	Cat #: A-21447, RRID:AB_141844	(1:1000)
recombinant DNA reagent	AAV9 hSyn-ACh3.0	Yulong Li (Jing et al., 2018, 2019)	Cat #: YL10002-AV9	
recombinant DNA reagent	AAV1 Syn-FLEX-GCaMP6s-WPRE-SV40	Addgene	Cat #: 100845-AAV1 RRID:Addgene_100845	
recombinant DNA reagent	AAV1-Syn-FLEX-jGCaMP7s-WPRE	Addgene	Cat #: 104491-AAV1 RRID:Addgene_104491	
recombinant DNA reagent	AAV1 Syn-FLEX-NES-jRCaMP1b-WPRE-SV40	Addgene	Cat #: 100850-AAV1 RRID:Addgene_100850	
recombinant DNA reagent	AAV2 EF1a-DIO-EYFP	UNC Viral Vector Core	RRID: SCR_002448	
recombinant DNA reagent	AAV2 EF1a-DIO-hChr2(H134R)-EYFP	UNC Viral Vector Core	RRID: SCR_002448	
chemical compound, drug	mecamylamine hydrochloride	Millipore Sigma	Cat #: M9020	
chemical compound, drug	(-) scopolamine hydrochloride	Millipore Sigma	Cat #: S1013	
software, algorithm	MATLAB	MathWorks	RRID: SCR_001622	Version 2020a
software, algorithm	GraphPad Prism 8	GraphPad Software	RRID: SCR_002798	

software, algorithm	EthoVision XT 10	Noldus	RRID: SCR_000441	
software, algorithm	FV10-ASW	Olympus	RRID:SCR_014215	Version 04.02.03.06
software, algorithm	Doric Neuroscience Studio	Doric Lenses		Version 5.3.3.14
software, algorithm	MED-PC IV	Med Associates Inc.	RRID:SCR_012156	
other	Allen Reference Atlas	(Lein et al., 2007)	RRID:SCR_013286	
other	DAPI stain	Thermo Fisher Scientific	Cat #: 62248	1:1000

594

595 **Animals**

596 All procedures were approved by the Yale University Institutional Animal Care &
597 Use Committee (protocol: 2019-07895) in compliance with the National Institute of
598 Health's Guide for the Care and Use of Laboratory Animals. Experiments were
599 performed in mice of both sexes, in keeping with the NIH policy of including sex as a
600 biological variable. Sex of mice in behavioral graphs is indicated by circles for females
601 and squares for males.

602 Female and male heterozygous mice with Cre recombinase knocked into the
603 choline acetyltransferase (ChAT) gene (ChAT-IRES-Cre, B6;129S6-*Chat*^{tm2(cre)Low/J},
604 Jackson Laboratory, Bar Harbor, ME) were bred in house by mating ChAT-IRES-Cre
605 with C57BL6/J mice. CaMKII α -Cre (Tg(*Camk2a-cre*)2Gsc) mice obtained from Ronald
606 Duman (Casanova et al., 2001; Wohleb et al., 2016) were bred in house as above.

607 C57BL6/J mice were obtained from The Jackson Laboratory at 6-10 weeks of age, and
608 tested at 5-7 months of age, following at least one week of acclimation. All mice were
609 maintained in a temperature-controlled animal facility on a 12-hour light/dark cycle
610 (lights on at 7:00 AM). Mice were group housed 3-5 per cage and provided with *ad*
611 *libitum* food and water until undergoing behavioral testing. Mice were single housed 1-3
612 weeks before surgery to facilitate food restriction and body weight maintenance.

613

614 **Surgical procedures**

615 Surgical procedures for behavior were performed in fully adult mice at 4-6
616 months of age, age-matched across conditions. For viral infusion and fiber implantation,
617 mice were anesthetized using isoflurane (induced at 4%, maintained at 1.5-2%) and
618 secured in a stereotactic apparatus (David Kopf Instruments, Tujunga, CA). The skull
619 was exposed using a scalpel and Bregma was determined using the syringe needle tip
620 (2 μ L Hamilton Neuros syringe, 30 gauge needle, flat tip; Reno, NV).

621 For fiber photometry surgeries, 0.4 μ L of AAV9 hSyn-ACh3.0 (Vigene
622 Biosciences Inc.) to measure BLA ACh levels (**Figure 2A-E + Figure 2-figure**
623 **supplement 1-2**) was delivered unilaterally to the BLA (A/P; -1.34 mm, M/L + or - 2.65
624 mm, D/V -4.6 mm, relative to Bregma) of ChAT-IRES-Cre or wild-type C57BL6/J mice at
625 a rate of 0.1 μ L/min. The needle was allowed to remain at the infusion site for 5 min
626 before and 5 min after injection. A mono fiber-optic cannula (1.25 mm outer diameter
627 metal ferrule; 6 mm long, 400 μ m core diameter/430 μ m outer diameter, 0.48 numerical
628 aperture (NA), hard polymer cladding outer layer cannula; Doric Lenses, Quebec City,
629 Quebec, Canada) was implanted above the BLA (A/P; -1.34 mm, M/L + 2.65 mm, D/V -

630 4.25 mm) and affixed to the skull using opaque dental cement (Parkell Inc., Edgewood,
631 NY). For BLA CaMKII α cell calcium dynamic recordings (**Figure 3 + Figure 3-figure**
632 **supplement 1-2**), 0.5 μ L of AAV1 Syn-FLEX-GCaMP6s-WPRE-SV40 (Addgene,
633 Watertown, MA) was injected into the left BLA using the same procedure and
634 coordinates but was injected into CaMKII α -Cre mice. Cholinergic NBM-BLA terminal
635 fiber calcium dynamic recording (**Figure 2F-J + Figure 2-figure supplement 5-8**)
636 surgeries were performed as above except AAV1-Syn-FLEX-jGCaMP7s-WPRE
637 (Addgene) was infused unilaterally into the NBM (A/P: - 0.7 mm, M/L + or - 1.75 mm,
638 D/V - 4.5 mm) of ChAT-IRES-Cre mice, with the optical fiber being placed above the
639 ipsilateral BLA. The jRCaMP1b + ACh3.0 surgeries to simultaneously measure
640 cholinergic NBM-BLA terminal fiber calcium dynamics and BLA ACh levels (**Figure 2-**
641 **figure supplement 9**) consisted of both the NBM and BLA infusions above, except
642 AAV1 Syn-FLEX-NES-jRCaMP1b-WPRE-SV40 (Addgene) was infused the NBM of
643 ChAT-IRES-Cre mice. The RCaMP sham mouse (**Figure 2-figure supplement 9E,H**)
644 was a wild-type littermate and thus had no jRCaMP1b expression.

645 pAAV.Syn.Flex.GCaMP6s.WPRE.SV40 (Addgene viral prep # 100845-AAV1;
646 <http://n2t.net/addgene:100845> ; RRID:Addgene_100845), pGP-AAV-syn-FLEX-
647 jGCaMP7s-WPRE was a gift from Douglas Kim & GENIE Project (Addgene viral prep #
648 104491-AAV1; <http://n2t.net/addgene:104491> ; RRID:Addgene_104491), and
649 pAAV.Syn.Flex.NES-jRCaMP1b.WPRE.SV40 (Addgene viral prep # 100850-AAV1;
650 <http://n2t.net/addgene:100850> ; RRID:Addgene_100850) were gifts from Douglas Kim &
651 GENIE Project (Chen et al., 2013; Dana et al., 2016, 2019).

652 Mice were allowed to recover in a cage without bedding with a microwavable
653 heating pad underneath it until recovery before being returned to home cage. For two
654 days following surgery, mice received 5 mg/Kg Rimadyl i.p (Zoetis Inc., Kalamazoo, MI)
655 as postoperative care.

656 For optical stimulation experiments (**Figure 4,6 + Figure 4-figure supplement 1-**
657 **5 + Figure 6-figure supplement 1-2**), surgeries were performed as above except as
658 follows: 0.5 μ L of control vector (AAV2 EF1a-DIO-EYFP) or channelrhodopsin (AAV2
659 EF1a-DIO-hChR2(H134R)-EYFP; University of North Carolina Gene Therapy Center
660 Vector Core, Chapel Hill, NC) was delivered bilaterally into the NBM (A/P: - 0.7 mm, M/L
661 \pm 1.75 mm, D/V – 4.5 mm) of ChAT-IRES-Cre mice. Mono fiber-optic cannulas (1.25
662 mm outer diameter zirconia ferrule; 5 mm long, 200 μ m core diameter/245 μ m outer
663 diameter, 0.37 NA, polyimide buffer outer layer cannula; Doric Lenses) were inserted
664 bilaterally above the basolateral amygdala (BLA, A/P; -1.22 mm, M/L \pm 2.75 mm, D/V -
665 4.25 mm). Mice were randomly assigned to EYFP or ChR2 groups, controlling for
666 average group age.

667 For *ex vivo* local field potential electrophysiology experiments (**Figure 4B**), the
668 NBM was injected with DIO-ChR2-EYFP as described above, except mice were 8
669 weeks of age (see Supplemental Methods for current clamp recording methods). The
670 coronal brain slices containing the NBM were prepared after 2-4 weeks of expression.
671 Briefly, mice were anesthetized with 1X Fatal-Plus (Vortech Pharmaceuticals, Dearborn,
672 MI) and were perfused through their circulatory systems to cool down the brain with an
673 ice-cold (4°C) and oxygenated cutting solution containing (mM): sucrose 220, KCl 2.5,
674 NaH₂PO₄ 1.23, NaHCO₃ 26, CaCl₂ 1, MgCl₂ 6 and glucose 10 (pH 7.3 with NaOH).

675 Mice were then decapitated with a guillotine immediately; the brain was removed and
676 immersed in the ice-cold (4°C) and oxygenated cutting solution to trim to a small tissue
677 block containing the NBM. Coronal slices (300 µm thick) were prepared with a Leica
678 vibratome (Leica Biosystems Inc., Buffalo Grove, IL) after the tissue block was glued on
679 the vibratome stage with Loctite 404 instant adhesive (Henkel Adhesive Technologies,
680 Düsseldorf, Germany). After preparation, slices were maintained at room temperature
681 (23-25 C°) in the storage chamber in the artificial cerebrospinal fluid (ACSF) (bubbled
682 with 5% CO₂ and 95% O₂) containing (in mM): NaCl 124, KCl 3, CaCl₂ 2, MgCl₂ 2,
683 NaH₂PO₄ 1.23, NaHCO₃ 26, glucose 10 (pH 7.4 with NaOH) for recovery and storage.
684 Slices were transferred to the recording chamber and constantly perfused with ACSF
685 with a perfusion rate of 2 ml/min at a temperature of 33 oC for electrophysiological
686 experiments. Cell-attached extracellular recording of action potentials was performed by
687 attaching a glass micropipette filled with ACSF on EYFP-expressing cholinergic neurons
688 with an input resistance of 10-20 MΩ under current clamp. Blue light (488 nm) pulse (60
689 ms) was applied to the recorded cells through an Olympus BX51WI microscope
690 (Olympus, Waltham, MA) under the control of the Sutter filter wheel shutter controller
691 (Lambda 10-2, Sutter Instrument, Novato, CA). All data were sampled at 3-10 kHz,
692 filtered at 3 kHz and analyzed with an Apple Macintosh computer using Axograph X
693 (AxoGraph). Events of field action potentials were detected and analyzed with an
694 algorithm in Axograph X as reported previously (Rao et al., 2008).

695

696 **Behavioral Testing**

697 ***Habituation***

698 One week after surgery, mice were weighed daily and given sufficient food
699 (2018S standard chow, Envigo, Madison, WI) to maintain 85% free-feeding body
700 weight. All behavioral tests were performed during the light cycle. Mice were allowed to
701 acclimate to the behavioral room for 30 min before testing and were returned to the
702 animal colony after behavioral sessions ended.

703 Two weeks after surgery, mice were handled 3 min per day for 7 days in the
704 behavioral room. Mice were given free access to the reward (Ensure[®] Plus Vanilla
705 Nutrition Shake solution mixed with equal parts water (Ensure); Abbott Laboratories,
706 Abbott Park, IL) in a 50 mL conical tube cap in their home cages on the last 3 days of
707 handling to familiarize them to the novel solution. Mice were also habituated to patch
708 cord attachment during the last 3 days of handling for optical stimulation and fiber
709 photometry experiments. Immediately before training each day, a patch cord was
710 connected to their optical fiber(s) via zirconia sleeve (s) (1.25 mm, Doric Lenses) before
711 being placed in the behavioral chamber.

712 ***Operant Training***

713 All operant training was carried out using Med Associates modular test chambers
714 and accessories (ENV-307A; Med Associates Inc., Georgia, VT). For optical stimulation
715 experiments, test chambers were housed in sound attenuating chambers (ENV-022M).
716 Two nose poke ports (ENV-313-M) were placed on the left wall of the chamber and the
717 reward receptacle (ENV-303LPHD-RL3) was placed on the right wall. The receptacle
718 cup spout was connected to a 5 mL syringe filled with Ensure loaded in a single speed
719 syringe pump (PHM-100). Nose pokes and receptacle entries were detected by infrared
720 beam breaks. The tone generator (ENV-230) and speaker (ENV-224BM) were placed

721 outside the test chamber, but within the sound attenuating chamber, to the left. The
722 house light (used for timeout, ENV-315M) was placed on top of the tone generator to
723 avoid snagging patch cords. Each chamber had a fan (ENV-025F28) running
724 throughout the session for ventilation and white noise. Behavior chambers were
725 connected to a computer running MEDPC IV to collect event frequency and timestamps.
726 For optical stimulation experiments, a hole drilled in the top of the sound attenuating
727 chambers allowed the patch cord to pass through. Initial BLA ACh3.0 (**Figure 2A-E**)
728 and BLA CaMKII α GCaMP6s (**Figure 3**) fiber photometry recordings occurred in a
729 darkened behavioral room outside of sound attenuating chambers due to steric
730 constraints with rigid fiber photometry patch cords. Later behavioral chamber
731 optimization (wall height was extended with 3D printed and laser cut acrylic panels to
732 allow removing the test chamber lid while preventing escape) allowed all other fiber
733 photometry cohorts to be tested inside sound attenuating chambers. For fiber
734 photometry experiments, a custom receptacle was 3D printed that extended the cup
735 beyond the chamber wall to allow mice to retrieve the reward with more rigid patch
736 cords. Each mouse was pseudo-randomly assigned to behavioral chamber when
737 multiple chambers were used, counterbalancing for groups across boxes.

738 Three weeks after surgery, initial operant familiarization consisted of one 35 min
739 session of Free Reward to demonstrate the location of reward delivery; all other
740 sessions were 30 mins. During Free Reward, only the reward receptacle was
741 accessible. After 5 min of habituation, Ensure (24 μ L over 2 seconds) was delivered in
742 the receptacle cup and a light was turned on above the receptacle. The receptacle light
743 was turned off upon receptacle entry. The next phase of operant familiarization, mice

744 learned to nose poke to receive reward on a fixed-ratio one (FR1) schedule of
745 reinforcement. Mice in experiments involving manipulations (optical stimulation and
746 antagonist studies) were pseudo-randomly assigned to left or right active (reinforced)
747 nose poke port. Mice in fiber photometry experiments were all assigned to right active
748 port to minimize potential across subject variability. The inactive (unreinforced) port
749 served as a locomotor control. During FR1 operant familiarization, each nose poke
750 response into the active port resulted in receptacle light and reward delivery. After the
751 mice reached criterion on FR1 operant familiarization (group average of 30 rewards for
752 2 consecutive days, usually 4-5 days), mice were advanced to the Pre-Training phase.
753 This phase incorporated an auditory tone (2.5-5 kHz, ~60 dB) that lasted for at most 10
754 seconds and signaled when active nose pokes would be rewarded. Only active nose
755 pokes made during the 10 sec auditory tone (correct nose pokes) resulted in reward
756 and receptacle light delivery. The tone co-terminated with Ensure delivery. During Pre-
757 Training, there was no consequence for improper nose pokes, neither in the active port
758 outside the tone (incorrect nose pokes) nor in the inactive port (inactive nose pokes).
759 The number of inactive nose pokes were typically very low after operant familiarization
760 and were not included in analysis. After reward retrieval (receptacle entry following
761 reward delivery) the receptacle light was turned off and the tone was presented again
762 on a variable intertrial interval schedule with an average interval of 30 sec (VI 30),
763 ranging from 10 to 50 sec (Ambroggi et al., 2008). After 4-5 days of Pre-Training, mice
764 progressed to the Training phase, which had the same contingency as Pre-Training
765 except incorrect nose pokes resulted in a 5 sec timeout signaled by house light
766 illumination, followed by a restarting of the previous intertrial interval. Mice were

767 considered to have acquired the task after earning 20 rewards during the Training
768 phase of the task. In order to promote task acquisition, mice that were not increasing
769 number of rewards earned reliably were moved to a VI 20 schedule after 9 days of VI 30
770 Training for BLA ACh3.0 or 6-7 days for BLA CaMKII α cell mice. The VI 20 schedule
771 was only needed for the two groups that were trained outside of the sound attenuating
772 chambers. Mice progressed to Extinction after 12 days of Training or, in the case of
773 fiber photometry cohorts, once all mice met the acquisition criteria. Extinction was
774 identical to Training except no Ensure was delivered in response to correct nose pokes.
775 The replicate cohorts of the BLA CaMKII α GCaMP6s and NBM-BLA terminal fiber
776 recording experiments were advanced to one day of Extinction after only 7 days of
777 Training due to the COVID-19 shutdown.

778 Between mice, excrement was removed from the chambers with a paper towel.
779 At the end of the day chambers were cleaned with Rescue Disinfectant (Virox Animal
780 Health, Oakville, Ontario, Canada) and Ensure syringe lines were flushed with water
781 then air. Mice were excluded from analyses if a behavioral chamber malfunctioned (e.g.
782 syringe pump failed) or they received the improper compound. Fiber photometry mice
783 were excluded from analyses if they did not meet the acquisition criterion by the last day
784 of Training. See **Supplementary File 1–Supplementary Table 1** for number of mice
785 that acquired, were excluded, and further explanations for behavioral paradigm
786 deviations.

787 ***Optical Stimulation***

788 Optical stimulation was generated by a 473 nm diode-pumped solid-state
789 continuous wave laser (Opto Engine LLC, Midvale, UT) controlled by a TTL adapter

790 (SG-231, Med Associates Inc.). The laser was connected to a fiber optic rotary joint
791 (Doric Lenses) via a mono fiber optic patch cord (200 μm core, 220 μm cladding, 0.53
792 NA, FC connectors; Doric Lenses). The rotary joint was suspended above the sound
793 attenuating chamber with a connected branching fiber optic patch cord (200 μm core,
794 220 μm cladding, 0.53 NA, FC connector with metal ferrule; Doric Lenses) fed into the
795 behavioral box. Laser power was adjusted to yield 10-12 mW of power at each fiber tip.
796 The stimulation pattern was 25 ms pulses at 20 Hz for 2 sec modified from parameters
797 in (Jiang et al., 2016). Jiang et al. used a 20Hz pulse frequency, 5 ms pulses, and 10-12
798 mW power at the fiber tips. In the current study we used a 2 sec stimulation duration
799 because it matched the time of syringe pump activation for reward delivery and co-
800 terminated with the pump and auditory tone. A 25 ms pulse width was used because
801 our lasers were not able to generate sufficient power with 5 ms pulses. Optical
802 stimulation was only delivered during the Pre-Training and Training phases of the
803 operant task. Both control (EYFP) and experimental (ChR2) groups received identical
804 light delivery, and stimulation was triggered by a correct nose poke and co-terminated
805 with the auditory tone and Ensure delivery. For the non-contingent experiment, the
806 number of light stimulations was yoked to the concurrently running ChR2 mouse. The
807 timing of the non-contingent stimulation was explicitly unpaired with correct nose pokes
808 or tones, and was held in queue until the mouse had not made a response in the last 2
809 sec, a tone was not going to be delivered within the next 2 sec, or at least 5 sec had
810 passed since the mouse entered the receptacle after earning reward.

811

812 **Fiber Photometry**

813 **Acquisition**

814 Fluorescent measurements of ACh and calcium levels were recorded using two
815 Doric Lenses 1-site Fiber Photometry Systems: a standard 405/465 nm system and a
816 405/470/560 nm system. The standard 405/465 system was configured as follows: the
817 fiber photometry console controlled the two connectorized LEDs (CLEDs, 405 nm
818 modulated at 208.616 Hz and 465 nm modulated at 572.205 Hz) through the LED
819 module driver (Cassidy et al., 2019). Each CLED was connected via attenuating patch
820 cord to the five-port Fluorescence MiniCube (FMC5_AE(405)_AF(420-450)_E1(460-
821 490)_F1(500-550)_S). A pigtailed fiber optic rotary joint was connected to the MiniCube
822 and suspended above the behavioral chamber with a rotary joint holder in order to
823 deliver and receive light through the implanted optical fiber. The other end of the rotary
824 joint was connected to the mono fiber optic patch cord via M3 connector and attached
825 with a zirconia sleeve to the implanted fiber optic as above. The F1 (500-550 nm) port of
826 the MiniCube was connected to the photoreceiver (AC low mode, New Focus 2151
827 Visible Femtowatt Photoreceiver, New Focus, San Jose, CA) via a fiber optic adapter
828 (Doric Lenses) that was finally connected back to the fiber photometry console through
829 an analog port. The 405/470/560 nm system was set up similarly, except a 560 nm LED
830 was incorporated (modulated at 333.786 Hz), a six-port MiniCube with two integrated
831 photodetector heads was used (iFMC6_IE(400-410)_E1(460-490)_F1(500-
832 540)_E2(555-570)_F2(580-680)_S), and Doric Fluorescence Detector Amplifiers were
833 used (AC 1X or 10X mode, DFD_FOA_FC). A TTL adapter (SG-231, Med Associates
834 Inc.) was connected to the digital input/output port to allow for timestamping when
835 events occurred in the behavioral chamber. Signal was recorded using Doric

836 Neuroscience Studio (V 5.3.3.14) via the Lock-In demodulation mode with a sampling
837 rate of 12.0 kS/s. Data were decimated by a factor of 100 and saved as a comma-
838 separated file.

839 **Pre-Processing**

840 Preprocessing of raw data was performed using a modified version of a MATLAB
841 (MathWorks, Natick, MA) script provided by Doric. The baseline fluorescence (F_0) was
842 calculated using a first order least mean squares regression over the ~30 min recording
843 session. Second order least mean squares regressions were used when
844 photobleaching of the sensor was more pronounced, as in the case of NBM-BLA
845 terminal fiber recordings. The change in fluorescence for a given timepoint (ΔF) was
846 calculated as the difference between it and F_0 , divided by F_0 , which was multiplied by
847 100 to yield $\% \Delta F / F_0$. The $\% \Delta F / F_0$ was calculated independently for both the signal
848 (465 nm) and reference (405 nm) channels to assess the degree of movement artifact.
849 Since little movement artifact was observed in the recordings (**Figure 2-figure**
850 **supplement 1B-C, Figure 2-figure supplement 5D-E, Figure 3-figure supplement**
851 **1C-D**, tan lines), the signal $\% \Delta F / F_0$ was analyzed alone (the code provided allows for
852 running the entire analysis pipeline with the reference channel $\% \Delta F / F_0$ if desired). The
853 $\% \Delta F / F_0$ was z-scored to give the final $Z \% \Delta F / F_0$ reported here. For the BLA CaMKII α
854 cell recordings (**Figure 3-figure supplement 1C-D**), the reference channel displayed
855 some mirroring (moving in the opposite direction) compared to the signal. This is likely
856 because 405 nm is not the “true” isosbestic point for GCaMP and we were instead
857 measuring some changes in calcium-unbound GCaMP rather than calcium-insensitive
858 GCaMP signal alone (Barnett et al., 2017; C. K. Kim et al., 2016; Sych et al., 2019).

859 Graphs and heatmaps for averaged traces aligned to actions were based on licking bout
860 epoch filtering code from TDT (Alachua, FL; link in code comments).

861 ***Heatmaps***

862 Combined action heatmaps were generated in MATLAB (2020a) by analyzing
863 data 5 sec preceding tone onset (rewarded trials only) to 5 sec after receptacle entry.
864 Actions were aligned despite variable latencies by evenly splitting a maximum of 4 sec
865 post-tone onset/pre-correct nose poke and 1 sec post-correct nose poke/pre-receptacle
866 entry for each trial within a day. The resulting aligned trials were averaged to generate
867 daily averages that made up the rows of the individual animal heatmaps. Blanks in the
868 rows of heatmaps (black time bins) indicate time bins added for alignment, meaning that
869 no trials for that day had a latency that stretched the entire window. Only rewarded trials
870 where the mouse entered the receptacle within 5 sec after nose poke were analyzed.
871 Full or partial training days were excluded from analysis if there were acquisition issues
872 such as the patch cord losing contact with the fiber or behavioral apparatus malfunction.
873 Lack of trials (fewer than three) for analysis or recording issues led to missing rows of
874 fiber photometry data in the heatmap despite having behavioral data, in which case
875 these rows were skipped rather than adding entire blank rows. Due to individual
876 differences in behavior, across-mouse average data was calculated by using a selection
877 of days in which behavior was roughly similar or milestones such as first and last day of
878 Pre-Training, first day earning 10 rewards in Training, first day crossing acquisition
879 threshold (and maintaining afterward), last day of Training, last day of Extinction (with 3
880 or more rewarded trials that met analysis criteria). Additional days were included in
881 across-mouse average heatmaps when possible. Incorrect nose poke heatmaps were

882 generated by averaging signals for 5 sec before and 5 sec after incorrect nose pokes
883 that were not preceded by an incorrect nose poke in the last 5 sec. The incorrect nose
884 poke heatmaps averaged across mice were generated using the same selection of days
885 as the combined action heatmaps for a given experiment.

886 **Bootstrapped Confidence Interval Analyses**

887 Bootstrapped Confidence Intervals (bCI's) of the Z-scored % $\Delta F/F_0$ fiber
888 photometry data within and across mice were generated using the methods described in
889 (Jean-Richard-dit-Bressel et al., 2020) for the following events: tone onset, correct nose
890 poke, receptacle entry, and incorrect nose poke. For the within-mouse analysis by day,
891 trials were aligned to event onset, and bCI's were generated for events that had at least
892 3 trials from 5 seconds prior to 10 seconds after each event. Each series of data were
893 bootstrapped 10,000 times and a two-sided 99% confidence interval was constructed.
894 Data were considered significantly different from baseline ($Z\% \Delta F/F_0 = 0$) when their
895 99% bCIs did not contain zero for an interval of time designated by a consecutive
896 threshold of 0.5 sec.

897 To avoid comparing vastly different numbers of trials, in graphs where correct
898 and incorrect nose pokes were plotted together, incorrect nose pokes were
899 downsampled to match the number of correct nose poke trials. For Incorrect Nose
900 Pokes graphs where last Pre-Training Day and Training Day 1 were plotted together,
901 both days were downsampled to the number of correct nose pokes on the last Pre-
902 Training Day.

903 For the combined action bCI plots (tone onset, correct nose poke, and
904 receptacle entry), the selection of days for each mouse matched that of the cohort-

905 averaged combined action heatmaps. The three event plots were combined by cropping
906 to match the maximum latencies used in the combined action heatmaps. For the
907 across-mouse averaged bCI plots, analyses were carried out as above except the
908 bootstrapping used mouse trial averages. The mean lines for across-mouse averaged
909 bCI plots were calculated by taking the mean of all individual trials together. The NBM-
910 BLA cholinergic terminal fiber experiment required combining the two independent
911 cohorts to obtain $n \geq 3$. For the incorrect nose poke bCI plots, the number of trials used
912 for each day were downsampled to 20 if a mouse performed more than 20.

913

914 **Pharmacology**

915 Male wildtype C57BL/6J mice were injected i.p. 30 min prior to each Pre-Training
916 and Training session with a volume of 10 mL/kg with the following compounds: 1X
917 DPBS (Thermo Fisher Scientific, Waltham, MA), 1 mg/kg mecamylamine hydrochloride
918 (Millipore Sigma, St. Louis, MO), 0.5 mg/kg (-) scopolamine hydrochloride (Millipore
919 Sigma), or 1 mg/kg mecamylamine + 0.5 mg/kg scopolamine (**Figure 5 + Figure 5-**
920 **figure supplement 1**)

921

922 **Histology**

923 After completion of behavioral experiments, animals were anesthetized with 1X
924 Fatal-Plus (Vortech Pharmaceuticals). Once there was no response to toe-pinch, mice
925 were transcardially perfused with 20 mL ice cold 1X DPBS followed by 20 mL 4%
926 paraformaldehyde (PFA, Electron Microscopy Sciences, Hatfield, PA). Brains were
927 extracted and post-fixed for at least 1 day in 4% PFA at 4°C and transferred to 30%

928 sucrose (Millipore Sigma) for at least 1 day at 4°C. Brains were sliced 40 µm thick on a
929 self-cooling microtome and stored in a 0.02% sodium azide (Millipore Sigma) PBS
930 solution. Brain slices were washed in PBS, blocked for 2-3 hours (0.3% Triton X-100,
931 American Bioanalytical, Canton, MA; 3% normal donkey serum, Jackson
932 ImmunoResearch, West Grove, PA), then incubated overnight with primary antibodies
933 (1:1000 + 1% normal donkey serum). Slices were then washed in PBS and incubated
934 with secondary antibodies (1:1000) for 2 hours, washed, stained with DAPI for 5 min,
935 washed, mounted, and coverslipped with Fluoromount-G (Electron Microscopy
936 Sciences). All incubations were at room temperature. Microscope slides were imaged
937 using a FLUOVIEW FV10i confocal microscope (Olympus). Injection sites and fiber
938 placements were designated on modified Allen Mouse Brain Atlas figures (Lein et al.,
939 2007). Mice were excluded from analyses if fluorescence was not observed at injection
940 sites or if fiber tips were not identified at the intended site.

941

942 **Statistical Analyses of Behavior**

943 Operant behavioral data saved by MEDPC IV was transferred to Excel using
944 MPC2XL. Data were organized in MATLAB and analyzed in Prism (V8.3.0, GraphPad
945 Software, San Diego, CA). Differences between groups and interactions across days for
946 Training were evaluated using Two-Way Repeated Measures ANOVAs. We computed
947 the required sample size for a 90% power level with an alpha of 0.05 by estimating the
948 control (EYFP) group mean would be 10 rewards and the mean experimental (Chr2)
949 group would be 20 rewards with a standard deviation of 5. We utilized a power
950 calculator for continuous outcomes of two independent samples, assuming a normal

951 distribution. The result was 6 samples per group. Each manipulation experiment started
952 with at least 6 mice included in each group (*Sealed Envelope | Power Calculator for*
953 *Continuous Outcome Superiority Trial*, n.d.). In each experiment, each animal within a
954 group served as a biological replicate. These studies did not include technical
955 replicates. Masking was not applied during data acquisition but data analyses were
956 semi-automated in MATLAB and performed blind to condition

957 **Supplemental Methods**

959 **Ex Vivo Electrophysiology**

960 ***Slice preparation:*** Coronal brain slices were prepared from virus injected mice after 3
961 weeks from surgery. Animals were anesthetized with a mixture of ketamine and
962 xylazine (100 mg ketamine and 6 mg xylazine/kg body weight injected ip). Then the
963 mice were transcardially perfused with a sucrose-based solution (see below). After
964 decapitation, the brain was rapidly transferred into a sucrose-based cutting solution
965 bubbled with 95%O₂ and 5% CO₂ and maintained at ~3°C. This solution contained (in
966 mM): sucrose 230; KCl 2.5; MgSO₄ 10; CaCl₂ 0.5; NaH₂PO₄ 1.25; NaHCO₃ 26; glucose
967 10 and pyruvate 1.5. Coronal brain slices (300µm) were prepared using a Leica
968 VT1000S vibratome (Leica Biosystems Inc). Slices were equilibrated with a mixture of
969 oxygenated artificial cerebrospinal fluid (aCSF) and sucrose-based cutting solution at
970 room temperature (24-26°C) for at least 1 hour prior to transfer to the recording
971 chamber. Pyruvate (0.15–0.75 mM) was added to reduce oxidative damage and
972 enhance survival. With this protocol, slices are initially incubated in a mixture of 50%
973 cutting solution with pyruvate and 50% aCSF (in mM): sucrose 115; NaCl 63; KCl 2.5;
974 NaH₂PO₄ 1.25; MgSO₄ 5; CaCl₂ 1.25; MgCl₂ 1; NaHCO₃ 26; glucose 10; and sodium

975 pyruvate 0.75 at 35°C for 30 min and then transferred to a mixture of 10% cutting
976 solution and 90% aCSF (in mM): sucrose 23; NaCl 113.4; KCl 2.5; NaH₂PO₄ 1.25;
977 MgSO₄ 1; CaCl₂ 1.85; MgCl₂ 1.8; NaHCO₃ 26; glucose 10; and sodium pyruvate 0.15 at
978 35°C for 1–4 h prior to recording. The slices were continuously superfused with aCSF at
979 a rate of 2ml/min containing (in mM); NaCl 126, KCl 2.5, NaH₂PO₄ 1.25, NaHCO₃ 26,
980 CaCl₂ 2, MgCl₂ 2 and glucose 10 bubbled with 95% O₂ and 5% CO₂ at room
981 temperature.

982 ***Electrophysiological recordings:*** Brain slices were placed on the stage of an upright,
983 infrared-differential interference contrast microscope (Olympus BX51WI, Olympus).
984 NBM neurons were visualized with a 40 X water-immersion objective by infrared
985 microscopy (COHU 4915 camera, COHU, Inc., Poway, CA). Patch electrodes with a
986 resistance of 4–6 MΩ were pulled with a laser-based micropipette puller (P-2000, Sutter
987 Instrument Company). Signals were recorded with a Multi Clamp 700A amplifier and
988 pClamp10 software (Molecular Devices, Inc., San Jose, CA). The pipette solution
989 contained (in mM) 130 K-gluconate, 2 KCl, 2 MgCl₂, 10 HEPES, 0.5 EGTA, 1 ATP and
990 0.2 GTP (pH=7.3).

991 To examine action potential firing frequency, NBM neurons were recorded in a current
992 clamp configuration after forming a giga-ohm seal. Membrane potentials were clamped
993 at -60 mV by injecting 0–50 pA current through the recording electrode as needed.
994 Cells that maintained steady membrane potentials for at least 5 mins were included in
995 the analysis.

996 ***Optogenetic stimulation ex vivo:*** Channelrhodopsin was activated with a train of light
997 flashes delivered through the 40x microscope objective. The light source was an
998 Olympus x-cite 120Q lamp (Olympus) gated with a TTL controlled shutter (LAMBDA
999 SC, Sutter Instrument). The filter cube contained an HQ480/40x excitation filter, a
1000 Q505lp bypass filter and an HQ535/50m emission filter (Chroma Technology Corp.,
1001 Bellows Falls, VT). The fluorescence illumination intensity delivered at the brain slices
1002 was adjusted to 1-3 mW/mm², measured with a PM100D optical power and energy
1003 meter (Thorlabs Inc., Newton, NJ). In the NBM, cholinergic neurons were identified by
1004 EGFP fluorescence and light flashes were delivered at 1 Hz, 5 Hz, 10 Hz, 15Hz, 20 Hz,
1005 25 Hz, and 30 Hz.

1006 **Cued Self-Stimulation**

1007 After Extinction, responding was reinstated in Training for 2 days. Then mice
1008 underwent a modified Training paradigm where correct nose pokes yielded only laser
1009 stimulation, without Ensure delivery.

1010 **Real Time Place Preference**

1011 An empty, clear mouse cage (29.5 cm x 19 cm x 12.5 cm) had half of its floor
1012 covered in printer paper to provide a distinct floor texture. A video camera was placed
1013 above the cage and was connected to a computer running EthoVision XT (version
1014 10.1.856, Noldus, Wageningen, Netherlands) to track the position of the mouse and
1015 deliver optical stimulation when the mouse was on the laser-paired side (via TTL pulse
1016 to OTPG_4 laser controller (Doric Lenses) connected to the laser; 20 Hz, 25 ms
1017 pulses). Mice were randomly assigned and counterbalanced to receive laser stimulation
1018 only on one side of the cage. Mice were allowed free access to either side for 15 min

1019 during a session. Baseline was established in the absence of optical stimulation on Day
1020 1. Mice then received optical stimulation on Day 2 only when on the laser-paired side.
1021 Data are presented as percent time spent on the laser-paired side.

1022 **Progressive Ratio testing**

1023 In the progressive ratio test, mice were given 60 min to nose poke for Ensure and
1024 2 sec of optical stimulation on a progressive ratio schedule (escalations given below).
1025 Training Day escalation: 1, 2, 2, 2, 2, 3, 3, 3, 3, 3, 5, 5, 5, 5, 5, 8, 8, 8, 8, 8, 8, 11, 11,
1026 11, 11, 11, 11, 15, 15, 15, 15, 15, 15, 22, 22, 22, 22, 22, 33, 33, 33, 33, 33, 44, 44, 44,
1027 44, 44, 55, 66, 77, 88, 99, 133, 166, 199, 255, 313, 399, 499, 599, 777, 900, 1222. Test
1028 Day escalation: 1, 2, 4, 6, 9, 12, 15, 20, 25, 32, 40, 50, 62, 77, 95, 118, 145, 178, 219,
1029 268, 328, 402, 492, 603, 777, 900, 1222.

1030 **Locomotor Activity**

1031 **Optical Stimulation:** Mice were placed in a square box (47 cm x 47 cm x 21 cm) for 20
1032 min with a floor of filter paper that was changed between mice. During the 3rd 5 min bin
1033 of the session, mice received optical stimulation (20 sec on/off, 20 Hz, 25 ms pulses).
1034 Locomotor activity was recorded via overhead camera and analyzed in 5 min bins with
1035 EthoVision.

1036 **Antagonists:** Locomotor data was collected using an Accuscan Instruments
1037 (Columbus, Ohio) behavior monitoring system and software. Mice were individually
1038 tested in empty cages, with bedding and nesting material removed to prevent
1039 obstruction of infrared beams. Mice were injected (i.p.) with saline, mecamlamine (1
1040 mg/kg, Sigma), scopolamine (0.5 mg/kg, Sigma), or mecamlamine+scopolamine (1
1041 mg/kg and 0.5 mg/kg, respectively) 30 min before locomotor testing. Locomotion was

1042 monitored for 20 min using 13 photocells placed 4 cm apart to obtain an ambulatory
1043 activity count, consisting of the number of beam breaks recorded during a period of
1044 ambulatory activity (linear motion rather than quick, repetitive beam breaks associated
1045 with behaviors such as scratching and grooming).

1046 **Light/Dark Box Exploration**

1047 A rectangular box was divided evenly into a light (clear top, illuminated by an 8W
1048 tube light) and dark (black walls, black top) side with a black walled divider in the middle
1049 with a small door. The lid and divider were modified to allow the optical fiber and patch
1050 cord to pass through freely. Mice were placed facing the corner on the light side furthest
1051 from the divider and the latency to crossing to the dark side was measured. The number
1052 of crosses and time spent on each side were measured for 6 min following the initial
1053 cross.

1054

1055 **Acknowledgements**

1056 These studies were supported by grants DA14241, DA037566, MH077681. LW, DT and
1057 PR were supported by NS022061, MH109104 from the National Institutes of Health,
1058 and by the intramural programs of NINDS and NIMH. X-BG was supported by
1059 DA046160. RBC was supported by T32-NS007224. This work was funded in part by the
1060 State of Connecticut, Department of Mental Health and Addiction Services, but this
1061 publication does not express the views of the Department of Mental Health and
1062 Addiction Services or the State of Connecticut. The views and opinions expressed are
1063 those of the authors. We thank Samantha Sheppard for the use of her mouse illustration
1064 and animal care assistance and Nadia Jordan-Spasov for genotyping and laboratory
1065 help. Li Jiang performed the *ex vivo* current clamp recordings. Angela Lee and
1066 Wenliang Zhou provided helpful input into experimental planning. Colin Bond, Marcelo
1067 Dietrich, Usman Farooq, Onur Iyilikci, Sharif Kronemer, Matthew Pettus, and Zach
1068 Saltzman provided insightful discussion and assistance with analysis and figure design.
1069 Ralph DiLeone, Stephanie Groman, Hyojung Seo, and Jane Taylor offered helpful
1070 discussion about experimental design and analysis. The support teams at Doric Lenses
1071 (Alex Côté and Olivier Dupont-Therrien) and Tucker-Davis Technologies provided
1072 discussion, analysis support, and MATLAB code assistance.

1073

1074 **References**

- 1075 Aitta-aho, T., Hay, Y. A., Phillips, B. U., Saksida, L. M., Bussey, T. J., Paulsen, O., & Apergis-Schoute, J.
1076 (2018). Basal Forebrain and Brainstem Cholinergic Neurons Differentially Impact Amygdala
1077 Circuits and Learning-Related Behavior. *Current Biology*, 28(16), 2557-2569.e4.
1078 <https://doi.org/10.1016/j.cub.2018.06.064>
- 1079 Ambroggi, F., Ishikawa, A., Fields, H. L., & Nicola, S. M. (2008). Basolateral Amygdala Neurons Facilitate
1080 Reward-Seeking Behavior by Exciting Nucleus Accumbens Neurons. *Neuron*, 59(4), 648–661.
1081 <https://doi.org/10.1016/j.neuron.2008.07.004>
- 1082 Barnett, L. M., Hughes, T. E., & Drobizhev, M. (2017). Deciphering the molecular mechanism responsible
1083 for GCaMP6m's Ca²⁺-dependent change in fluorescence. *PLOS ONE*, 12(2), e0170934.
1084 <https://doi.org/10.1371/journal.pone.0170934>
- 1085 Baxter, M. G., & Murray, E. A. (2002). The amygdala and reward. *Nature Reviews Neuroscience*, 3(7),
1086 563. <https://doi.org/10.1038/nrn875>
- 1087 Baysinger, A. N., Kent, B. A., & Brown, T. H. (2012). Muscarinic Receptors in Amygdala Control Trace Fear
1088 Conditioning. *PLOS ONE*, 7(9), e45720. <https://doi.org/10.1371/journal.pone.0045720>
- 1089 Butler, R. K., Sharko, A. C., Oliver, E. M., Brito-Vargas, P., Kaigler, K. F., Fadel, J. R., & Wilson, M. A.
1090 (2011). Activation of phenotypically-distinct neuronal subpopulations of the rat amygdala
1091 following exposure to predator odor. *Neuroscience*, 175, 133–144.
1092 <https://doi.org/10.1016/j.neuroscience.2010.12.001>
- 1093 Cador, M., Robbins, T. W., & Everitt, B. J. (1989). Involvement of the amygdala in stimulus-reward
1094 associations: Interaction with the ventral striatum. *Neuroscience*, 30(1), 77–86.
- 1095 Casanova, E., Fehsenfeld, S., Mantamadiotis, T., Lemberger, T., Greiner, E., Stewart, A. F., & Schütz, G.
1096 (2001). A CamKII α iCre BAC allows brain-specific gene inactivation. *Genesis*, 31(1), 37–42.
1097 <https://doi.org/10.1002/gene.1078>

1098 Cassidy, R. M., Lu, Y., Jere, M., Tian, J.-B., Xu, Y., Mangieri, L. R., Felix-Okoroji, B., Selever, J., Xu, Y.,
1099 Arenkiel, B. R., & Tong, Q. (2019). A lateral hypothalamus to basal forebrain neurocircuit
1100 promotes feeding by suppressing responses to anxiogenic environmental cues. *Science*
1101 *Advances*, 5(3), eaav1640. <https://doi.org/10.1126/sciadv.aav1640>

1102 Chen, T.-W., Wardill, T. J., Sun, Y., Pulver, S. R., Renninger, S. L., Baohan, A., Schreiter, E. R., Kerr, R. A.,
1103 Orger, M. B., Jayaraman, V., Looger, L. L., Svoboda, K., & Kim, D. S. (2013). Ultrasensitive
1104 fluorescent proteins for imaging neuronal activity. *Nature*, 499(7458), 295–300.
1105 <https://doi.org/10.1038/nature12354>

1106 Chubykin, A. A., Roach, E. B., Bear, M. F., & Shuler, M. G. H. (2013). A Cholinergic Mechanism for Reward
1107 Timing within Primary Visual Cortex. *Neuron*, 77(4), 723–735.
1108 <https://doi.org/10.1016/j.neuron.2012.12.039>

1109 Dana, H., Mohar, B., Sun, Y., Narayan, S., Gordus, A., Hasseman, J. P., Tsegaye, G., Holt, G. T., Hu, A.,
1110 Walpita, D., Patel, R., Macklin, J. J., Bargmann, C. I., Ahrens, M. B., Schreiter, E. R., Jayaraman, V.,
1111 Looger, L. L., Svoboda, K., & Kim, D. S. (2016). Sensitive red protein calcium indicators for
1112 imaging neural activity. *eLife*, 5, e12727. <https://doi.org/10.7554/eLife.12727>

1113 Dana, H., Sun, Y., Mohar, B., Hulse, B. K., Kerlin, A. M., Hasseman, J. P., Tsegaye, G., Tsang, A., Wong, A.,
1114 Patel, R., Macklin, J. J., Chen, Y., Konnerth, A., Jayaraman, V., Looger, L. L., Schreiter, E. R.,
1115 Svoboda, K., & Kim, D. S. (2019). High-performance calcium sensors for imaging activity in
1116 neuronal populations and microcompartments. *Nature Methods*, 16(7), 649–657.
1117 <https://doi.org/10.1038/s41592-019-0435-6>

1118 Egorov, A. V., Unsicker, K., & Halbach, O. V. B. und. (2006). Muscarinic control of graded persistent
1119 activity in lateral amygdala neurons. *European Journal of Neuroscience*, 24(11), 3183–3194.
1120 <https://doi.org/10.1111/j.1460-9568.2006.05200.x>

1121 Felix-Ortiz, A. C., & Tye, K. M. (2014). Amygdala Inputs to the Ventral Hippocampus Bidirectionally
1122 Modulate Social Behavior. *Journal of Neuroscience*, *34*(2), 586–595.
1123 <https://doi.org/10.1523/JNEUROSCI.4257-13.2014>

1124 Gu, Z., & Yakel, J. L. (2011). Timing-Dependent Septal Cholinergic Induction of Dynamic Hippocampal
1125 Synaptic Plasticity. *Neuron*, *71*(1), 155–165. <https://doi.org/10.1016/j.neuron.2011.04.026>

1126 Guo, W., Robert, B., & Polley, D. B. (2019). The Cholinergic Basal Forebrain Links Auditory Stimuli with
1127 Delayed Reinforcement to Support Learning. *Neuron*, *103*(6), 1164–1177.e6.
1128 <https://doi.org/10.1016/j.neuron.2019.06.024>

1129 Hangya, B., Ranade, S. P., Lorenc, M., & Kepecs, A. (2015). Central Cholinergic Neurons Are Rapidly
1130 Recruited by Reinforcement Feedback. *Cell*, *162*(5), 1155–1168.
1131 <https://doi.org/10.1016/j.cell.2015.07.057>

1132 Janak, P. H., & Tye, K. M. (2015). From circuits to behaviour in the amygdala. *Nature*, *517*(7534), 284–
1133 292. <https://doi.org/10.1038/nature14188>

1134 Jean-Richard-dit-Bressel, P., Clifford, C. W. G., & McNally, G. P. (2020). Analyzing Event-Related
1135 Transients: Confidence Intervals, Permutation Tests, and Consecutive Thresholds. *Frontiers in*
1136 *Molecular Neuroscience*, *13*, 14. <https://doi.org/10.3389/fnmol.2020.00014>

1137 Jiang, L., Kundu, S., Lederman, J. D., López-Hernández, G. Y., Ballinger, E. C., Wang, S., Talmage, D. A., &
1138 Role, L. W. (2016). Cholinergic Signaling Controls Conditioned Fear Behaviors and Enhances
1139 Plasticity of Cortical-Amygdala Circuits. *Neuron*, *90*(5), 1057–1070.
1140 <https://doi.org/10.1016/j.neuron.2016.04.028>

1141 Jing, M., Li, Y., Zeng, J., Huang, P., Skirzewski, M., Kljakic, O., Peng, W., Qian, T., Tan, K., Wu, R., Zhang, S.,
1142 Pan, S., Xu, M., Li, H., Saksida, L. M., Prado, V. F., Bussey, T., Prado, M. A. M., Chen, L., ... Li, Y.
1143 (2019). *An optimized acetylcholine sensor for monitoring in vivo cholinergic activity* [Preprint].
1144 Neuroscience. <https://doi.org/10.1101/861690>

1145 Jing, M., Zhang, P., Wang, G., Feng, J., Mesik, L., Zeng, J., Jiang, H., Wang, S., Looby, J. C., Guagliardo, N.
1146 A., Langma, L. W., Lu, J., Zuo, Y., Talmage, D. A., Role, L. W., Barrett, P. Q., Zhang, L. I., Luo, M.,
1147 Song, Y., ... Li, Y. (2018). A genetically encoded fluorescent acetylcholine indicator for *in vitro* and
1148 *in vivo* studies. *Nature Biotechnology*, *36*(8), 726–737. <https://doi.org/10.1038/nbt.4184>

1149 Kim, C. K., Yang, S. J., Pichamoorthy, N., Young, N. P., Kauvar, I., Jennings, J. H., Lerner, T. N., Berndt, A.,
1150 Lee, S. Y., Ramakrishnan, C., Davidson, T. J., Inoue, M., Bito, H., & Deisseroth, K. (2016).
1151 Simultaneous fast measurement of circuit dynamics at multiple sites across the mammalian
1152 brain. *Nature Methods*, *13*(4), 325–328. <https://doi.org/10.1038/nmeth.3770>

1153 Kim, J., Pignatelli, M., Xu, S., Itohara, S., & Tonegawa, S. (2016). Antagonistic negative and positive
1154 neurons of the basolateral amygdala. *Nature Neuroscience*. <https://doi.org/10.1038/nn.4414>

1155 LeDoux, J. E., Cicchetti, P., Xagoraris, A., & Romanski, L. M. (1990). The lateral amygdaloid nucleus:
1156 Sensory interface of the amygdala in fear conditioning. *Journal of Neuroscience*, *10*(4), 1062–
1157 1069.

1158 Lein, E. S., Hawrylycz, M. J., Ao, N., Ayres, M., Bensinger, A., Bernard, A., Boe, A. F., Boguski, M. S.,
1159 Brockway, K. S., Byrnes, E. J., Chen, L., Chen, L., Chen, T.-M., Chi Chin, M., Chong, J., Crook, B. E.,
1160 Czaplinska, A., Dang, C. N., Datta, S., ... Jones, A. R. (2007). Genome-wide atlas of gene
1161 expression in the adult mouse brain. *Nature*, *445*(7124), 168–176.
1162 <https://doi.org/10.1038/nature05453>

1163 Liu, C.-H., Coleman, J. E., Davoudi, H., Zhang, K., & Hussain Shuler, M. G. (2015). Selective Activation of a
1164 Putative Reinforcement Signal Conditions Cued Interval Timing in Primary Visual Cortex. *Current*
1165 *Biology*, *25*(12), 1551–1561. <https://doi.org/10.1016/j.cub.2015.04.028>

1166 Lutas, A., Kucukdereli, H., Alturkistani, O., Carty, C., Sugden, A. U., Fernando, K., Diaz, V., Flores-
1167 Maldonado, V., & Andermann, M. L. (2019). State-specific gating of salient cues by midbrain

1168 dopaminergic input to basal amygdala. *Nature Neuroscience*, 22(11), 1820–1833.

1169 <https://doi.org/10.1038/s41593-019-0506-0>

1170 Ma, S., Hangya, B., Leonard, C. S., Wisden, W., & Gundlach, A. L. (2018). Dual-transmitter systems
1171 regulating arousal, attention, learning and memory. *Neuroscience & Biobehavioral Reviews*, 85,
1172 21–33. <https://doi.org/10.1016/j.neubiorev.2017.07.009>

1173 Marvin, J. S., Borghuis, B. G., Tian, L., Cichon, J., Harnett, M. T., Akerboom, J., Gordus, A., Renninger, S.
1174 L., Chen, T.-W., Bargmann, C. I., Orger, M. B., Schreiter, E. R., Demb, J. B., Gan, W.-B., Hires, S. A.,
1175 & Looger, L. L. (2013). An optimized fluorescent probe for visualizing glutamate
1176 neurotransmission. *Nature Methods*, 10(2), 162–170. <https://doi.org/10.1038/nmeth.2333>

1177 Marvin, J. S., Scholl, B., Wilson, D. E., Podgorski, K., Kazemipour, A., Müller, J. A., Schoch, S., Quiroz, F. J.
1178 U., Rebola, N., Bao, H., Little, J. P., Tkachuk, A. N., Cai, E., Hantman, A. W., Wang, S. S.-H.,
1179 DePiero, V. J., Borghuis, B. G., Chapman, E. R., Dietrich, D., ... Looger, L. L. (2018). Stability,
1180 affinity, and chromatic variants of the glutamate sensor iGluSnFR. *Nature Methods*, 15(11), 936–
1181 939. <https://doi.org/10.1038/s41592-018-0171-3>

1182 Marvin, J. S., Shimoda, Y., Magloire, V., Leite, M., Kawashima, T., Jensen, T. P., Kolb, I., Knott, E. L.,
1183 Novak, O., Podgorski, K., Leidenheimer, N. J., Rusakov, D. A., Ahrens, M. B., Kullmann, D. M., &
1184 Looger, L. L. (2019). A genetically encoded fluorescent sensor for in vivo imaging of GABA.
1185 *Nature Methods*, 16(8), 763–770. <https://doi.org/10.1038/s41592-019-0471-2>

1186 McDonald, A. J. (1992). Projection neurons of the basolateral amygdala: A correlative Golgi and
1187 retrograde tract tracing study. *Brain Research Bulletin*, 28(2), 179–185.
1188 [https://doi.org/10.1016/0361-9230\(92\)90177-Y](https://doi.org/10.1016/0361-9230(92)90177-Y)

1189 McIntyre, C. K., Ragozzino, M. E., & Gold, P. E. (1998). Intra-amygdala infusions of scopolamine impair
1190 performance on a conditioned place preference task but not a spatial radial maze task.
1191 *Behavioural Brain Research*, 95(2), 219–226. [https://doi.org/10.1016/S0166-4328\(97\)00161-7](https://doi.org/10.1016/S0166-4328(97)00161-7)

1192 McKernan, M. G., & Shinnick-Gallagher, P. (1997). Fear conditioning induces a lasting potentiation of
1193 synaptic currents in vitro. *Nature*, *390*(6660), 607–611. <https://doi.org/10.1038/37605>

1194 Mineur, Y. S., Somenzi, O., & Picciotto, M. R. (2007). Cytisine, a partial agonist of high-affinity nicotinic
1195 acetylcholine receptors, has antidepressant-like properties in male C57BL/6J mice.
1196 *Neuropharmacology*, *52*(5), 1256–1262. <https://doi.org/10.1016/j.neuropharm.2007.01.006>

1197 Parikh, V., Kozak, R., Martinez, V., & Sarter, M. (2007). Prefrontal Acetylcholine Release Controls Cue
1198 Detection on Multiple Timescales. *Neuron*, *56*(1), 141–154.
1199 <https://doi.org/10.1016/j.neuron.2007.08.025>

1200 Picciotto, M. R., Higley, M. J., & Mineur, Y. S. (2012). Acetylcholine as a Neuromodulator: Cholinergic
1201 Signaling Shapes Nervous System Function and Behavior. *Neuron*, *76*(1), 116–129.
1202 <https://doi.org/10.1016/j.neuron.2012.08.036>

1203 Pisansky, M. T., Lefevre, E. M., Retzlaff, C. L., Trieu, B. H., Leipold, D. W., & Rothwell, P. E. (2019).
1204 Nucleus Accumbens Fast-Spiking Interneurons Constrain Impulsive Action. *Biological Psychiatry*,
1205 *86*(11), 836–847. <https://doi.org/10.1016/j.biopsych.2019.07.002>

1206 Poulin, A. N., Guerci, A., Mestikawy, S. E., & Semba, K. (2006). Vesicular glutamate transporter 3
1207 immunoreactivity is present in cholinergic basal forebrain neurons projecting to the basolateral
1208 amygdala in rat. *Journal of Comparative Neurology*, *498*(5), 690–711.
1209 <https://doi.org/10.1002/cne.21081>

1210 Rao, Y., Lu, M., Ge, F., Marsh, D. J., Qian, S., Wang, A. H., Picciotto, M. R., & Gao, X.-B. (2008). Regulation
1211 of Synaptic Efficacy in Hypocretin/Orexin-Containing Neurons by Melanin Concentrating
1212 Hormone in the Lateral Hypothalamus. *The Journal of Neuroscience*, *28*(37), 9101–9110.
1213 <https://doi.org/10.1523/JNEUROSCI.1766-08.2008>

1214 Rogan, M. T., Stäubli, U. V., & LeDoux, J. E. (1997). Fear conditioning induces associative long-term
1215 potentiation in the amygdala. *Nature*, *390*(6660), 604–607. <https://doi.org/10.1038/37601>

1216 Sanghera, M. K., Rolls, E. T., & Roper-Hall, A. (1979). Visual responses of neurons in the dorsolateral
1217 amygdala of the alert monkey. *Experimental Neurology*, *63*(3), 610–626.
1218 [https://doi.org/10.1016/0014-4886\(79\)90175-4](https://doi.org/10.1016/0014-4886(79)90175-4)

1219 Sarter, M., & Lustig, C. (2020). Forebrain Cholinergic Signaling: Wired and Phasic, Not Tonic, and Causing
1220 Behavior. *Journal of Neuroscience*, *40*(4), 712–719. [https://doi.org/10.1523/JNEUROSCI.1305-](https://doi.org/10.1523/JNEUROSCI.1305-19.2019)
1221 [19.2019](https://doi.org/10.1523/JNEUROSCI.1305-19.2019)

1222 Saunders, A., Granger, A. J., & Sabatini, B. L. (2015). Corelease of acetylcholine and GABA from
1223 cholinergic forebrain neurons. *ELife*, *4*, e06412. <https://doi.org/10.7554/eLife.06412>

1224 Schoenbaum, G., Chiba, A. A., & Gallagher, M. (1998). Orbitofrontal cortex and basolateral amygdala
1225 encode expected outcomes during learning. *Nature Neuroscience*, *1*(2), 155–159.
1226 <https://doi.org/10.1038/407>

1227 Schultz, W. (1998). Predictive Reward Signal of Dopamine Neurons. *Journal of Neurophysiology*, *80*(1),
1228 1–27.

1229 Schultz, W., Dayan, P., & Montague, P. R. (1997). A Neural Substrate of Prediction and Reward. *Science*,
1230 *275*(5306), 1593–1599. <https://doi.org/10.1126/science.275.5306.1593>

1231 *Sealed Envelope | Power calculator for continuous outcome superiority trial.* (n.d.). Retrieved October
1232 10, 2016, from <https://www.sealedenvelope.com/power/continuous-superiority/>

1233 Sengupta, A., Yau, J. O. Y., Jean-Richard-Dit-Bressel, P., Liu, Y., Millan, E. Z., Power, J. M., & McNally, G. P.
1234 (2018). Basolateral Amygdala Neurons Maintain Aversive Emotional Salience. *Journal of*
1235 *Neuroscience*, *38*(12), 3001–3012. <https://doi.org/10.1523/JNEUROSCI.2460-17.2017>

1236 Sturgill, J. F., Hegedus, P., Li, S. J., Chevy, Q., Siebels, A., Jing, M., Li, Y., Hangya, B., & Kepecs, A. (2020).
1237 Basal forebrain-derived acetylcholine encodes valence-free reinforcement prediction error.
1238 *BioRxiv*, 2020.02.17.953141. <https://doi.org/10.1101/2020.02.17.953141>

1239 Sych, Y., Chernysheva, M., Sumanovski, L. T., & Helmchen, F. (2019). High-density multi-fiber
1240 photometry for studying large-scale brain circuit dynamics. *Nature Methods*, 16(6), 553–560.
1241 <https://doi.org/10.1038/s41592-019-0400-4>

1242 Tye, K. M., & Janak, P. H. (2007). Amygdala Neurons Differentially Encode Motivation and
1243 Reinforcement. *Journal of Neuroscience*, 27(15), 3937–3945.
1244 <https://doi.org/10.1523/JNEUROSCI.5281-06.2007>

1245 Tye, K. M., Prakash, R., Kim, S.-Y., Fenno, L. E., Grosenick, L., Zarabi, H., Thompson, K. R., Gradinaru, V.,
1246 Ramakrishnan, C., & Deisseroth, K. (2011). Amygdala circuitry mediating reversible and
1247 bidirectional control of anxiety. *Nature*, 471(7338), 358–362.
1248 <https://doi.org/10.1038/nature09820>

1249 Tye, K. M., Stuber, G. D., de Ridder, B., Bonci, A., & Janak, P. H. (2008). Rapid strengthening of thalamo-
1250 amygdala synapses mediates cue–reward learning. *Nature*, 453(7199), 1253–1257.
1251 <https://doi.org/10.1038/nature06963>

1252 Unal, C. T., Pare, D., & Zaborszky, L. (2015). Impact of Basal Forebrain Cholinergic Inputs on Basolateral
1253 Amygdala Neurons. *Journal of Neuroscience*, 35(2), 853–863.
1254 <https://doi.org/10.1523/JNEUROSCI.2706-14.2015>

1255 Wohleb, E. S., Wu, M., Gerhard, D. M., Taylor, S. R., Picciotto, M. R., Alreja, M., & Duman, R. S. (2016).
1256 GABA interneurons mediate the rapid antidepressant-like effects of scopolamine. *The Journal of*
1257 *Clinical Investigation*, 126(7), 2482–2494. <https://doi.org/10.1172/JCI85033>

1258 Woolf, N. J. (1991). Cholinergic systems in mammalian brain and spinal cord. *Progress in Neurobiology*,
1259 37(6), 475–524. [https://doi.org/10.1016/0301-0082\(91\)90006-M](https://doi.org/10.1016/0301-0082(91)90006-M)

1260 Zaborszky, L., van den Pol, A., & Gyengesi, E. (2012). The Basal Forebrain Cholinergic Projection System
1261 in Mice. In *The Mouse Nervous System* (pp. 684–718). Elsevier. [https://doi.org/10.1016/B978-0-](https://doi.org/10.1016/B978-0-12-369497-3.10028-7)
1262 [12-369497-3.10028-7](https://doi.org/10.1016/B978-0-12-369497-3.10028-7)

1263 Zhong, W., Li, Y., Feng, Q., & Luo, M. (2017). Learning and Stress Shape the Reward Response Patterns
1264 of Serotonin Neurons. *The Journal of Neuroscience*, 37(37), 8863–8875.
1265 <https://doi.org/10.1523/JNEUROSCI.1181-17.2017>

1266

1267

1268

1269 **Figure 1**

1270 **Experimental timeline and cue-reward learning paradigm.**

1271 A) Experimental timeline. Mice began food restriction 7 days after surgery and were
1272 maintained at 85% free-feeding body weight for the duration of the experiment. After 7
1273 days of handling, 5-6 days of operant familiarization prepared the mice for the cue-
1274 reward learning task (Pre-Training through Extinction).

1275 B) Behavioral chamber setup. Mice were placed in modular test chambers that included
1276 two nose poke ports on the left wall (Active and Inactive) and the Reward Receptacle on
1277 the right wall. A tone generator and timeout light were placed outside the modular test
1278 chamber. For fiber photometry (FP) and optical stimulation (Laser) experiments, mice
1279 were tethered to a patch cord(s).

1280 C-D) Details of the Cue-Reward Learning Paradigm C) In Pre-Training, an auditory tone
1281 was presented on a variable interval 30 schedule (VI30), during which an active nose
1282 poke yielded Ensure reward delivery but there was no consequence for incorrect nose
1283 pokes (active nose pokes not during tone). D) Training was identical to Pre-Training,
1284 except incorrect nose pokes resulted in a 5 sec timeout, signaled by timeout light
1285 illumination, followed by a restarting of the intertrial interval (ITI).

1286

1287 **Figure 2**

1288 **Basolateral amygdala (BLA) ACh signaling aligns with salient events during**

1289 **reward learning.**

1290 A) Diagram and example of injection and fiber placement sites in the BLA for recording

1291 from mice expressing a fluorescent acetylcholine sensor (ACh3.0). Left: Diagram of BLA

1292 ACh3.0 injection and fiber tip placement. Right: Representative coronal brain slice with

1293 fiber tip and ACh3.0 expression. Blue: DAPI, Green: ACh3.0. White dashed line: BLA

1294 outline. Grey dashed rectangle: fiber track. Scale = 500 μm . Individual fiber placements

1295 are shown in **Figure 2-figure supplement 1A**.

1296 B) Behavioral responding of mice expressing ACh3.0 in BLA. Individual mice acquired

1297 the task at different rates as measured by rewards earned. Horizontal white line:

1298 acquisition threshold, when a mouse began to earn 20 rewards consistently in Training.

1299 Incorrect nose pokes shown in **Figure 2-figure supplement 2A**. Pre-Training (PT): blue

1300 shaded area, Training: pink shaded area, Extinction (Ext): orange shaded area.

1301 C) Fluorescence traces from BLA of ACh3.0-expressing mouse. A significant increase

1302 in fluorescence representing BLA ACh release consistently coincided with correct

1303 (green line) but not incorrect (grey line) nose pokes on last day of PT (data are shown

1304 from Mouse 1). Mean Z-scored ($Z\% \Delta F/F_0$) overlaid on bootstrapped 99% confidence

1305 intervals (99% bCI's). Shaded significance bars under traces represent time points

1306 where 99% bCI's do not contain 0 for at least 0.5 sec. Correct: n = 24; downsampled

1307 incorrect: n = 24 of 58. Traces of signal and reference channels ($\% \Delta F/F_0$) during nose

1308 pokes are shown in **Figure 2-figure supplement 1B-C**. Incorrect nose pokes on last

1309 day of PT vs Training Day 1 shown in **Figure 2-figure supplement 2B**.

1310 D) Heatmap of BLA ACh signaling in Mouse 1 across all training phases, aligned to tone
1311 onset (Tone), correct nose poke (NP), and receptacle entry (Rec). Each row is the
1312 average of rewarded trials across a training session. White dashed horizontal line: first
1313 Training day earning 10 rewards. Horizontal white line: acquisition threshold, when a
1314 mouse began to earn 20 rewards consistently in Training. Black horizontal lines:
1315 divisions between training phases. Black vertical lines: divisions between breaks in time
1316 to allow for variable latencies in tone onset, correct nose poke, and receptacle entry
1317 (reward retrieval). bCI plot for Mouse 1 in **Figure 2-figure supplement 1G**. Individual
1318 heatmaps for mice 2-4 in **Figure 2-figure supplement 1D-F**. Incorrect nose pokes
1319 heatmaps for individual mice shown in **Figure 2-figure supplement 2C-F**.

1320 E) Heatmap of BLA ACh signaling averaged across mice. Signal aligned as in D) with a
1321 selection of data from key days in the behavioral paradigm shown. From bottom to top:
1322 PT Day 1, PT Day 5, Early Training Day, First Training day earning 10 rewards (white
1323 dashed horizontal line), Mid Training Day, Acquisition Day (white horizontal line), Last
1324 Training Day, Last Extinction Day. Black horizontal lines: divisions between training
1325 phases. Black vertical lines: divisions between breaks in time to allow for variable
1326 latencies in tone onset, correct nose poke, and receptacle entry. bCI plot for cohort
1327 averaged data in **Figure 2-figure supplement 1H**. Incorrect nose poke heatmap and
1328 bCI plot averaged across mice shown in **Figure 2-figure supplement 2G-H**

1329 F) Diagram and example of Nucleus Basalis of Mynert (NBM)-BLA terminal fiber
1330 recordings. Left: DIO-GCaMP7s was injected in the NBM of ChAT-IRES-Cre mice,
1331 individual injection sites are shown in **Figure 2-figure supplement 5A**. Representative
1332 coronal brain slice showing GCaMP7s expression. White dashed lines: internal capsule

1333 and globus pallidus outlines. Blue: DAPI, Green: GCaMP7s, Red: ChAT. Scale = 500
1334 μm ; separate channels shown in **Figure 2-figure supplement 5B**. Right: An optical
1335 fiber was implanted above the ipsilateral BLA, individual fiber placements are shown in
1336 **Figure 2-figure supplement 5A**. Representative coronal brain slice showing GCaMP7
1337 expression and fiber tip placement. White dashed line: BLA outline. Grey dashed
1338 rectangle: fiber tract. Blue: DAPI, Green: GCaMP7s, Red: ChAT. Scale = 500 μm ;
1339 separate channels shown in **Figure 2-figure supplement 5C**.

1340 G) Behavioral responding of mice during NBM-BLA terminal fiber recordings. Individual
1341 mice acquired the task at different rates as measured by rewards earned. White
1342 horizontal line: acquisition threshold, when a mouse began to earn 20 rewards
1343 consistently in Training. Incorrect nose pokes shown in **Figure 2-figure supplement**
1344 **6A**.

1345 H) NBM-BLA terminal fiber activity is similar to ACh3.0 recordings. NBM-BLA terminal
1346 fiber activity significantly increased with correct (green line) but not incorrect (grey line)
1347 nose pokes on last day of PT (data shown for Mouse 1). Mean $Z\% \Delta F/F_0$ overlaid on
1348 bootstrapped 99% confidence intervals (99% bCI's). Shaded significance bars under
1349 traces represent time points where 99% bCI's do not contain 0 for at least 0.5 sec.
1350 Correct: $n = 42$; downsampled incorrect: $n = 42$ of 101. Signal and reference channels
1351 ($\% \Delta F/F_0$) during nose pokes are shown in **Figure 2-figure supplement 5D-E**. Incorrect
1352 nose pokes on last day of PT vs Training Day 1 shown in **Figure 2-figure supplement**
1353 **6B**. See **Figure 2-figure supplement 9A-H** for simultaneous ACh3.0 and NBM-BLA
1354 terminal fiber recordings.

1355 I) Heatmap of NBM-BLA terminal fiber activity in Mouse 1 across all training phases,
1356 aligned to tone onset (Tone), correct nose poke (NP), and receptacle entry (Rec). Each
1357 row is the average of rewarded trials across a training session. Horizontal white line:
1358 acquisition threshold, when a mouse began to earn 20 rewards consistently in Training.
1359 Black horizontal lines: divisions between training phases. Black vertical lines: divisions
1360 between breaks in time to allow for variable latencies in tone onset, correct nose poke,
1361 and receptacle entry (reward retrieval). Blanks in the heatmaps indicate time bins added
1362 for alignment. bCI plot for Mouse 1 in **Figure 2-figure supplement 7F**. Mouse 2
1363 individual heatmap shown in **Figure 2-figure supplement 5F**. Incorrect nose pokes
1364 heatmaps for individual mice shown in **Figure 2-figure supplement 6C-D**.

1365 J) Heatmap of NBM-BLA terminal fiber activity averaged across mice. Signal aligned as
1366 in D-E) with a selection of key days shown, from bottom to top: PT Day 1, PT Day 4,
1367 Early Training, Acquisition Day (white horizontal line), Last Training Day, Last Extinction
1368 Day. Black horizontal lines: divisions between training phases. Black vertical lines:
1369 divisions between breaks in time to allow for variable latencies in tone onset, correct
1370 nose poke, and receptacle entry (reward retrieval). bCI plot for cohort averaged data in
1371 **Figure 2-figure supplement 7G**. Incorrect nose poke heatmap and bCI plot averaged
1372 across mice shown in **Figure 2-figure supplement 6E + 8E**.

1373

1374 **Figure 3**

1375 **BLA CaMKII α neuron activity aligns to reward retrieval and cue-reward learning.**

1376 A) Diagram and example of injection and fiber placement sites in the BLA for recording

1377 from CaMKII α -Cre mice expressing a fluorescent calcium indicator (DIO-GCaMP6s).

1378 Left: Diagram of injection and fiber placement. Right: Representative coronal brain slice

1379 with fiber tip and GCaMP6s expression. White dashed line: BLA outline. Grey dashed

1380 rectangle: fiber tract. Blue: DAPI, Green: GCaMP6s. Scale 500 μ m. Individual fiber

1381 placements are shown in **Figure 3-figure supplement 1A**.

1382 B) Fluorescence traces from BLA of GCaMP6s-expressing CaMKII α -Cre mice. During

1383 the last day PT, (data shown for Mouse 1) correct nose pokes (green line) were

1384 followed by a modest, but significant rise in BLA CaMKII α cell activity that increased

1385 steeply following receptacle entry (**Figure 3-figure supplement 1B**) while incorrect

1386 nose pokes (grey line) were followed by a modest decrease in activity. Mean $Z\% \Delta F/F_0$

1387 overlaid on bootstrapped 99% confidence intervals (99% bCI's). Shaded significance

1388 bars under traces represent time points where 99% bCI's do not contain 0 for at least

1389 0.5 sec. Correct: n = 44; downsampled incorrect: n = 44 of 141. Signal and reference

1390 channels ($\% \Delta F/F_0$) during nose pokes are shown in **Figure 3-figure supplement 1C-**

1391 **D**. Incorrect nose pokes on last day of PT vs Training Day 1 shown in **Figure 3-figure**

1392 **supplement 2B**.

1393 C) Behavioral responding of CaMKII α -Cre mice expressing GCaMP6s in BLA. Individual

1394 mice acquired the task at different rates as measured by rewards earned. Horizontal

1395 white line: acquisition threshold, when a mouse began to earn 20 rewards consistently

1396 in Training. Incorrect nose pokes shown in **Figure 3-figure supplement 2A**.

1397 D) Heatmap of BLA CaMKII α cell activity (Mouse 1) across all training phases, aligned
1398 to tone onset (Tone), correct nose poke (NP), and receptacle entry (Rec). Each row is
1399 the average of rewarded trials across a training session. White horizontal line: Day
1400 acquisition threshold met, as determined by rewards earned. Black horizontal lines:
1401 divisions between training phases. Black vertical lines: divisions between breaks in time
1402 to allow for variable latencies in tone onset, correct nose poke, and receptacle entry.
1403 Blanks in the heatmaps indicate time bins added for alignment. bCI plot for Mouse 1 in
1404 **Figure 3-figure supplement 1G.** Individual heatmaps for mice 2-3 in **Figure 3-figure**
1405 **supplement 1E-F.** Incorrect nose pokes heatmaps for individual mice shown in **Figure**
1406 **3-figure supplement 2C-E.**

1407 E) Heatmap of BLA CaMKII α cell activity averaged across mice. Signal aligned as in D)
1408 with a selection of key days shown, from bottom to top: PT Day 1, PT Day 4, Early
1409 Training Day, Acquisition Day (white horizontal line), Last Extinction Day. Black
1410 horizontal lines: divisions between training phases. Black vertical lines: divisions
1411 between breaks in time to allow for variable latencies in tone onset, correct nose poke,
1412 and receptacle entry. bCI plot for cohort averaged data in **Figure 3-figure supplement**
1413 **1H.** Incorrect nose poke heatmaps averaged across mice shown in **Figure 3-figure**
1414 **supplement 2F.**

1415

1416

1417 **Figure 4**
1418 **Stimulation of cholinergic terminal fibers in the BLA enhances cue-reward**
1419 **learning.**

1420 A) Schematic of optical stimulation of ChAT⁺ terminal fibers projecting to the BLA. Left:
1421 Bilateral AAV injection into the NBM of ChAT-IRES-Cre mice to gain optical control over
1422 ChAT⁺ NBM cells and representative coronal brain slice showing ChR2-EYFP
1423 expression. White dashed lines: internal capsule and globus pallidus outlines. Blue:
1424 DAPI, red: ChAT, green: ChR2-EYFP. Scale: 500 μ m, individual injection sites shown in
1425 **Figure 4-figure supplement 1A** and separate channels shown in **Figure 4-figure**
1426 **supplement 1B.** Right: Bilateral optical fiber implantation above BLA to stimulate BLA-
1427 projecting ChAT⁺ NBM cells. Representative coronal brain slice showing ChR2-EYFP
1428 expression and fiber tip placement. Grey dashed rectangle: fiber tract. White dashed:
1429 BLA outline. Blue: DAPI, red: ChAT, green: ChR2-EYFP. Scale: 500 μ m, individual fiber
1430 tip placements shown in **Figure 4-figure supplement 1C** and separate channels shown
1431 in **Figure 4-figure supplement 1D.** Injection sites and fiber tip placements for males
1432 from **Figure 4-figure supplement 3C-F** shown in **Figure 4-figure supplement 4A-B.**

1433 B) Optical stimulation validation via local field potential recordings. Extracellular
1434 recording of action potentials induced by optical stimulation of ChAT⁺ NBM cells
1435 expressing ChR2. Arrows indicate 60 ms laser pulse.

1436 C-D) Details of the Cue-Reward Learning Paradigm C) During Pre-Training, auditory
1437 tones were presented on a variable interval 30 schedule (VI30), during which an active
1438 nose poke (correct) yielded Ensure reward delivery and 2 sec of optical stimulation but
1439 there was no consequence for incorrect nose pokes (active nose pokes not during

1440 tone). D) Training was identical to Pre-Training, except incorrect nose pokes resulted in
1441 a 5 sec timeout, signaled by house light illumination, followed by a restarting of the ITI.

1442 E) Behavioral performance in a cue-reward learning task improves with optical
1443 stimulation of ChAT⁺ fibers in BLA. EYFP- and ChR2-expressing mice earn similar
1444 numbers of rewards during PT (blue shaded region). ChR2-expressing mice more
1445 rapidly earn significantly more rewards than EYFP-expressing mice during Training
1446 (pink shaded region). No significant differences were observed during extinction training
1447 (orange shaded region). Horizontal white line: acquisition threshold, when a mouse
1448 began to earn ~20 rewards consistently in Training. Mean \pm SEM, EYFP: n = 5, ChR2: n
1449 = 6. Individual data are shown in **Figure 4-figure supplement 3A**. Data for males
1450 shown in **Figure 4-figure supplement 3C,E**.

1451 F) EYFP- and ChR2-expressing mice made similar numbers of incorrect nose pokes
1452 during Pre-Training. ChR2-expressing mice made significantly fewer incorrect nose
1453 pokes than EYFP-expressing mice in Training. No significant differences were observed
1454 during extinction training. Mean \pm SEM, EYFP: n = 5, ChR2: n = 6. Individual data are
1455 shown in **Figure 4-figure supplement 3B**. Data for males shown in **Figure 4-figure**
1456 **supplement 3D,F**. Additional behavioral assays shown in **Figure 4-figure supplement**
1457 **5A-F**.

1458

1459 **Figure 5**

1460 **Muscarinic, but not nicotinic, ACh receptor antagonism prevents learning of a**

1461 **cue-reward contingency.**

1462 A) Timeline of drug administration. Saline or ACh receptor (AChR) antagonists were

1463 delivered i.p., 30 min before PT and Training sessions, the same phases of the task as

1464 optical stimulation in **Figure 4.**

1465 B) Behavioral performance of mice administered AChR antagonists. AChR antagonists

1466 had no significant effect on rewards earned during Pre-Training. Muscarinic AChR

1467 antagonism (Scop and Mec+Scop) resulted in significantly fewer rewards earned during

1468 Training. There was no significant difference between saline controls and those

1469 receiving the nicotinic AChR antagonist (Mec) during Training and mice extinguished

1470 responding at similar rates. Mean \pm SEM Saline (n = 8), Mec (n = 9), Scop (n = 8),

1471 Mec+Scop (n = 9). Horizontal white line: acquisition threshold, when a mouse began to

1472 earn ~20 rewards consistently in Training. Individual data are shown in **Figure 5-figure**

1473 **supplement 1A.**

1474 C) Incorrect nose pokes. Incorrect nose poking was not affected by AChR antagonism

1475 during PT but Scop- and Scop+Mec-treated mice maintained high levels of incorrect

1476 nose pokes compared to Saline- and Mec-treated mice throughout Training. Mean \pm

1477 SEM, Saline (n = 8), Mec (n = 9), Scop (n = 8), or Mec+Scop (n = 9). Individual data are

1478 shown in **Figure 5-figure supplement 1B.** AChR antagonist locomotor test shown in

1479 **Figure 5-figure supplement 1C.**

1480

1481 **Figure 6**

1482 **Non-contingent stimulation of cholinergic NBM-BLA terminals is sufficient to**

1483 **enhance cue-reward learning.**

1484 A) Experimental details of laser stimulation in non-contingent ChR2mice. Non-

1485 contingent-ChR2-expressing mice received the same number of light stimulations as

1486 contingent-ChR2-expressing mice, but stimulation was only given during the ITI, when

1487 non-contingent mice had not made a response within 2 sec. Injection sites and fiber

1488 placements are shown in **Figure 6-figure supplement 1A-B.**

1489 B) Non-contingent NBM-BLA optical stimulation also improves behavioral performance

1490 in cue-reward learning task. There was no significant difference in the number of

1491 rewards earned between EYFP (n = 6), contingent-ChR2 (n = 5), or non-contingent-

1492 ChR2 (n = 5) mice during Pre-Training. Contingent- and non-contingent-ChR2-

1493 expressing mice more rapidly earned significantly more rewards during Training than

1494 EYFP-expressing mice. No differences were observed between groups during extinction

1495 training. Mean \pm SEM EYFP: n = 6, contingent-ChR2: n = 5, non-contingent-ChR2: n =

1496 5. Horizontal white line: acquisition threshold, when a mouse began to earn 20 rewards

1497 consistently in Training. Individual data are shown in **Figure 6-figure supplement 2A.**

1498 C) Incorrect nose pokes. There was no significant difference in the number of incorrect

1499 nose pokes between groups during Pre-Training. Contingent- and non-contingent-

1500 ChR2-expressing mice made significantly fewer incorrect nose pokes during Training

1501 than EYFP-expressing mice. No differences between groups were observed during

1502 extinction training. Mean \pm SEM EYFP: n = 6, contingent-ChR2: n = 5, non-contingent: n

1503 = 5. Individual data are shown in **Figure 6-figure supplement 2B.**

1504 **Figure 2-figure supplement 1**

1505 **BLA ACh3.0 recording.**

1506 A) Squares indicate optical fiber tips for individual mice. 1 (red), 2 (blue), 3 (teal), 4
1507 (purple).

1508 B) Increase in fluorescence ($\% \Delta F/F_0$) following correct nose pokes is specific to the
1509 signal (465 nm, green) channel and is not observed in the reference channel (405 nm,
1510 tan). Data from Mouse 1 PT Day 5 as in **Figure 2C**. Mean \pm SEM, n = 24.

1511 C) Minimal increase in fluorescence ($\% \Delta F/F_0$) following incorrect nose pokes. Signal
1512 (465 nm, grey) channel, reference channel (405 nm, tan). Data from Mouse 1 PT Day 5
1513 as in **Figure 2C**. Downsampled mean \pm SEM, n = 24 of 58.

1514 D-F) Individual mouse data for mice 2-4 as shown in **Figure 2D**. Dashed white
1515 horizontal line: first Training day earning 10 rewards (10 Rew.). White horizontal line:
1516 acquisition threshold (Acq.).

1517 G) Mouse 1 combined action bCI plot for subset of days used in cohort averaged
1518 heatmap **Figure 2E** (From bottom to top: PT Day 1, PT Day 5, Early Training Day, First
1519 Training day earning 10 rewards, Mid Training Day, Acquisition Day, Last Training Day,
1520 Last Extinction Day). Mean overlaid on 99% bCI's for tone onset, correct nose poke,
1521 and receptacle entry. Pink and blue significance bars under traces denote time points
1522 where 99% bCI's are above or below 0 for at least 0.5 sec, respectively. Horizontal
1523 scale = 1 sec. Vertical scale = 5 Z $\% \Delta F/F_0$.

1524 H) Cohort averaged combined action bCI plot for subset of days used in G) and cohort
1525 averaged heatmap **Figure 2E**. Trial level mean overlaid on 99% bCI's for tone onset,
1526 correct nose poke, and receptacle entry. Pink and blue significance bars under traces

1527 denote time points where 99% bCI's are above or below 0 for at least 0.5 sec,
1528 respectively. Horizontal scale = 1 sec. Vertical scale = $5 Z\% \Delta F / F_0$.
1529

1530 **Figure 2-figure supplement 2**

1531 **BLA ACh3.0 recording: incorrect nose pokes.**

1532 A) Incorrect nose poking of individual mice throughout training.

1533 B) Incorrect nose pokes that yield timeouts (downsampled Training Day 1, pink line, n =

1534 24 of 66) result in a modest increase in BLA ACh signaling but incorrect nose pokes

1535 before timeouts are introduced (downsampled PT Day 5, blue line, n = 24 of 58) do not.

1536 Data from Mouse 1 as in **Figure 2C**, Mean $Z\% \Delta F/F_0$ overlaid on bootstrapped 99%

1537 confidence intervals (99% bCI's). Shaded significance bars under traces represent time

1538 points where 99% bCI's do not contain 0 for at least 0.5 sec.

1539 C-F) Individual mouse heatmaps of BLA ACh signaling across all training phases,

1540 aligned to incorrect nose poke. Each row is the average of incorrect nose pokes that led

1541 to (or would have led to for PT) a timeout across a session. White dashed horizontal

1542 line: first Training day earning 10 rewards. Horizontal white line: acquisition threshold,

1543 when a mouse began to earn ~20 rewards consistently in Training. Black horizontal

1544 lines: divisions between training phases.

1545 G) Heatmap of BLA ACh signaling during incorrect nose poke averaged across mice.

1546 Signal aligned as in C-F) with a selection of data from key days in the behavioral

1547 paradigm shown. From bottom to top: PT Day 1, PT Day 5, Early Training Day, First

1548 Training day earning 10 rewards (white dashed horizontal line), Mid Training Day,

1549 Acquisition Day (white horizontal line), Last Training Day, Last Extinction Day. Black

1550 horizontal lines: divisions between training phases.

1551 H) Cohort averaged bCI plot for subset of days used in G). Trial level mean

1552 (downsampled to 20) overlaid on 99% bCI's for incorrect nose poke. Pink and blue

1553 significance bars under traces denote time points where 99% bCI's are above or below
1554 0 for at least 0.5 sec, respectively. It is unclear how to interpret the timepoints
1555 significantly below 0 before and after incorrect nose pokes pulled out by bootstrapping.
1556 This may be an artefact of the small signal across incorrect trials, although this remains
1557 to be investigated. Horizontal scale = 1 sec. Vertical scale = 5 Z% $\Delta F/F_0$.
1558

1559 **Figure 2-figure supplement 3**

1560 **BLA ACh3.0 recording replicate.**

1561 A) Squares indicate optical fiber tips for individual mice. 5 (orange), 6 (cyan), 7 (brown),
1562 8 (navy).

1563 B) Behavioral responding of mice during BLA ACh3.0 recordings. Individual mice
1564 acquired the task at different rates as measured by rewards earned. White horizontal
1565 line: acquisition threshold, when a mouse began to earn 20 rewards consistently in
1566 Training. Incorrect nose pokes shown in **Figure 2-figure supplement 4A**.

1567 C-F) Heatmaps of BLA ACh signaling in mice 5-8 across all training phases, aligned to
1568 tone onset (Tone), correct nose poke (NP), and receptacle entry (Rec). Each row is the
1569 average of rewarded trials across a training session. Horizontal white line: acquisition
1570 threshold, when a mouse began to earn 20 rewards consistently in Training. Black
1571 horizontal lines: divisions between training phases. Black vertical lines: divisions
1572 between breaks in time to allow for variable latencies in tone onset, correct nose poke,
1573 and receptacle entry (reward retrieval). Blanks in the heatmaps indicate time bins added
1574 for alignment.

1575 G) Heatmap of BLA ACh signaling averaged across mice 5-8. Signal aligned as in C-F)
1576 with a selection of key days shown, from bottom to top: PT Day 1, PT Day 4, Early
1577 Training, Acquisition Day (white horizontal line), Last Training Day, Last Extinction Day.
1578 Black horizontal lines: divisions between training phases. Black vertical lines: divisions
1579 between breaks in time to allow for variable latencies in tone onset, correct nose poke,
1580 and receptacle entry (reward retrieval).

1581 H) Mouse 5 combined action bCI plot for subset of days used in G). Mean overlaid on
1582 99% bCI's for tone onset, correct nose poke, and receptacle entry. Pink and blue
1583 significance bars under traces denote time points where 99% bCI's are above or below
1584 0 for at least 0.5 sec, respectively. Horizontal scale = 1 sec. Vertical scale = 5
1585 $Z\% \Delta F / F_0$.

1586 I) Cohort (mice 5-8) averaged combined action bCI plot for subset of days used in G-H).
1587 Trial level mean overlaid on 99% bCI's for tone onset, correct nose poke, and
1588 receptacle entry. Pink and blue significance bars under traces denote time points where
1589 99% bCI's are above or below 0 for at least 0.5 sec, respectively. Horizontal scale = 1
1590 sec. Vertical scale = 5 $Z\% \Delta F / F_0$.

1591

1592

1593 **Figure 2-figure supplement 4**

1594 **BLA ACh3.0 recording replicate: incorrect nose pokes.**

1595 A) Incorrect nose poking of individual mice throughout training.

1596 B-E) Individual mouse heatmaps of BLA ACh signaling across all training phases,
1597 aligned to incorrect nose poke. Each row is the average of incorrect nose pokes that led
1598 to (or would have led to for PT) a timeout across a session. Horizontal white line:
1599 acquisition threshold, when a mouse began to earn 20 rewards consistently in Training.

1600 Black horizontal lines: divisions between training phases.

1601 F) Heatmap of BLA ACh signaling during incorrect nose poke averaged across mice.

1602 Signal aligned as in B-E) with a selection of data from key days in the behavioral
1603 paradigm shown. From bottom to top: PT Day 1, PT Day 4, Early Training Day,
1604 Acquisition Day (white horizontal line), Last Training Day, Last Extinction Day. Black
1605 horizontal lines: divisions between training phases.

1606 G) Cohort averaged bCI plot for subset of days used in F). Downsampled trial level
1607 mean overlaid on 99% bCI's for incorrect nose poke. Pink and blue significance bars
1608 under traces denote time points where 99% bCI's are above or below 0 for at least 0.5
1609 sec, respectively. Horizontal scale = 1 sec. Vertical scale = 5 $Z\% \Delta F/F_0$.

1610

1611 **Figure 2-figure supplement 5**

1612 **NBM-BLA GCaMP7s recording in cholinergic terminal fibers.**

1613 A) Circles indicate NBM DIO-GCaMP7s injection sites for individual mice, 1 (red), 2
1614 (blue). Triangles indicate estimated optical fiber tips based on adjacent slices for
1615 individual mice. 1 (red), 2 (blue).

1616 B) Representative injection site coronal slice from **Figure 2F** with channels separated.
1617 Scale = 500 μ m.

1618 C) Representative fiber tip site coronal slice from **Figure 2F** with channels separated.
1619 Scale = 500 μ m.

1620 D) Increase in fluorescence ($\% \Delta F/F_0$) following correct nose pokes is specific to the
1621 signal (465 nm, green) channel and is not observed in the reference channel (405 nm,
1622 tan). Data from Mouse 1 PT Day 4 as in **Figure 2H**. Mean \pm SEM, n = 42.

1623 E) Minimal increase in fluorescence ($\% \Delta F/F_0$) following incorrect nose pokes. Signal
1624 (465 nm, grey) channel, reference channel (405 nm, tan). Data from Mouse 1 PT Day 4
1625 as in **Figure 2H**. Downsampled mean \pm SEM, n = 42 of 101.

1626 F) Individual data for mouse 2 as shown in **Figure 2I**. White horizontal line: acquisition
1627 threshold.

1628 G) Mouse 1 combined action bCI plot for subset of days used in cohort averaged
1629 heatmap **Figure 2J** (From bottom to top: PT Day 1, PT Day 4, Early Training Day,
1630 Acquisition Day, Last Training Day, Last Extinction Day). Mean overlaid on 99% bCI's
1631 for tone onset, correct nose poke, and receptacle entry. Pink and blue significance bars
1632 under traces denote time points where 99% bCI's are above or below 0 for at least 0.5
1633 sec, respectively. Horizontal scale = 1 sec. Vertical scale = 5 $Z\% \Delta F/F_0$.

1634 **Figure 2-figure supplement 6**

1635 **NBM-BLA GCAMP7s recording in cholinergic terminal fibers: incorrect nose**
1636 **pokes.**

1637 A) Incorrect nose poking of individual mice throughout training.

1638 B) Incorrect nose pokes that yield timeouts (downsampled Training Day 1, pink line, n =
1639 42 of 105) result in a significant increase in NBM-BLA terminal fiber activity, but
1640 incorrect nose pokes before timeouts are introduced (downsampled PT Day 4, blue line,
1641 n = 42 of 101) do not. Data from Mouse 1 as in **Figure 2H**, mean $Z\% \Delta F/F_0$ overlaid on
1642 bootstrapped 99% confidence intervals (99% bCI's). Shaded significance bars under
1643 traces represent time points where 99% bCI's do not contain 0 for at least 0.5 sec.

1644 C-D) Individual mouse heatmaps of NBM-BLA terminal fiber activity across all training
1645 phases, aligned to incorrect nose poke. Each row is the average of incorrect nose
1646 pokes that led to (or would have led to for PT) a timeout across a session. Horizontal
1647 white line: acquisition threshold, when a mouse began to earn 20 rewards consistently
1648 in Training. Black horizontal lines: divisions between training phases.

1649 E) Heatmap of NBM-BLA terminal fiber activity during incorrect nose poke averaged
1650 across mice. Signal aligned as in C-D) with a selection of data from key days in the
1651 behavioral paradigm shown. From bottom to top: PT Day 1, PT Day 4, Early Training
1652 Day, Acquisition Day (white horizontal line), Last Training Day, Last Extinction Day.
1653 Black horizontal lines: divisions between training phases.

1654 **Figure 2-figure supplement 7**

1655 **NBM-BLA GCaMP7s recording in cholinergic terminal fibers replicate.**

1656 A) Circles indicate NBM DIO-GCaMP7s injection sites for individual mice, 3 (teal), 4
1657 (purple). Squares indicate optical fiber tips for individual mice, 3 (teal), 4 (purple).

1658 B) Behavioral responding of mice during NBM-BLA recordings. Individual mice acquired
1659 the task at different rates as measured by rewards earned. White horizontal line:
1660 acquisition threshold, when a mouse began to earn 20 rewards consistently in Training.
1661 Incorrect nose pokes shown in **Figure 2-figure supplement 8A**.

1662 C-D) Heatmaps of NBM-BLA terminal fiber activity in mice 3-4 across all training
1663 phases, aligned to tone onset (Tone), correct nose poke (NP), and receptacle entry
1664 (Rec). Each row is the average of rewarded trials across a training session. Horizontal
1665 white line: acquisition threshold, when a mouse began to earn 20 rewards consistently
1666 in Training. Black horizontal lines: divisions between training phases. Black vertical
1667 lines: divisions between breaks in time to allow for variable latencies in tone onset,
1668 correct nose poke, and receptacle entry (reward retrieval). Blanks in the heatmaps
1669 indicate time bins added for alignment.

1670 E) Heatmap of NBM-BLA terminal fiber activity averaged across mice 3-4. Signal
1671 aligned as in C-D) with a selection of key days shown, from bottom to top: PT Day 1, PT
1672 Day 4, Early Training, Acquisition Day (white horizontal line), Last Training Day, Last
1673 Extinction Day. Black horizontal lines: divisions between training phases. Black vertical
1674 lines: divisions between breaks in time to allow for variable latencies in tone onset,
1675 correct nose poke, and receptacle entry (reward retrieval).

1676 F) Mouse 3 combined action bCI plot for subset of days used in cohort averaged
1677 heatmap E). Mean overlaid on 99% bCI's for tone onset, correct nose poke, and
1678 receptacle entry. Pink and blue significance bars under traces denote time points where
1679 99% bCI's are above or below 0 for at least 0.5 sec, respectively. Horizontal scale = 1
1680 sec. Vertical scale = $5 Z\% \Delta F / F_0$.

1681 G) Cohort (mice 1-4) averaged combined action bCI plot for subset of days used in E-
1682 F). Trial level mean overlaid on 99% bCI's for tone onset, correct nose poke, and
1683 receptacle entry. Pink and blue significance bars under traces denote time points where
1684 99% bCI's are above or below 0 for at least 0.5 sec, respectively. Horizontal scale = 1
1685 sec. Vertical scale = $5 Z\% \Delta F / F_0$.

1686 **Figure 2-figure supplement 8**

1687 **NBM-BLA GCAMP7s recording in cholinergic terminal fibers replicate: incorrect**
1688 **nose pokes.**

1689 A) Incorrect nose poking of individual mice throughout training.

1690 B-C) Individual mouse heatmaps of NBM-BLA terminal fiber activity across all training
1691 phases, aligned to incorrect nose poke. Each row is the average of incorrect nose
1692 pokes that led to (or would have led to for PT) a timeout across a session. Horizontal
1693 white line: acquisition threshold, when a mouse began to earn 20 rewards consistently
1694 in Training. Black horizontal lines: divisions between training phases.

1695 D) Heatmap of NBM-BLA terminal fiber activity during incorrect nose poke averaged
1696 across mice 3-4. Signal aligned as in B-C) with a selection of data from key days in the
1697 behavioral paradigm shown. From bottom to top: PT Day 1, PT Day 4, Early Training
1698 Day, Acquisition Day (white horizontal line), Last Training Day, Last Extinction Day.
1699 Black horizontal lines: divisions between training phases.

1700 E) Cohort (mice 1-4) averaged bCI plot for subset of days used in D). Trial level mean
1701 (downsampled to 20) overlaid on 99% bCI's for incorrect nose poke. Pink and blue
1702 significance bars under traces denote time points where 99% bCI's are above or below
1703 0 for at least 0.5 sec, respectively. As for other experiments measuring signal before
1704 and after incorrect nose pokes, it is unclear how to interpret the timepoints significantly
1705 below 0 pulled out by bootstrapping. As mentioned previously, this may be an artefact of
1706 the small signal across incorrect trials, although this remains to be investigated.

1707 Horizontal scale = 1 sec. Vertical scale = 5 Z% $\Delta F/F_0$.

1708

1709 **Figure 2-figure supplement 9**

1710 **Simultaneous BLA ACh3.0 + GCAMP7s recording in NBM-BLA cholinergic**
1711 **terminal fibers.**

1712 A) Left: DIO-jRCaMP1b was injected in the NBM of ChAT-IRES-Cre mice.

1713 Representative coronal brain slice showing jRCaMP1b expression. Yellow dashed lines:
1714 internal capsule and globus pallidus outlines. Scale = 500 μm . White box: higher
1715 magnification area shown in B).

1716 B) Higher magnification of injection site. Scale = 100 μm .

1717 C) Circle indicates NBM DIO-jRCaMP1b injection site for mouse 1.

1718 D) ACh3.0 was injected into the ipsilateral BLA and an optical fiber was implanted
1719 above the BLA. White dashed line: BLA outline. Scale = 500 μm .

1720 E) Squares indicate optical fiber tips for individual mice. ACh3.0 + RCaMP (red),
1721 ACh3.0 + RCaMP sham (grey),

1722 F) A substantial increase in both fluorescence representing BLA ACh release (green
1723 line) and NBM-BLA cholinergic terminal activity (magenta line) coincided with correct

1724 nose pokes on last day of PT. Mean $Z\%\Delta F/F_0$ overlaid on bootstrapped 99%

1725 confidence intervals (99% bCI's). Shaded significance bars under traces represent time

1726 points where 99% bCI's do not contain 0 for at least 0.5 sec. $n = 42$.

1727 G) Modest increase in fluorescence in both channels following incorrect nose pokes on

1728 last day of PT. Mean $Z\%\Delta F/F_0$ overlaid on bootstrapped 99% confidence intervals (99%

1729 bCI's). Shaded significance bars under traces represent time points where 99% bCI's

1730 do not contain 0 for at least 0.5 sec. Downsampled $n = 42$ of 94.

1731 H) jRCaMP1b signal is not simply crosstalk from ACh3.0 channel. A substantial
1732 increase in fluorescence representing BLA ACh release (green line) following correct
1733 nose pokes did not necessitate signal in RCaMP sham red channel (grey line). Last day
1734 of PT. Mean $Z\% \Delta F/F_0$ overlaid on bootstrapped 99% confidence intervals (99% bCI's).
1735 Shaded significance bars under traces represent time points where 99% bCI's do not
1736 contain 0 for at least 0.5 sec. n = 44.

1737 I) Incorrect nose pokes on Last day of PT, as in G), for ACh3.0 + RCaMP sham mouse.
1738 Downsampled n = 44 of 135.

1739
1740

1741 **Figure 3-figure supplement 1**

1742 **GCaMP6s recording in BLA CaMKII α cells.**

1743 A) Squares indicate optical fiber tips for individual mice. 1 (red), 2 (blue), 3 (teal).

1744 B) Increase in fluorescence ($Z\% \Delta F/F_0$) during last day of PT (data shown for Mouse 1)

1745 aligns more closely to receptacle entry (reward retrieval) on rewarded trials. Mean \pm

1746 SEM, n = 44.

1747 C) Increase in fluorescence ($\% \Delta F/F_0$) following correct nose pokes is specific to the

1748 signal (465 nm, green) channel and is not observed in the reference channel (405 nm,

1749 tan). Mirroring in reference channel following correct nose poke is likely due to a change

1750 in the pool of unbound tracer, because data are not acquired at the “true” isosbestic

1751 point of GCaMP (Barnett et al., 2017; C. K. Kim et al., 2016; Sych et al., 2019)). Data

1752 from Mouse 1, PT Day 4 as in **Figure 3B**. Mean \pm SEM, n = 44.

1753 D) Decrease in fluorescence ($\% \Delta F/F_0$) following incorrect nose pokes is seen in signal

1754 channel (465 nm, grey), but not reference channel (405 nm, tan). Data from Mouse 1,

1755 PT Day 4 as in **Figure 3B**. Downsampled mean \pm SEM, n = 44 of 141.

1756 E-F) Individual data for mice not shown in **Figure 3D**. White horizontal line: acquisition

1757 threshold.

1758 G) Mouse 1 combined action bCI plot for subset of days used in cohort averaged

1759 heatmap **Figure 3E** (from bottom to top: PT Day 1, PT Day 4, Early Training Day,

1760 Acquisition Day, Last Extinction Day). Mean overlaid on 99% bCI's for tone onset,

1761 correct nose poke, and receptacle entry. Pink and blue significance bars under traces

1762 denote time points where 99% bCI's are above or below 0 for at least 0.5 sec,

1763 respectively. Horizontal scale = 1 sec. Vertical scale = 1 $Z\% \Delta F/F_0$.

1764 H) Cohort averaged combined action bCI plot for subset of days used in cohort
1765 averaged heatmap **Figure 3E**. Trial level mean overlaid on 99% bCI's for tone onset,
1766 correct nose poke, and receptacle entry. Pink and blue significance bars under traces
1767 denote time points where 99% bCI's are above or below 0 for at least 0.5 sec,
1768 respectively. Horizontal scale = 1 sec. Vertical scale = 1 $Z\% \Delta F/F_0$.
1769

1770 **Figure 3-figure supplement 2**

1771 **GCAMP6s recording in BLA CaMKII α cells: incorrect nose pokes.**

1772 A) Incorrect nose pokes of individual mice throughout training.

1773 B) Both incorrect nose pokes that yield timeouts (downsampled Training Day 1, pink
1774 line, n = 44 of 124) and incorrect nose pokes before timeouts are introduced

1775 (downsampled PT Day 4, blue line, n = 44 of 141) result in a modest decrease in BLA

1776 CaMKII α neuron activity. Data from Mouse 1 as in **Figure 3B**, mean Z% Δ F/F₀ overlaid

1777 on bootstrapped 99% confidence intervals (99% bCI's). Shaded significance bars under

1778 traces represent time points where 99% bCI's do not contain 0 for at least 0.5 sec.

1779 C-E) Individual mouse heatmaps of BLA CaMKII α neuron activity across all training

1780 phases, aligned to incorrect nose poke. Each row is the average of incorrect nose

1781 pokes that led to (or would have led to for PT) a timeout across a session. Horizontal

1782 white line: acquisition threshold, when a mouse began to earn ~20 rewards consistently

1783 in Training. Black horizontal lines: divisions between training phases.

1784 F) Heatmap of BLA CaMKII α neuron activity during incorrect nose poke averaged

1785 across mice. Signal aligned as in C-E) with a selection of data from key days in the

1786 behavioral paradigm shown. From bottom to top: PT Day 1, PT Day 4, Early Training

1787 Day, Acquisition Day (white horizontal line), Last Extinction Day. Black horizontal lines:

1788 divisions between training phases.

1789 G) Cohort averaged bCI plot for subset of days used in F). Trial level mean

1790 (downsampled to 20) overlaid on 99% bCI's for incorrect nose poke. Pink and blue

1791 significance bars under traces denote time points where 99% bCI's are above or below

1792 0 for at least 0.5 sec, respectively. It is unclear how to interpret the substantial number

1793 of timepoints significantly below 0 before and after incorrect nose pokes and may be an
1794 artifact. Horizontal scale = 1 sec. Vertical scale = 1 $Z\% \Delta F / F_0$.

1795

1796 **Figure 3-figure supplement 3**

1797 **GCaMP6s recording in BLA CaMKII α replicate.**

1798 A) Squares indicate optical fiber tips for individual mice. 4(purple), 5 (orange), 6 (cyan),
1799 7 (brown).

1800 B) Behavioral responding of mice during BLA CaMKII α GCaMP6s recordings. Individual
1801 mice acquired the task at different rates as measured by rewards earned. White
1802 horizontal line: acquisition threshold, when a mouse began to earn 20 rewards
1803 consistently in Training. Incorrect nose pokes shown in **Figure 3-figure supplement**
1804 **4A.**

1805 C-F) Heatmaps of BLA CaMKII α cell activity in mice 4-7 across all training phases,
1806 aligned to tone onset (Tone), correct nose poke (NP), and receptacle entry (Rec). Each
1807 row is the average of rewarded trials across a training session. Horizontal white line:
1808 acquisition threshold, when a mouse began to earn 20 rewards consistently in Training.
1809 Black horizontal lines: divisions between training phases. Black vertical lines: divisions
1810 between breaks in time to allow for variable latencies in tone onset, correct nose poke,
1811 and receptacle entry (reward retrieval). Blanks in the heatmaps indicate time bins added
1812 for alignment.

1813 G) Mouse 4 combined action bCI plot for subset of days, from bottom to top: PT Day 1,
1814 PT Day 4, Early Training Day, Acquisition Day, Last Training Day, Last Extinction Day.
1815 Mean overlaid on 99% bCI's for tone onset, correct nose poke, and receptacle entry.
1816 Pink and blue significance bars under traces denote time points where 99% bCI's are
1817 above or below 0 for at least 0.5 sec, respectively. Horizontal scale = 1 sec. Vertical
1818 scale = 5 Z% $\Delta F/F_0$.

1819 **Figure 3-figure supplement 4**

1820 **GCAMP6s recording in BLA CaMKII α replicate: incorrect nose pokes.**

1821 A) Incorrect nose poking of individual mice throughout training.

1822 B-E) Individual mouse heatmaps of BLA CaMKII α cell activity across all training phases,

1823 aligned to incorrect nose poke. Each row is the average of incorrect nose pokes that led

1824 to (or would have led to for PT) a timeout across a session. Horizontal white line:

1825 acquisition threshold, when a mouse began to earn 20 rewards consistently in Training.

1826 Black horizontal lines: divisions between training phases.

1827

1828 **Figure 4-figure supplement 1**

1829 **Injection sites and optical fiber placements.**

1830 A) Circles indicate NBM injection sites for individual mice, EYFP (green) and ChR2
1831 (blue). Anterior/Posterior position relative to Bregma indicated.

1832 B) Representative injection site coronal slice from **Figure 4A** with channels separated.
1833 Scale = 500 μ m.

1834 C) Squares indicate observable optical fiber tips for individual mice, EYFP- (green) and
1835 ChR2-expressing mice (blue). Triangles indicate estimated optical fiber tips based on
1836 adjacent slices. Anterior/Posterior position relative to Bregma indicated.

1837 D) Representative fiber tip site coronal slice from **Figure 4A** with channels separated.
1838 Scale = 500

1839

1840 **Figure 4-figure supplement 2**

1841 ***Ex vivo* electrophysiology.**

1842 A-G) Current clamp recordings of ChAT⁺ NBM cells expressing ChR2. Optical
1843 stimulation was delivered at the indicated frequency.

1844

1845 **Figure 4-figure supplement 3**

1846 **Individual behavioral data and male cohort.**

1847 A) Rewards earned for individual mice from **Figure 4E**. Horizontal white line: acquisition
1848 threshold, when a mouse began to earn ~20 rewards consistently in Training.

1849 B) Incorrect nose pokes for individual mice from **Figure 4F**.

1850 C) Optical stimulation of ChAT⁺ NBM-BLA terminal fibers (ChR2-expressing mice, blue
1851 squares) had a similar effect on rewards earned during Training in male mice compared
1852 to female mice. Mean \pm SEM, EYFP: n = 7, ChR2: n = 7. Horizontal white line:
1853 acquisition threshold, when a mouse began to earn ~20 rewards consistently in
1854 Training.

1855 D) Optical stimulation of ChAT⁺ NBM-BLA terminal fibers (ChR2-expressing mice, blue
1856 squares) had a similar effect on incorrect nose pokes during Training in male mice
1857 compared to female mice. Mean \pm SEM, EYFP: n = 7, ChR2: n = 7.

1858 E) Individual data for graph shown in C).

1859 F) Individual data for graph shown in D).

1860

1861 **Figure 4-figure supplement 4**

1862 **Injection sites and optical fiber placements.**

1863 A) Circles indicate NBM injection sites for individual mice, EYFP- (green) and ChR2-
1864 expressing mice (blue). Anterior/Posterior position relative to Bregma indicated.

1865 B) Squares indicate observable optical fiber tips for individual mice, EYFP- (green) and
1866 ChR2-expressing mice (blue). Triangles indicate estimated site of optical fiber tips
1867 based on adjacent slices. Anterior/Posterior position relative to Bregma indicated.

1868

1869 **Figure 4-figure supplement 5**

1870 **Additional behavioral assays with NBM-BLA optical stimulation.**

1871 A) Stimulation of ChAT⁺ NBM-BLA terminal fibers did not support self-stimulation. Mice
1872 were allowed to nose poke for 2 sec of stimulation in the Training paradigm. Data for
1873 female mice from **Figure 4, Figure 4-figure supplement 1, Figure 4-figure**
1874 **supplement 3A-B.**

1875 B) Stimulation of ChAT⁺ NBM-BLA terminal fibers did not support real time place
1876 preference. Mice were allowed to move freely between two sides of an empty cage with
1877 distinct floor contexts for 15 min. Data are reported as percent time spent on the laser-
1878 paired side. Closed circles: Mean \pm SEM, open circles: data for individual mice. Data for
1879 female mice from **Figure 4, Figure 4-figure supplement 1, Figure 4-figure**
1880 **supplement 3A-B.**

1881 C) Stimulation of ChAT⁺ NBM-BLA terminal fibers during a progressive ratio test did not
1882 affect active nose poking. Closed squares: Mean \pm SEM, open squares: individual mice.
1883 Data for male mice from **Figure 4-figure supplement 3C-F + 4.**

1884 D) There were no differences between EYFP- and ChR2-expressing mice in locomotor
1885 activity. X-axis ticks = 5 min bins, Laser = 5 min of 20 sec on/off optical stimulation.
1886 Closed circles: Mean \pm SEM, open circles: data for individual mice. Data for female
1887 mice from **Figure 4, Figure 4-figure supplement 1, Figure 4-figure supplement 3A-**
1888 **B.**

1889 E-F) No difference in behavior was seen between EYFP- and ChR2-expressing mice on
1890 any measures in the Light/Dark Box Test. Data for female mice from **Figure 4, Figure**
1891 **4-figure supplement 1, Figure 4-figure supplement 3A-B.**

1892 **Figure 5-figure supplement 1**

1893 **Individual behavioral data and locomotion.**

1894 A) Rewards earned for individual mice from **Figure 5B**. Horizontal white line: acquisition
1895 threshold, when a mouse began to earn ~20 rewards consistently in Training.

1896 B) Incorrect nose pokes for individual mice from **Figure 5C**.

1897 C) There were no differences in locomotion for antagonists.

1898

1899 **Figure 6-figure supplement 1**

1900 **Injection sites and optical fiber placements.**

1901 A) Circles indicate NBM injection sites for individual mice, EYFP-expressing (green),
1902 contingent-ChR2-expressing (blue), and non-contingent-ChR2-expressing mice (cyan).

1903 Anterior/Posterior position relative to Bregma indicated.

1904 B) Squares indicate observable optical fiber tips for individual mice, EYFP-expressing
1905 (green), contingent-ChR2-expressing (blue), and non-contingent-ChR2-expressing mice
1906 (cyan). Triangles indicate estimated site of optical fiber tips based on adjacent slices.

1907 Anterior/Posterior position relative to Bregma indicated.

1908

1909 **Figure 6-figure supplement 2**

1910 **Individual behavioral data.**

1911 A) Rewards earned for individual mice from **Figure 6B**. Horizontal white line: acquisition
1912 threshold, when a mouse began to earn ~20 rewards consistently in Training.

1913 B) Incorrect nose pokes for individual mice from **Figure 6C**.

1914

1915 **Supplementary File 1**

1916 **Supplementary Table 1: Number of mice that acquired the reward learning**
1917 **behavior, number that were excluded and any training deviations.**

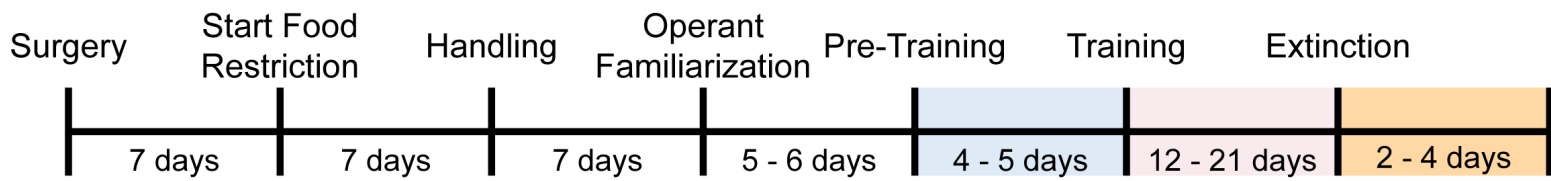
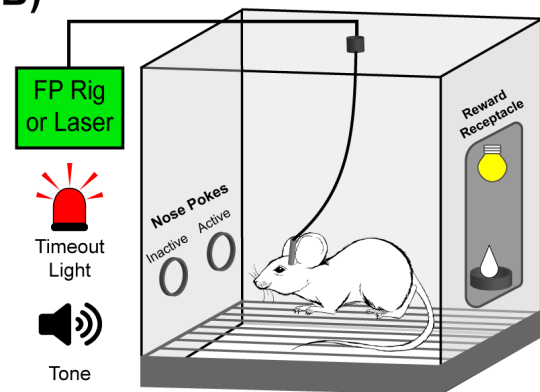
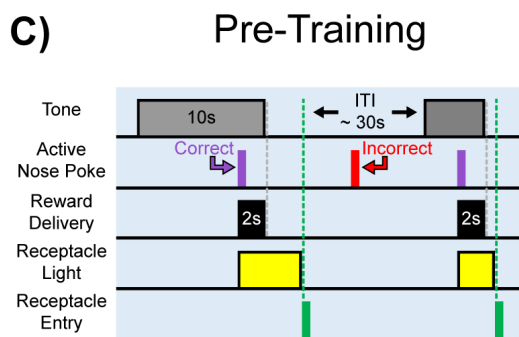
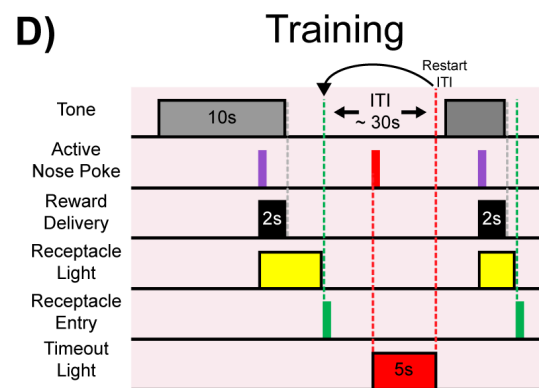
1918 A) Mice in the initial BLA ACh3.0 group were trained outside of the sound attenuating
1919 chambers. These mice had 5 days of Pre-Training because they were trained
1920 concurrently with another cohort of mice (not shown) that required an extra day to reach
1921 two consecutive days of 20 rewards earned and were advanced to a VI 20 schedule of
1922 reinforcement during Training after 9 days to promote responding. Training was
1923 extended to allow all mice to acquire. Due to time constraints during acquisition, mouse
1924 3 in this cohort was moved to Extinction after 20 days of Training because it had
1925 acquired earlier, was earning the most rewards, and we wanted to record more
1926 extinction days.

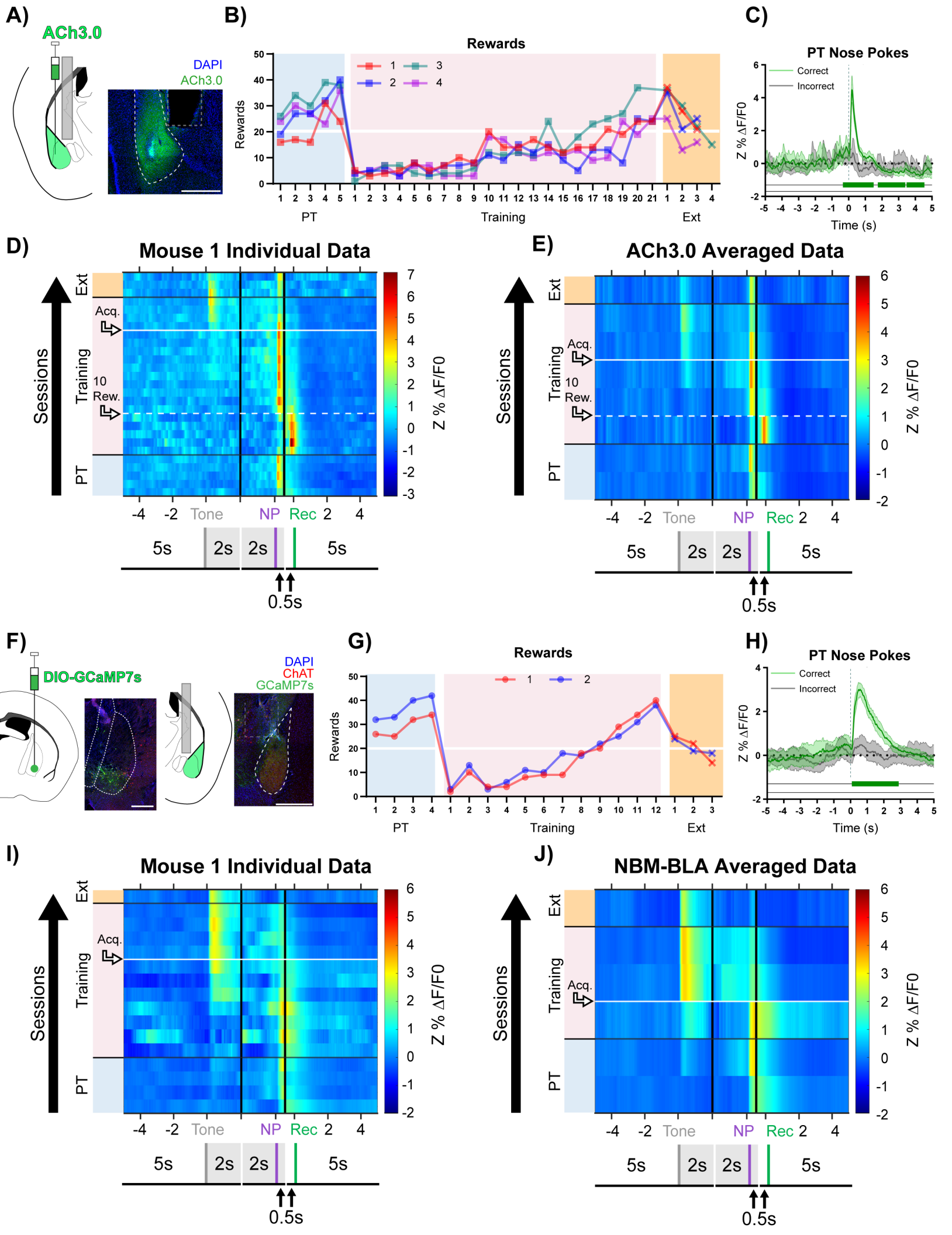
1927 B) Mice in the BLA ACh3.0 and NBM-BLA terminal fiber replicate experiments were
1928 advanced to one day of Extinction after only 7 days of Training due to the COVID-19
1929 shutdown.

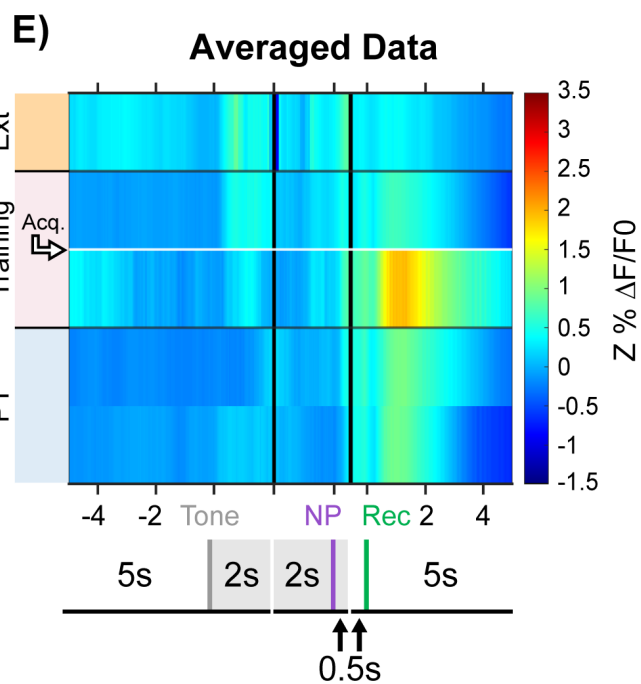
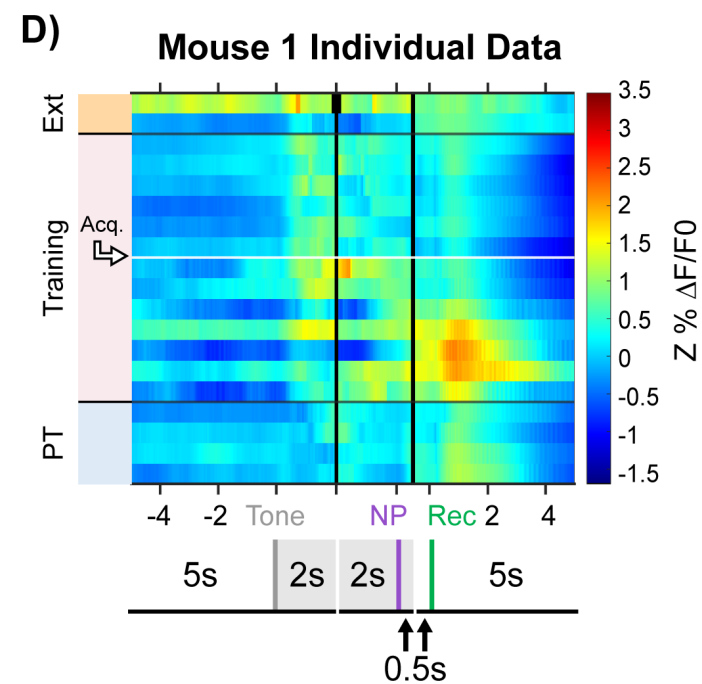
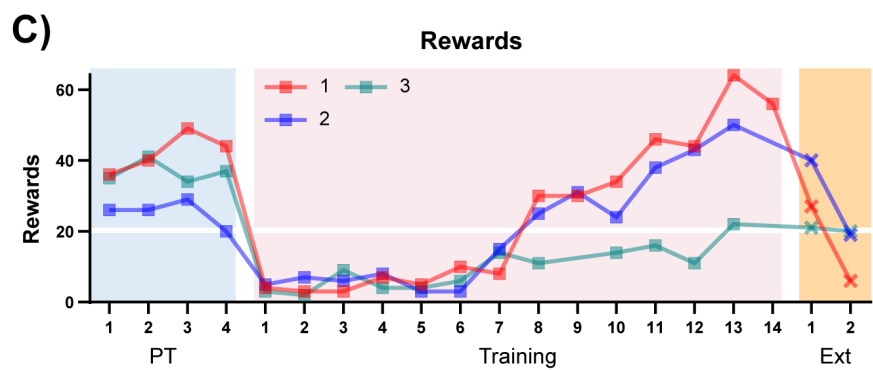
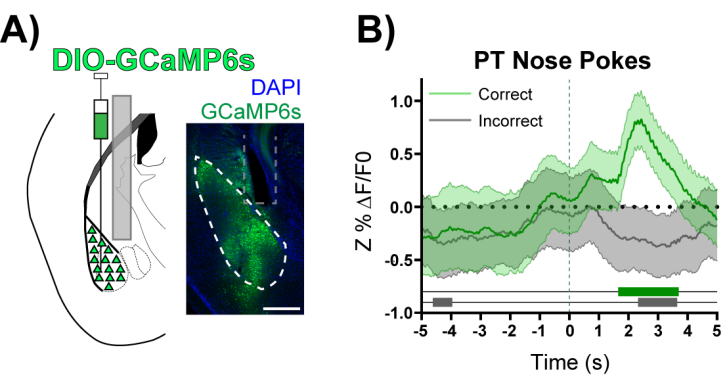
1930 C) BLA ACh3.0 and NBM-BLA terminal fiber jRCaMP1b mice were analyzed as dual
1931 channel mice just through Pre-Training and were instead used as replicates of the BLA
1932 ACh3.0 experiment. One of the mice had apparatus errors during Training and had to
1933 be excluded.

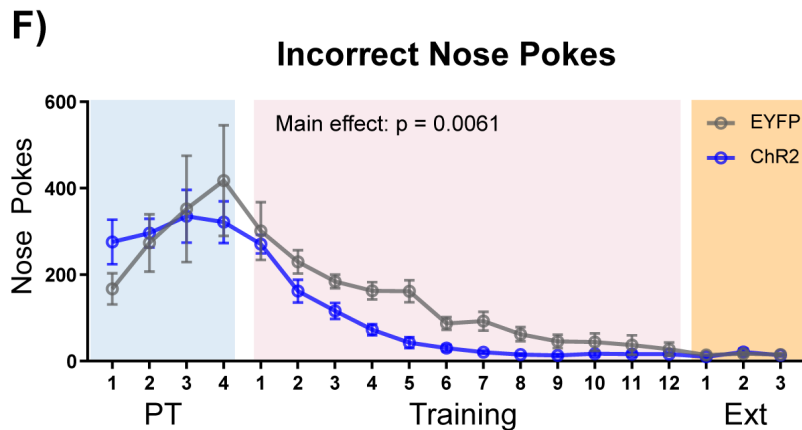
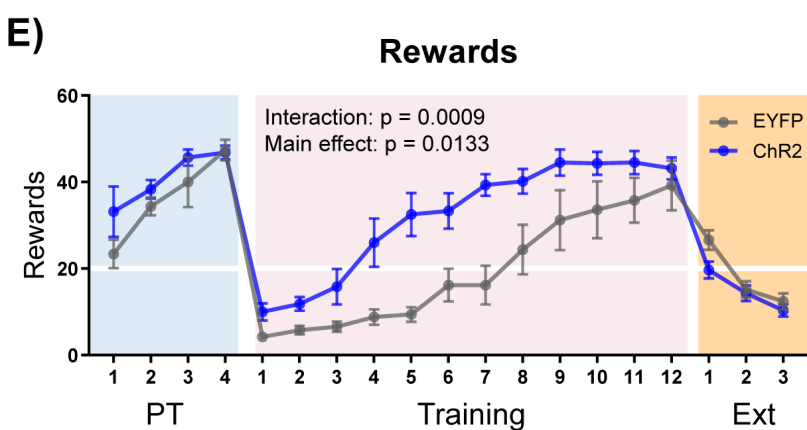
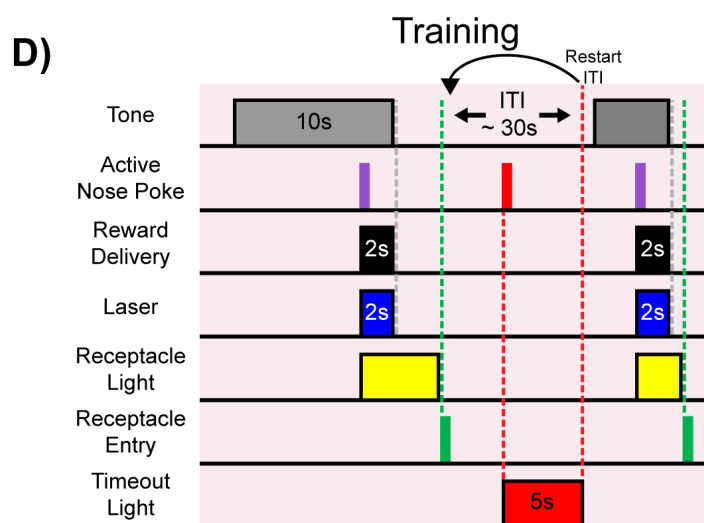
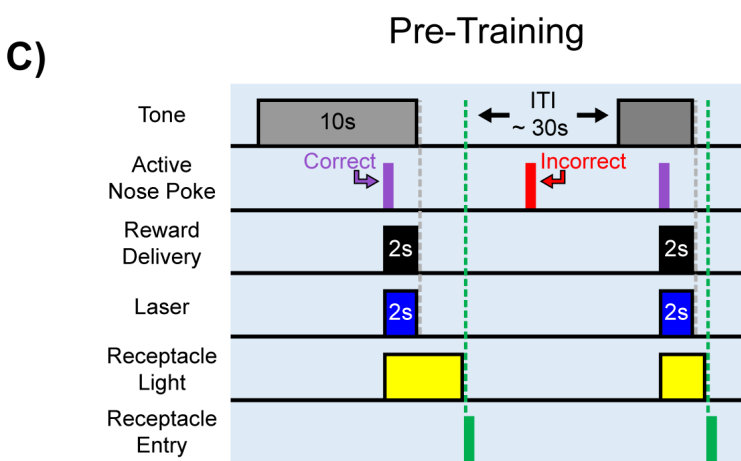
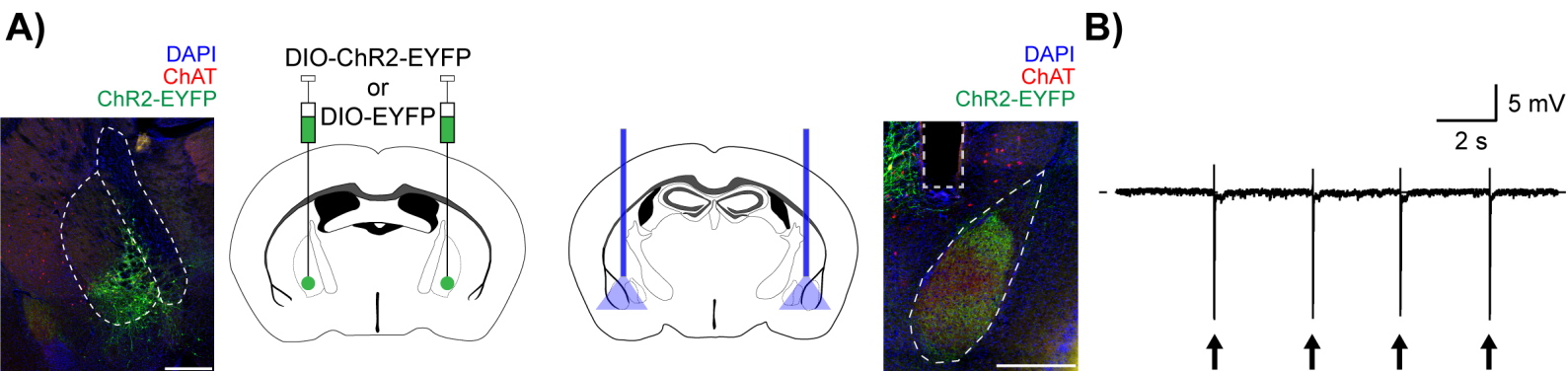
1934 D) Mice in the initial BLA CaMKII α GCaMP6 were trained outside of the sound
1935 attenuating chambers. Mouse 1 progressed from Pre-Training to Training a day earlier
1936 than the rest of the group and was able to have an extra day of Training before the 2
1937 days of Extinction. Mice in this group were advanced to a VI 20 schedule of

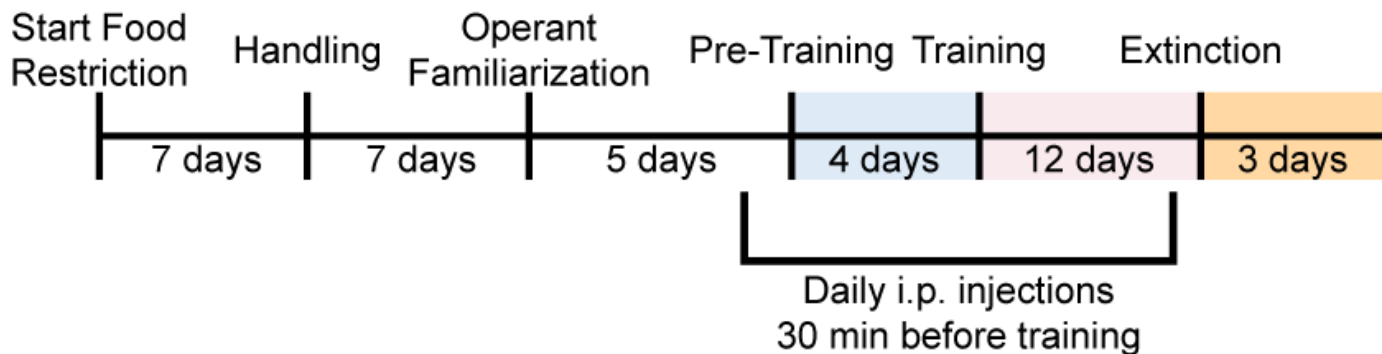
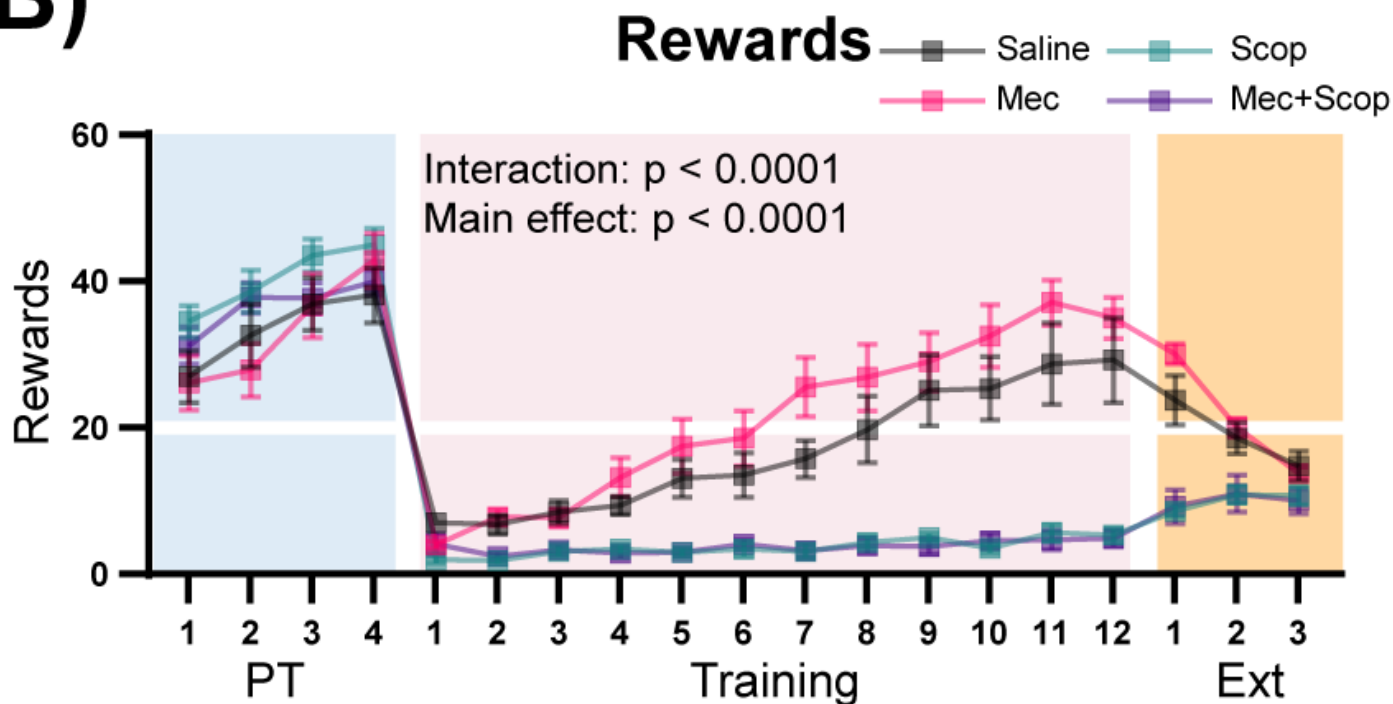
1938 reinforcement during Training after 6-7 days to promote responding. Training was
1939 extended to allow more mice to acquire.
1940

A)**B)****C)****D)**

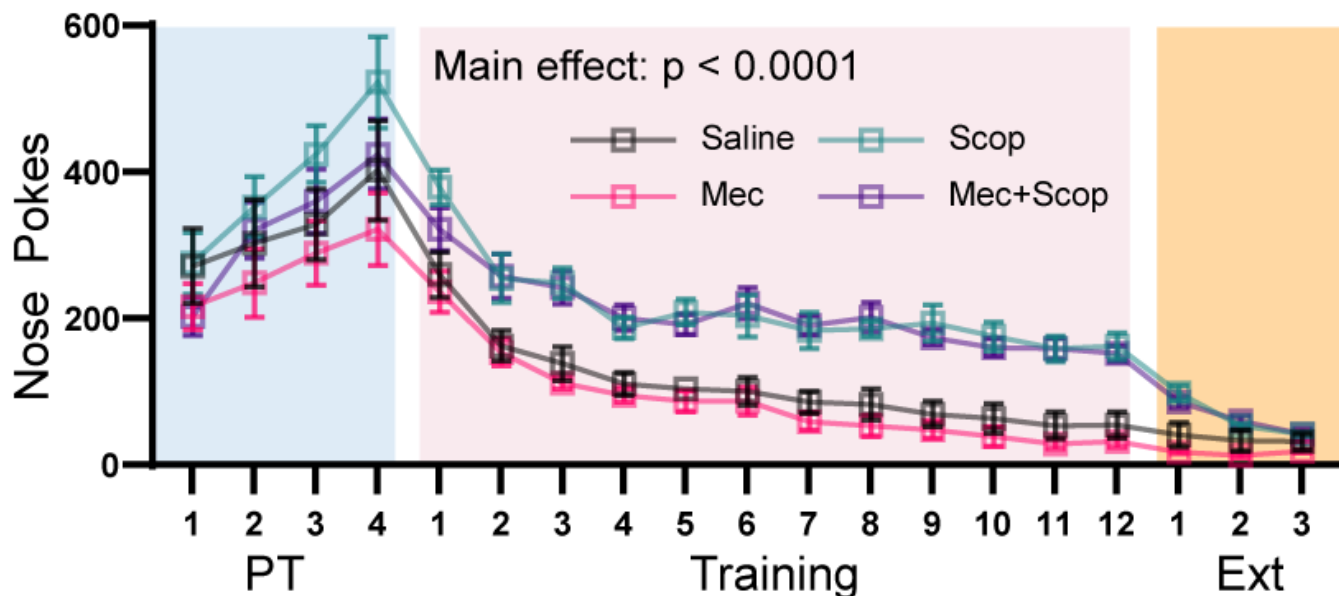




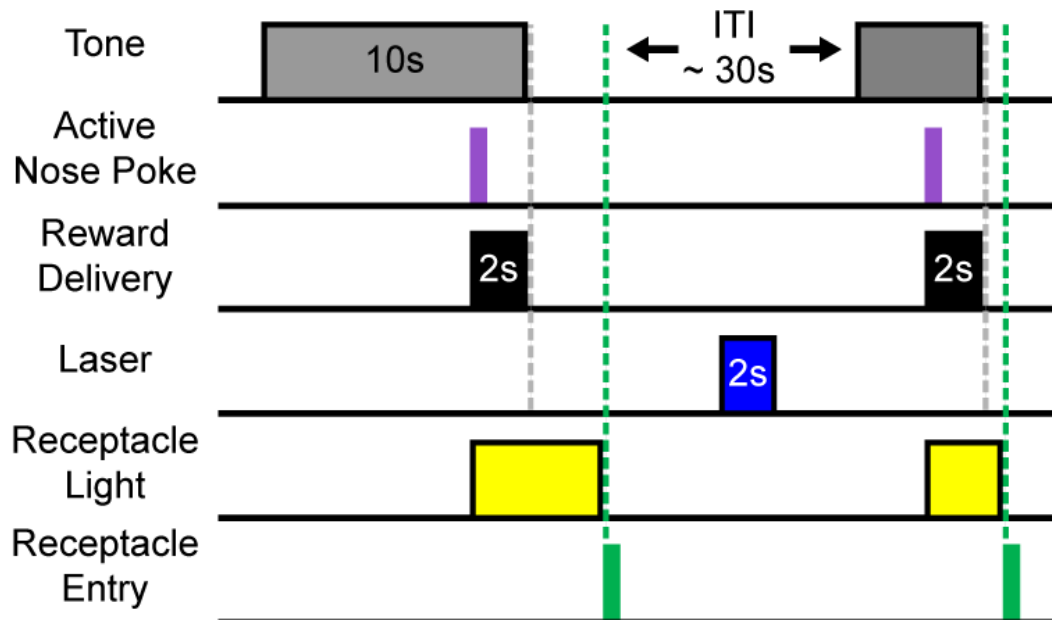


A)**B)****C)**

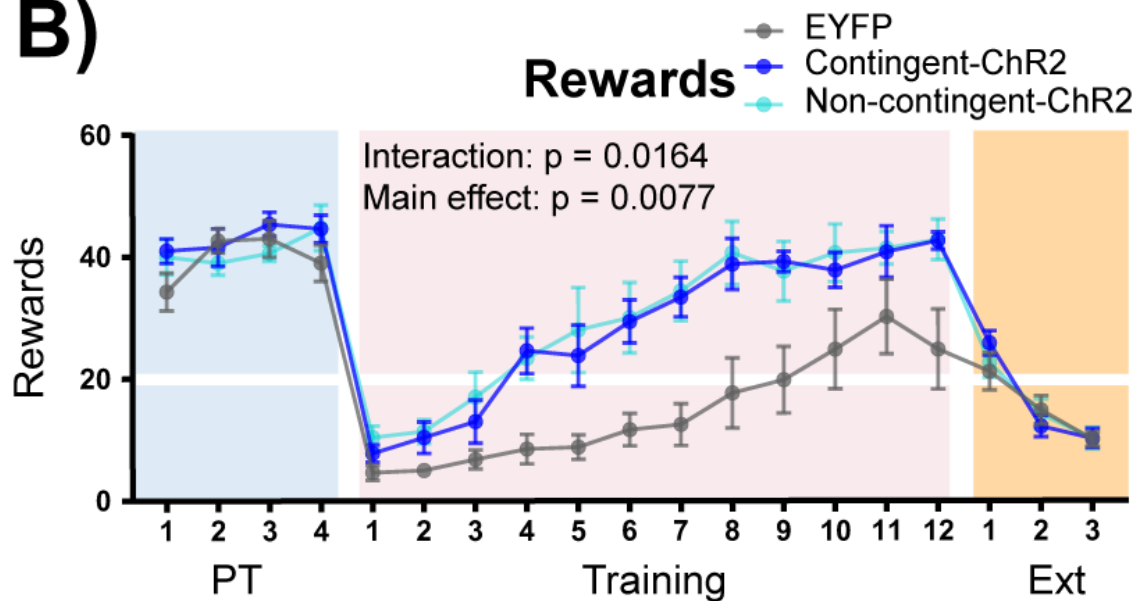
Incorrect Nose Pokes



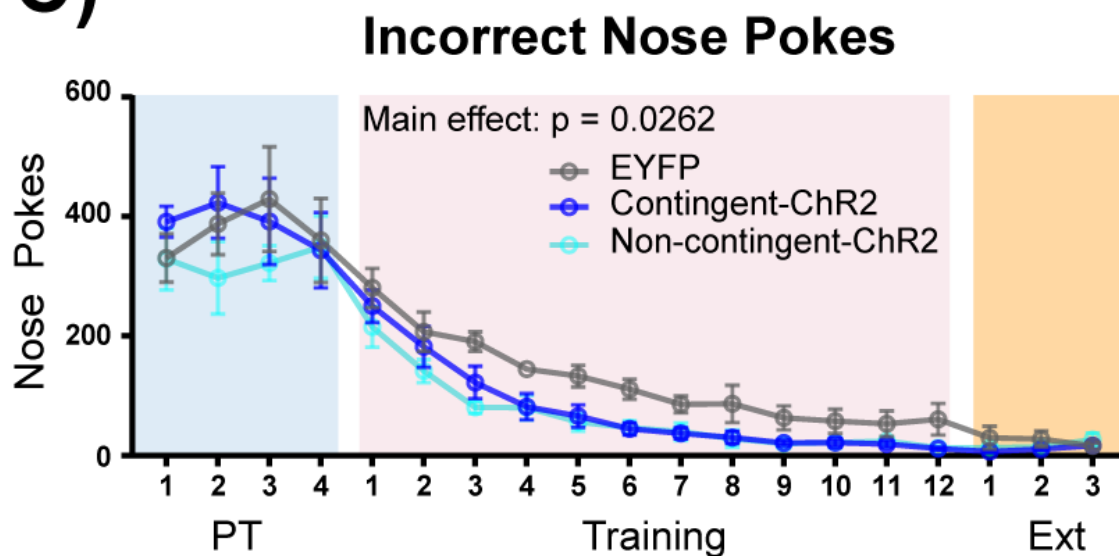
A) Non-Contingent-ChR2

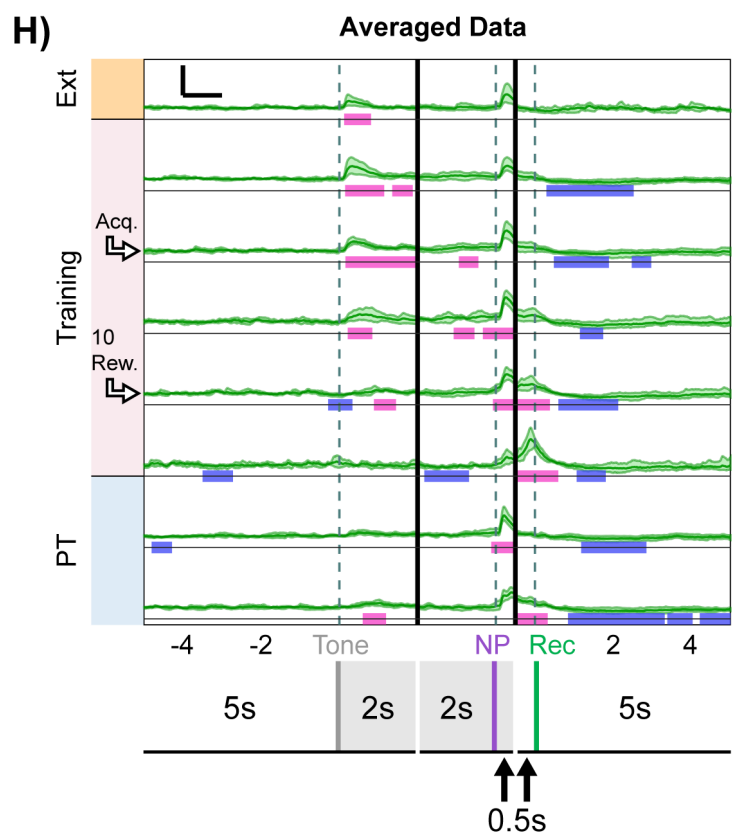
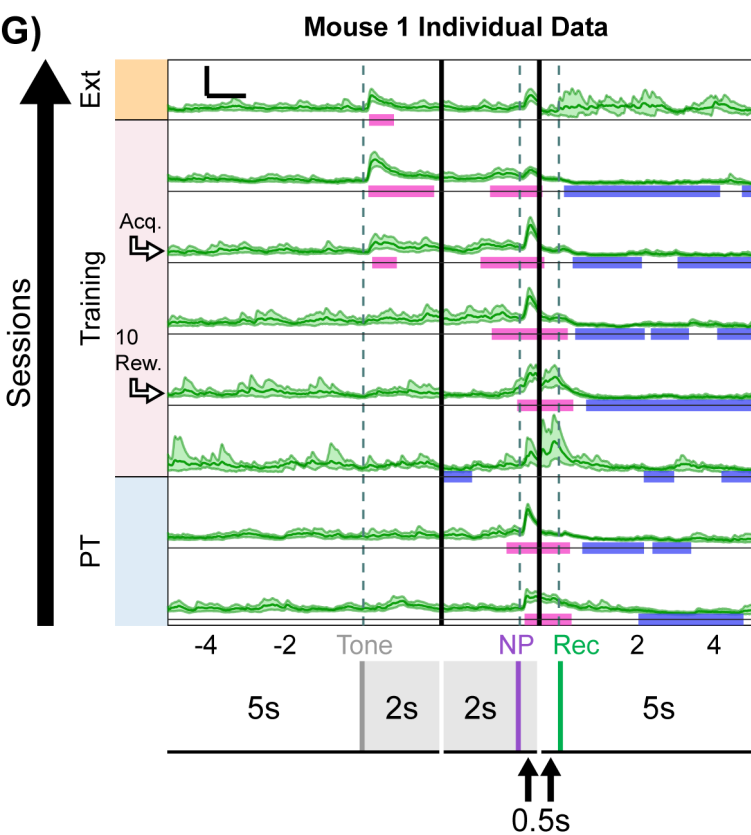
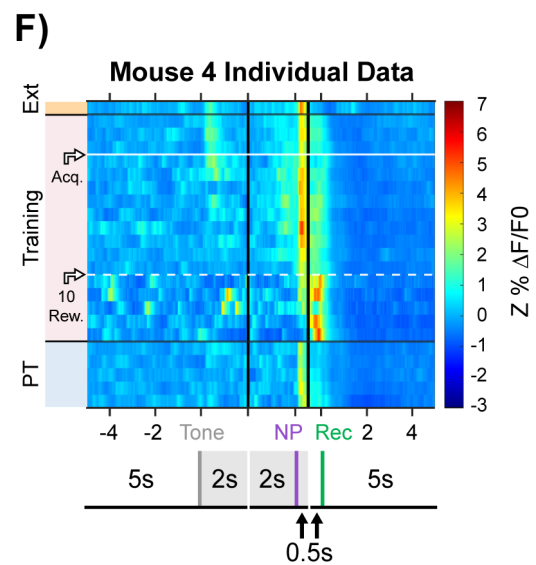
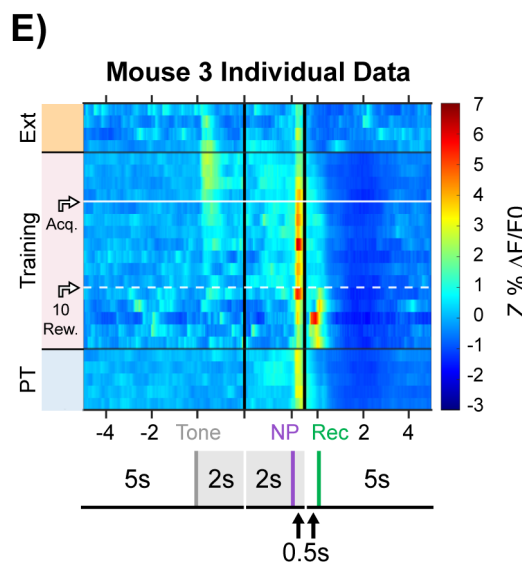
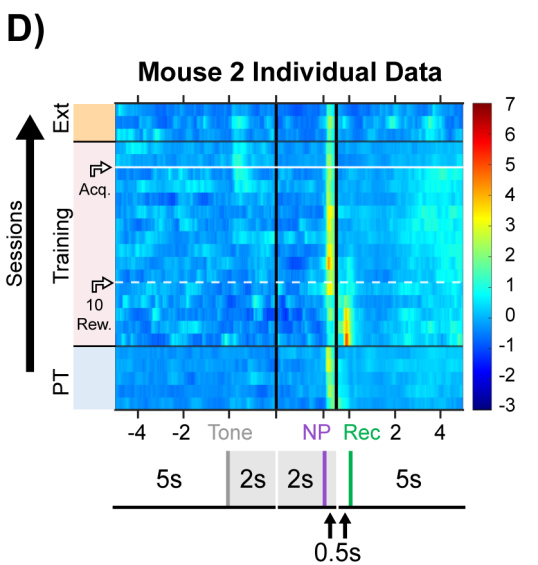
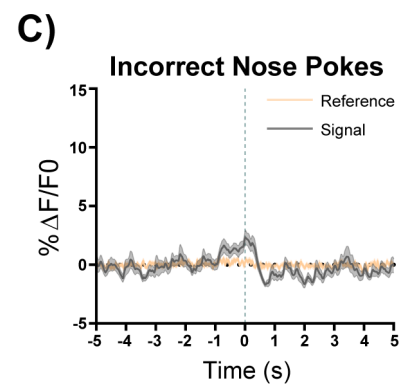
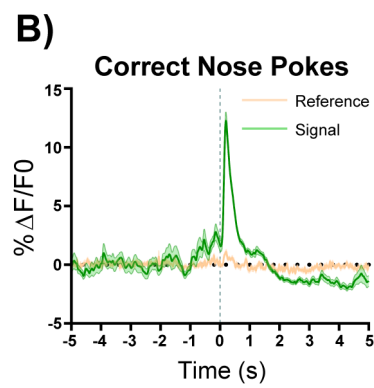
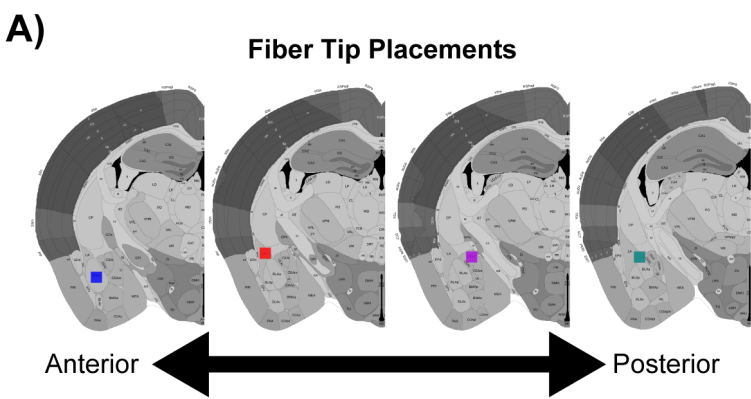


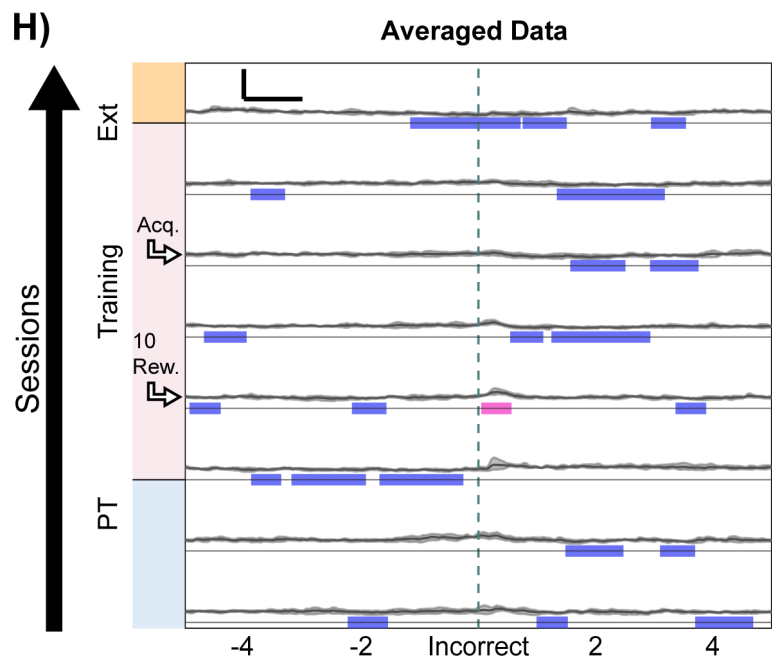
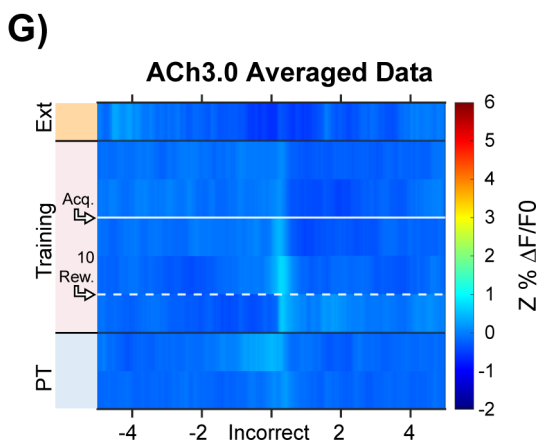
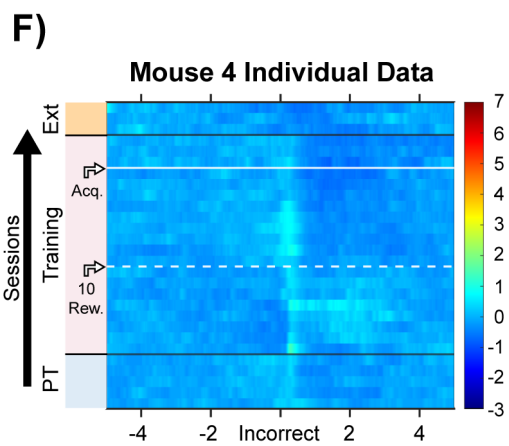
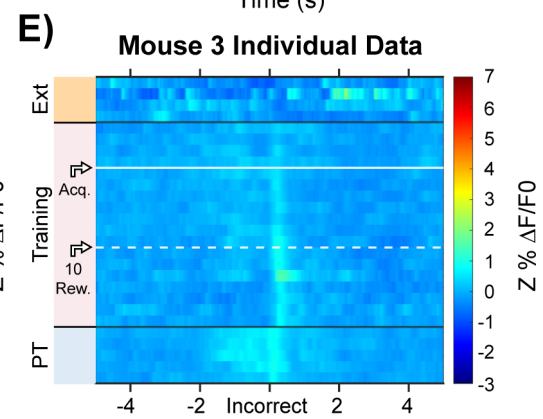
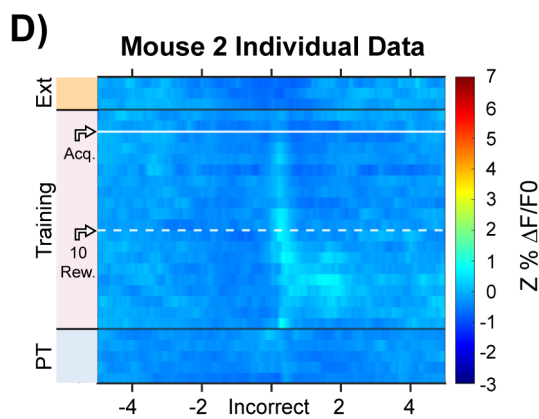
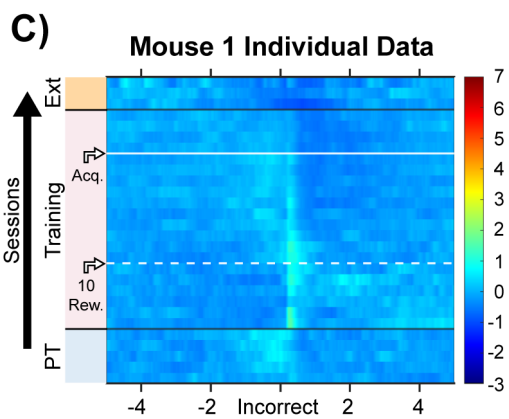
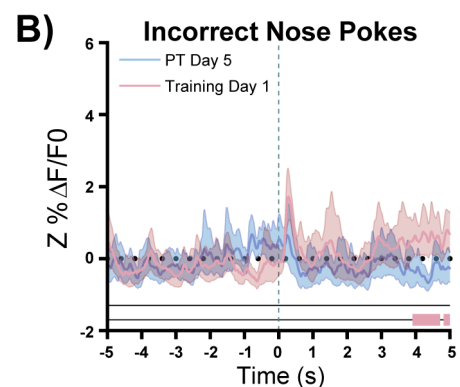
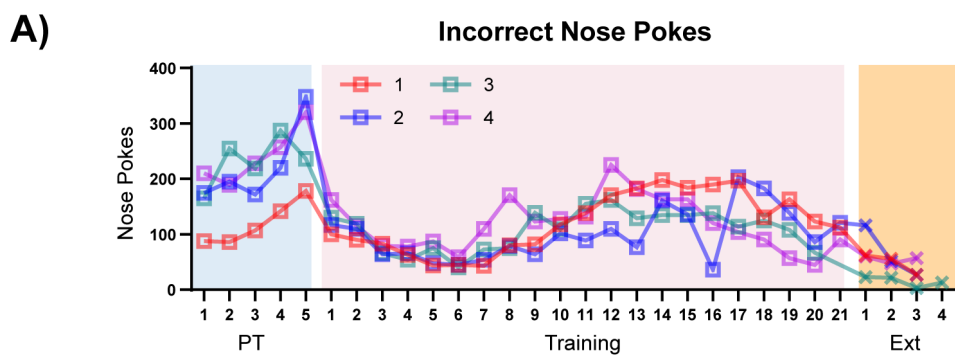
B)

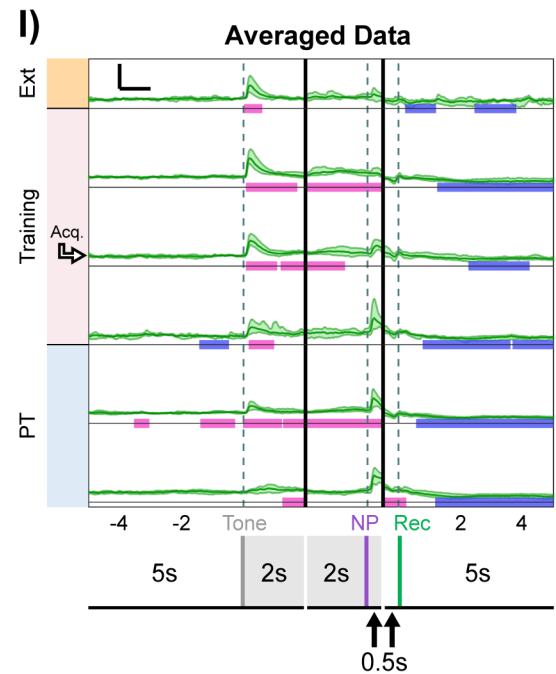
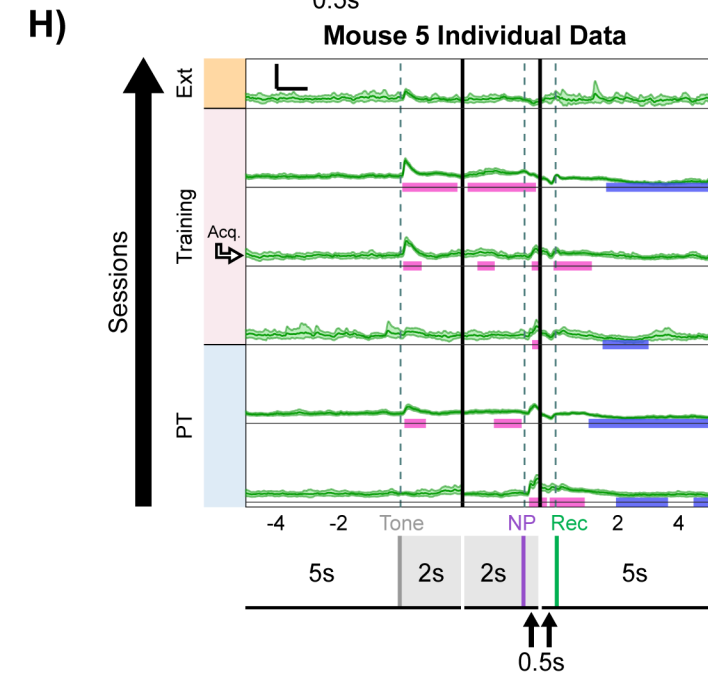
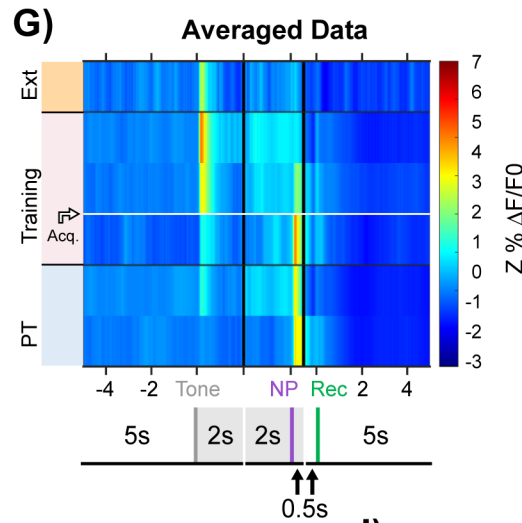
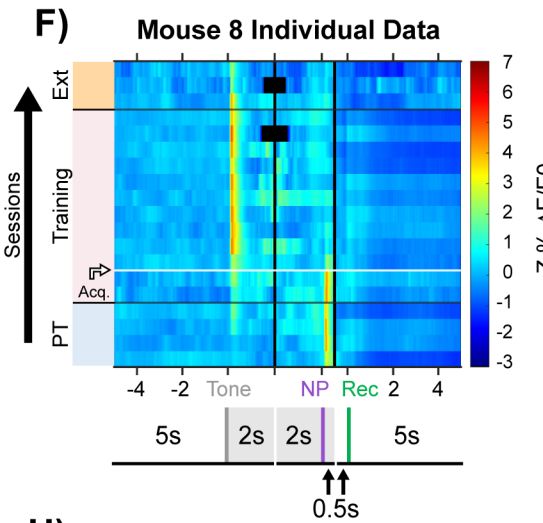
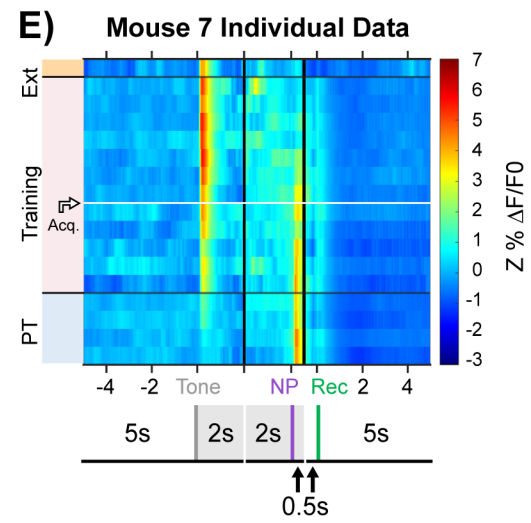
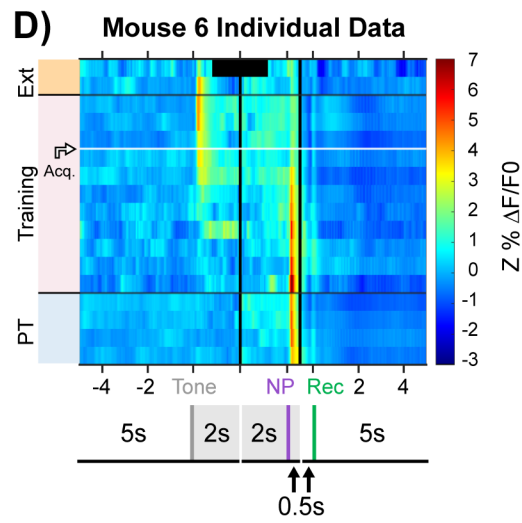
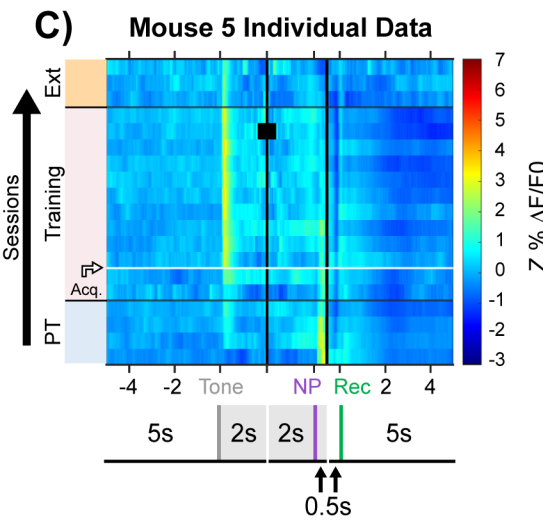
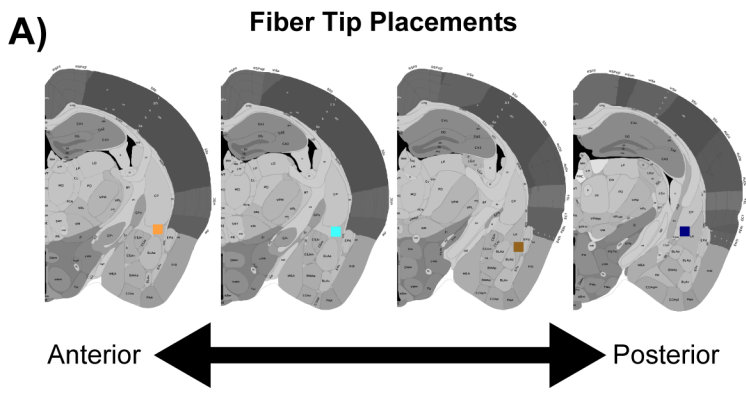


C)

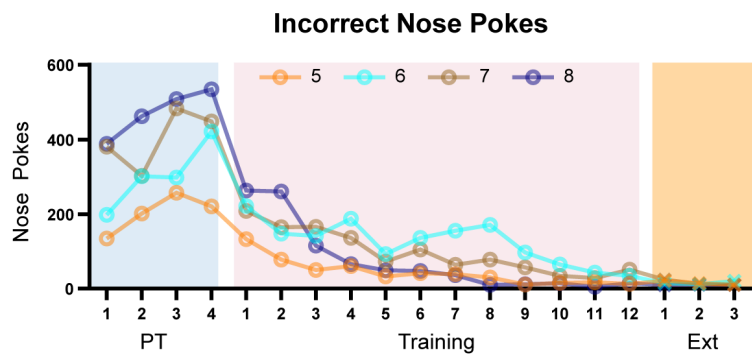




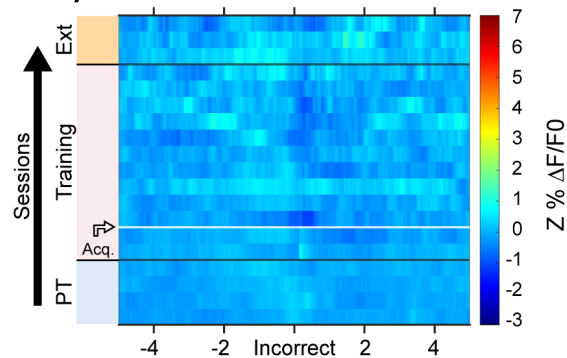




A)

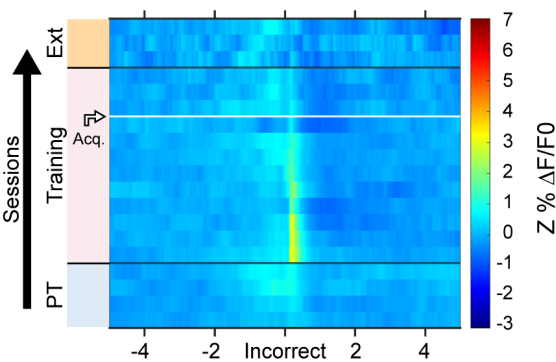


B) Mouse 5 Individual Data



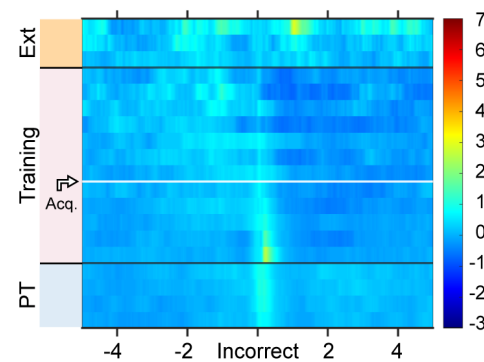
C)

Mouse 6 Individual Data



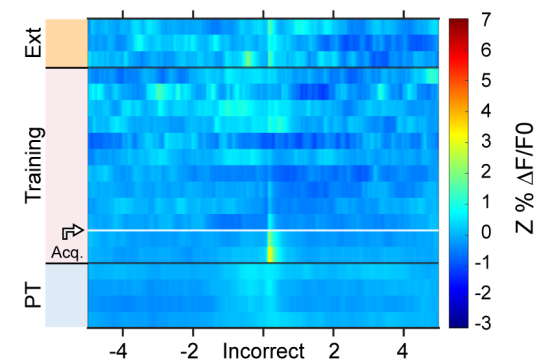
D)

Mouse 7 Individual Data



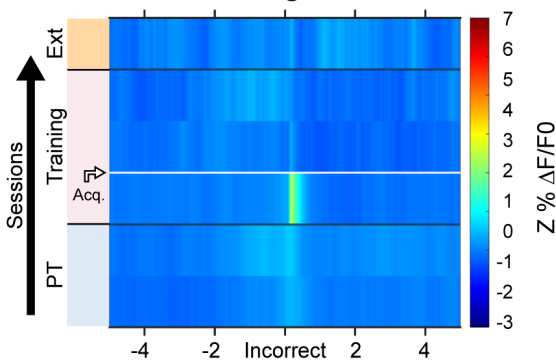
E)

Mouse 8 Individual Data



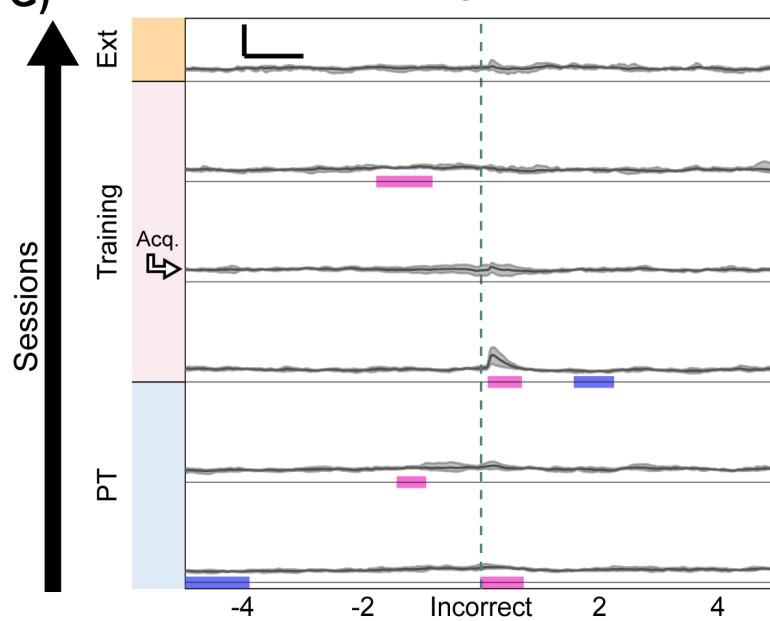
F)

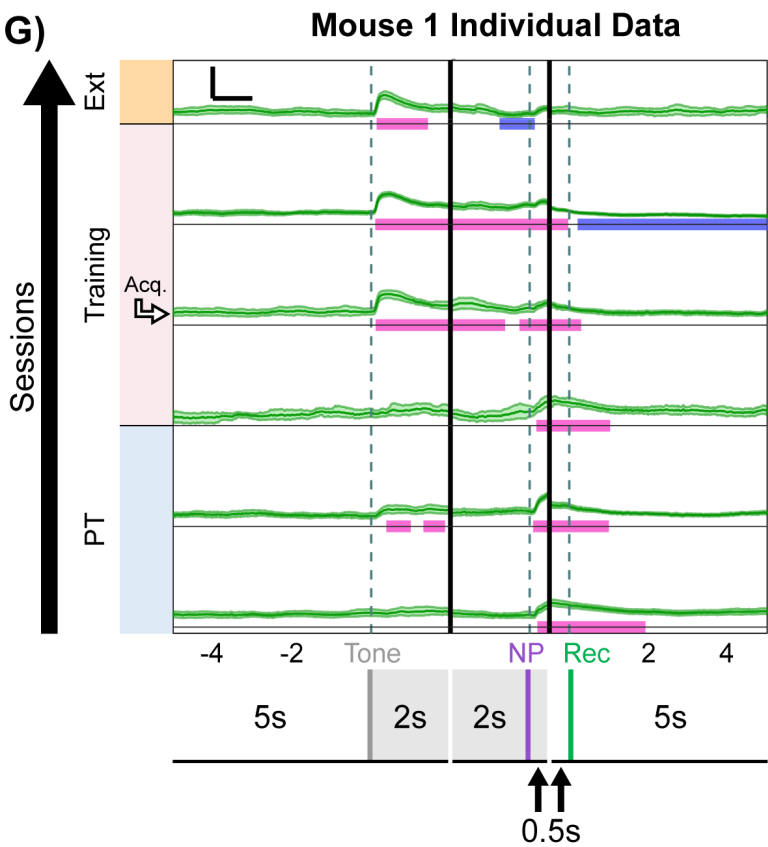
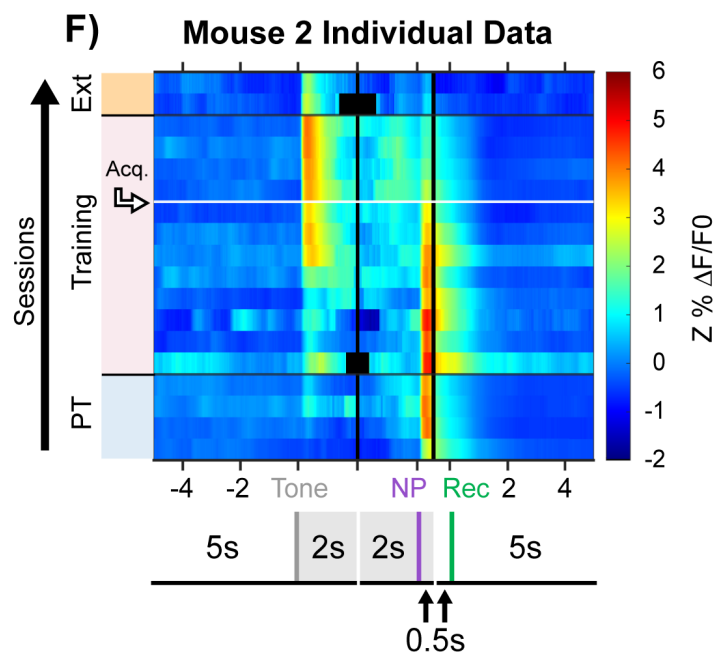
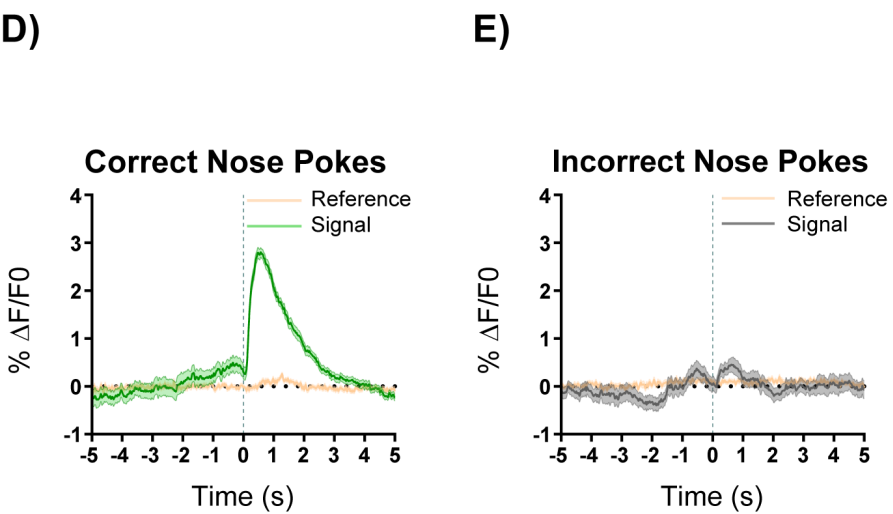
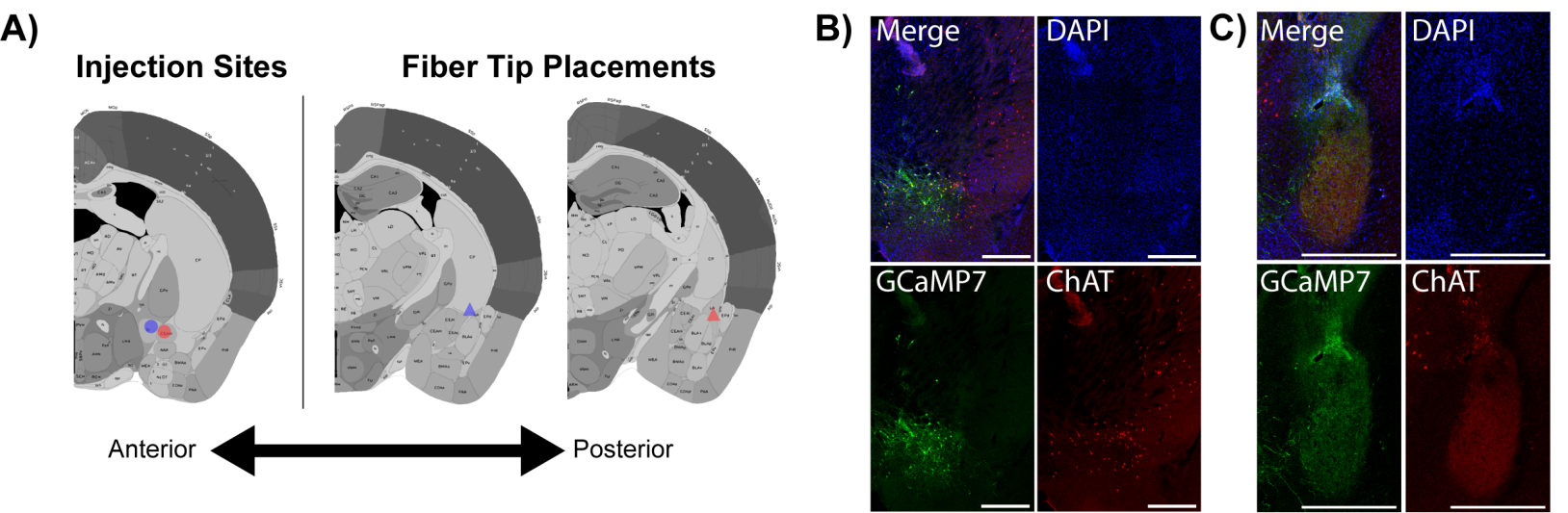
Averaged Data

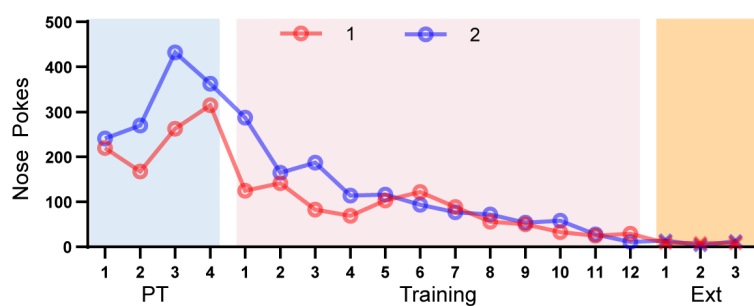
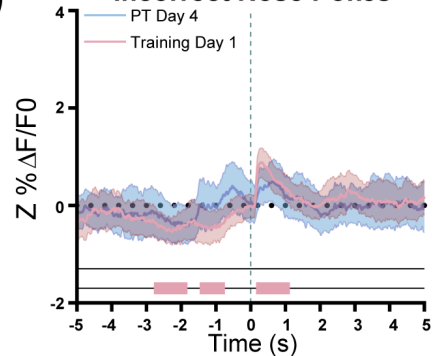
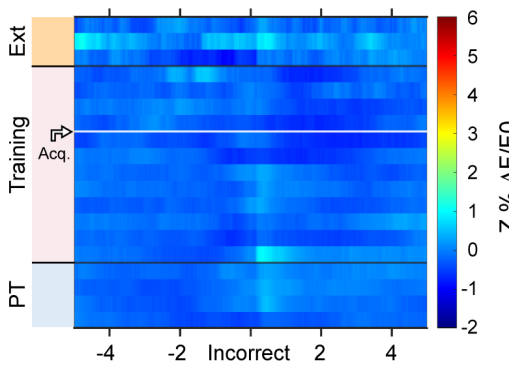
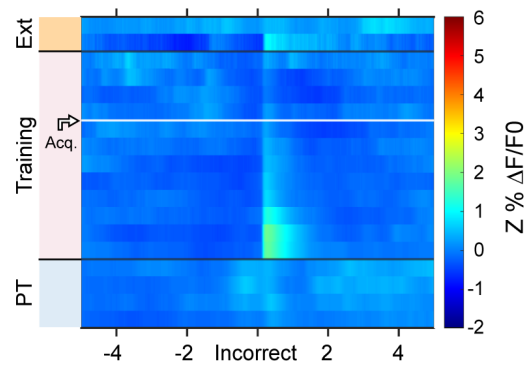
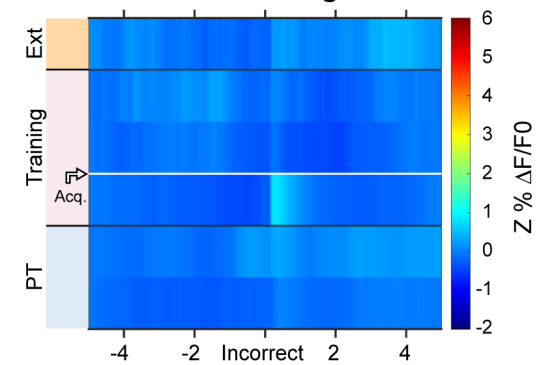


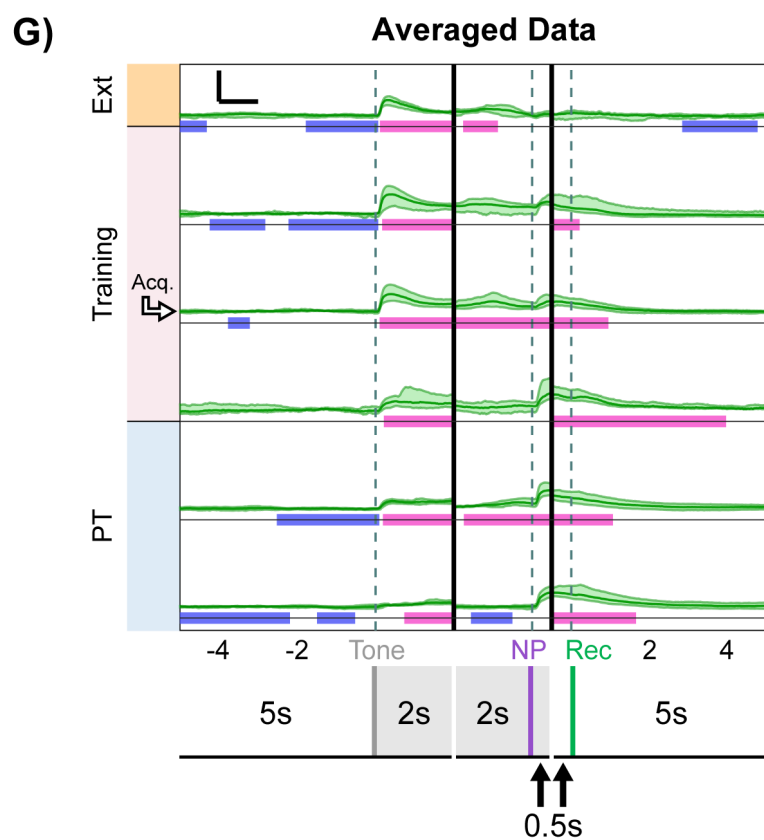
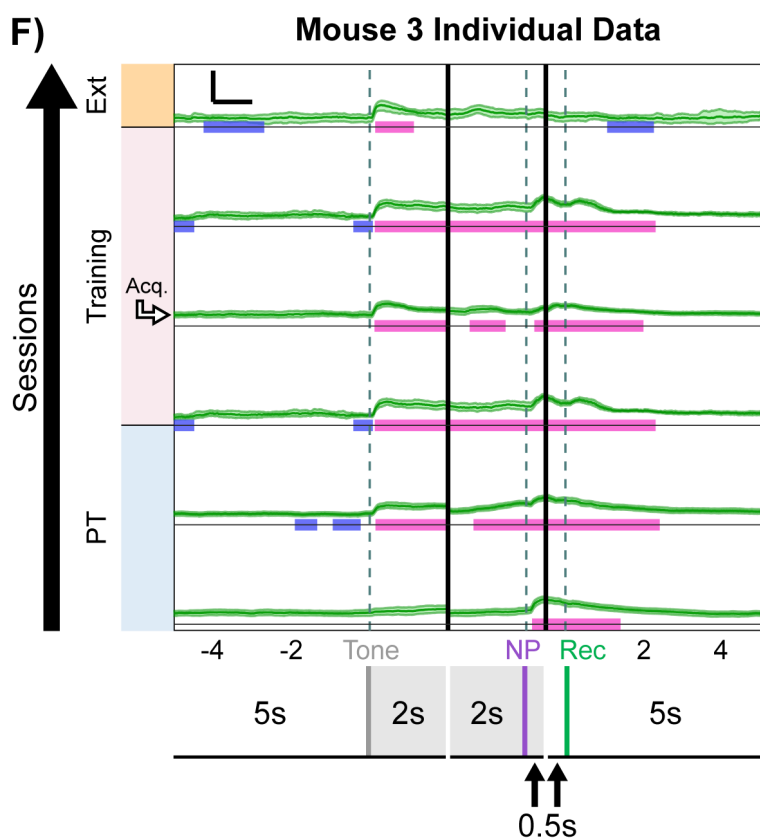
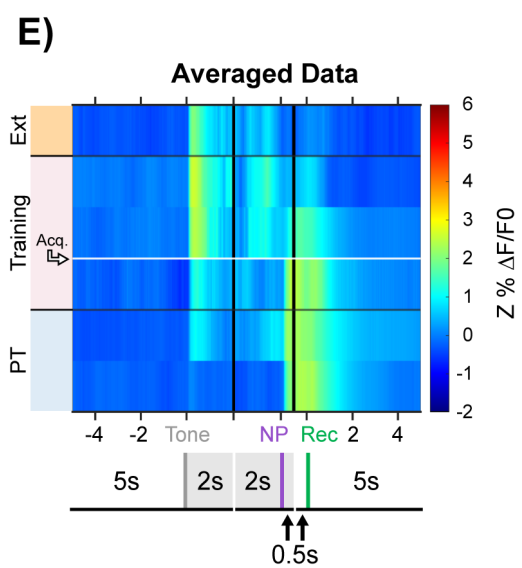
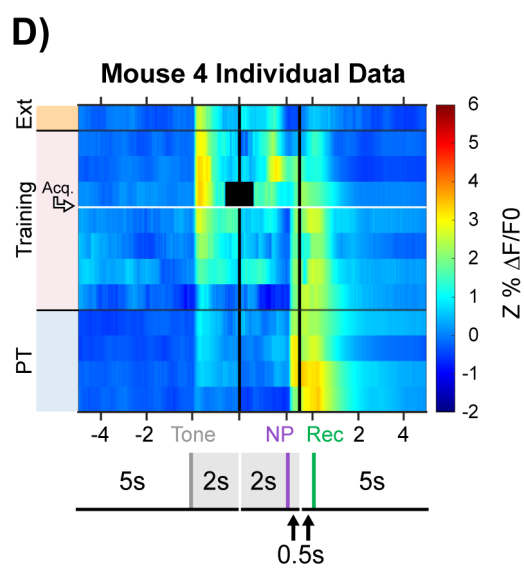
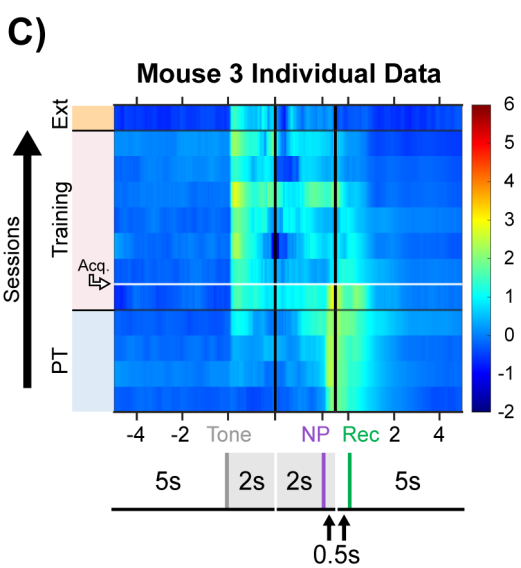
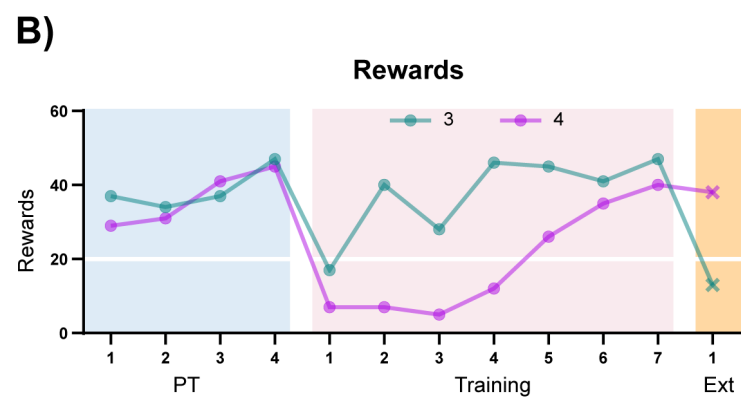
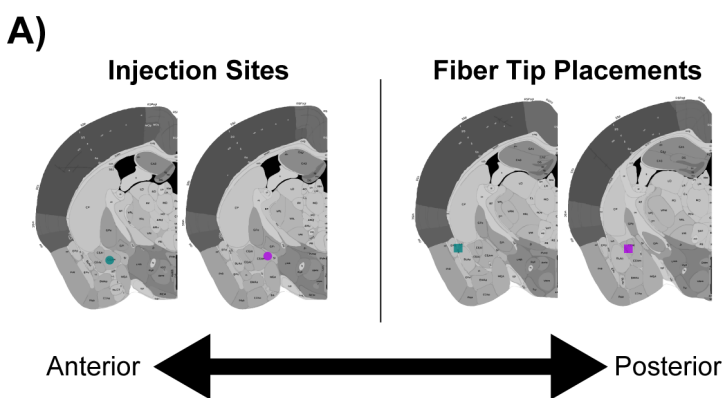
G)

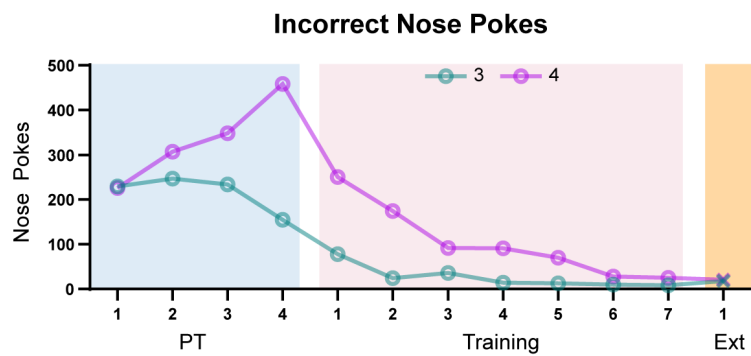
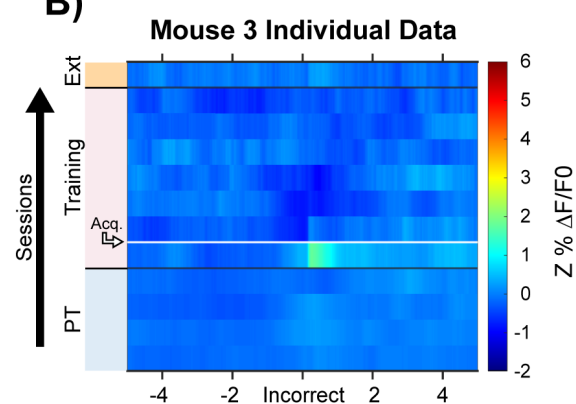
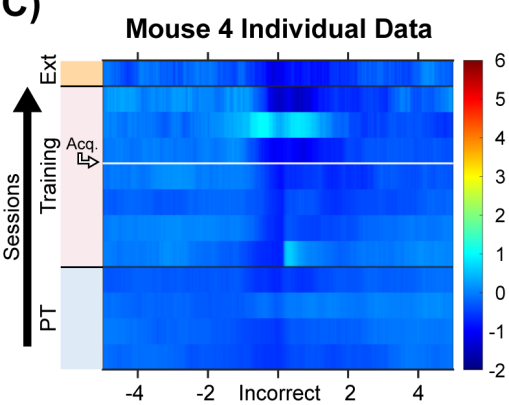
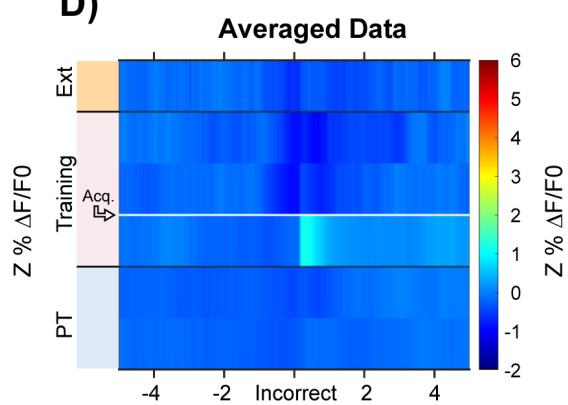
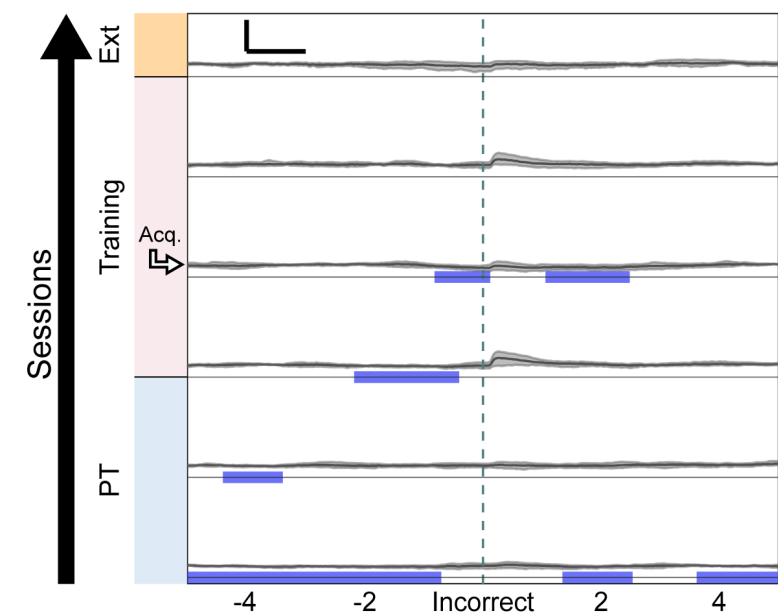
Averaged Data

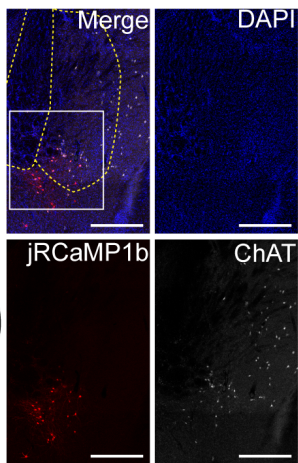
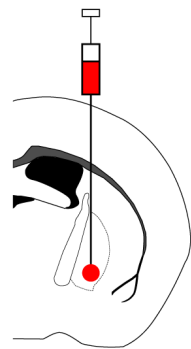
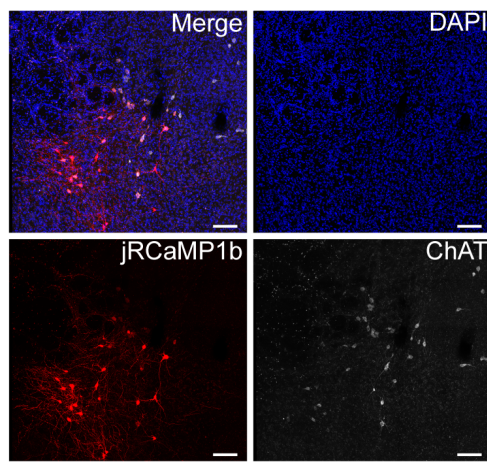
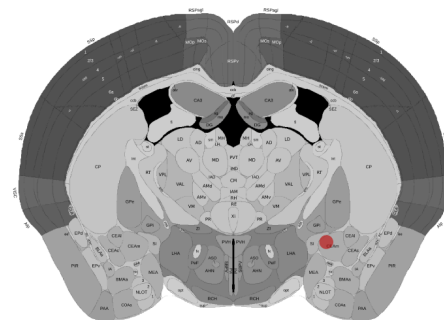
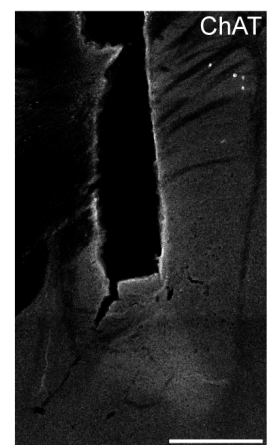
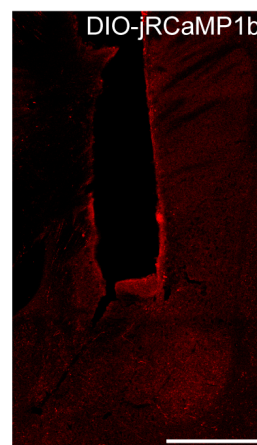
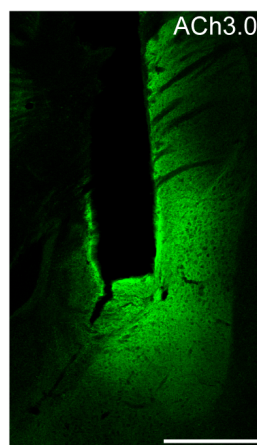
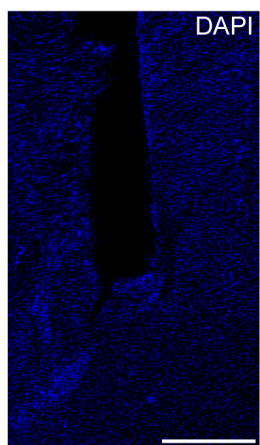
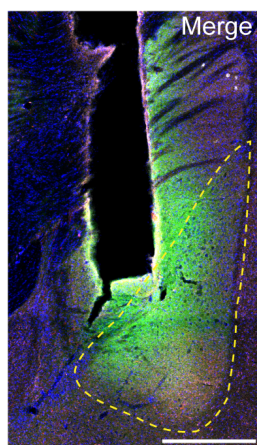
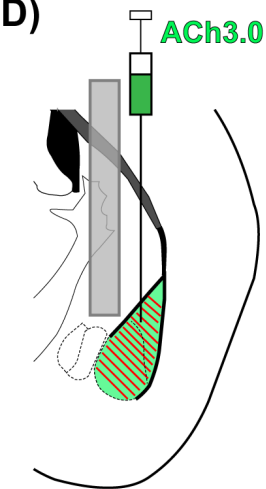
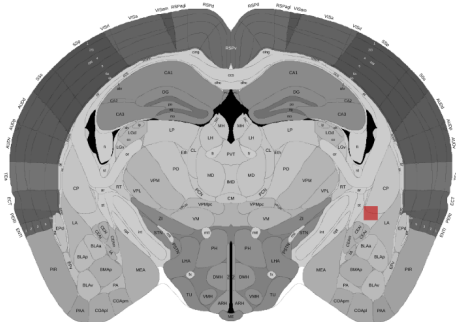
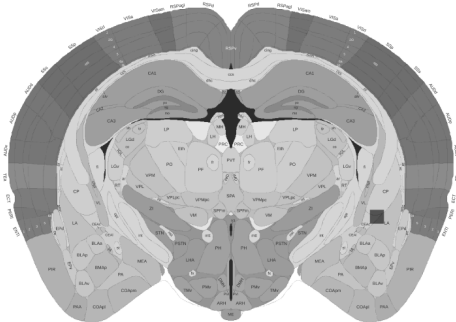
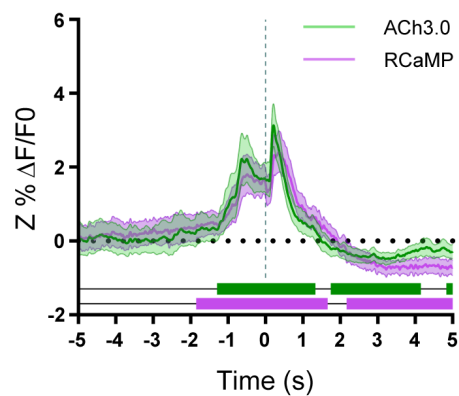
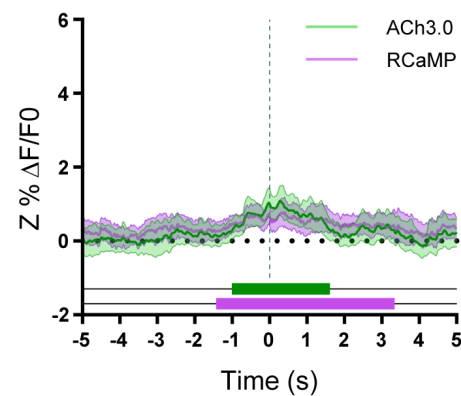
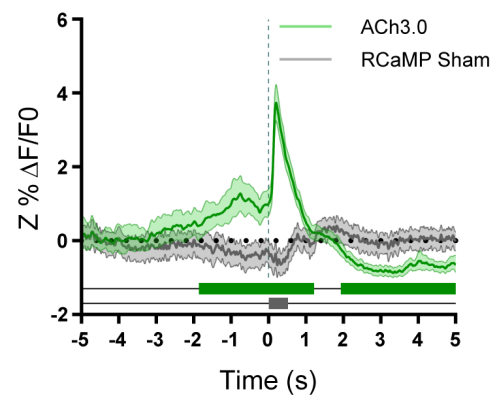
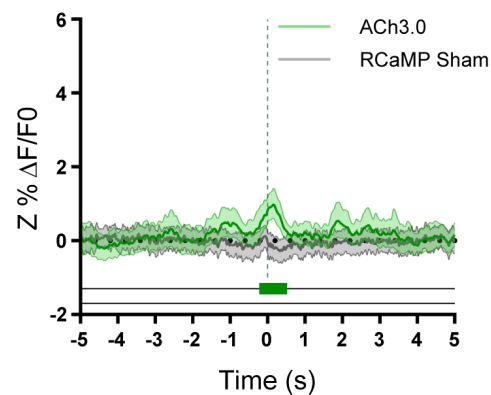


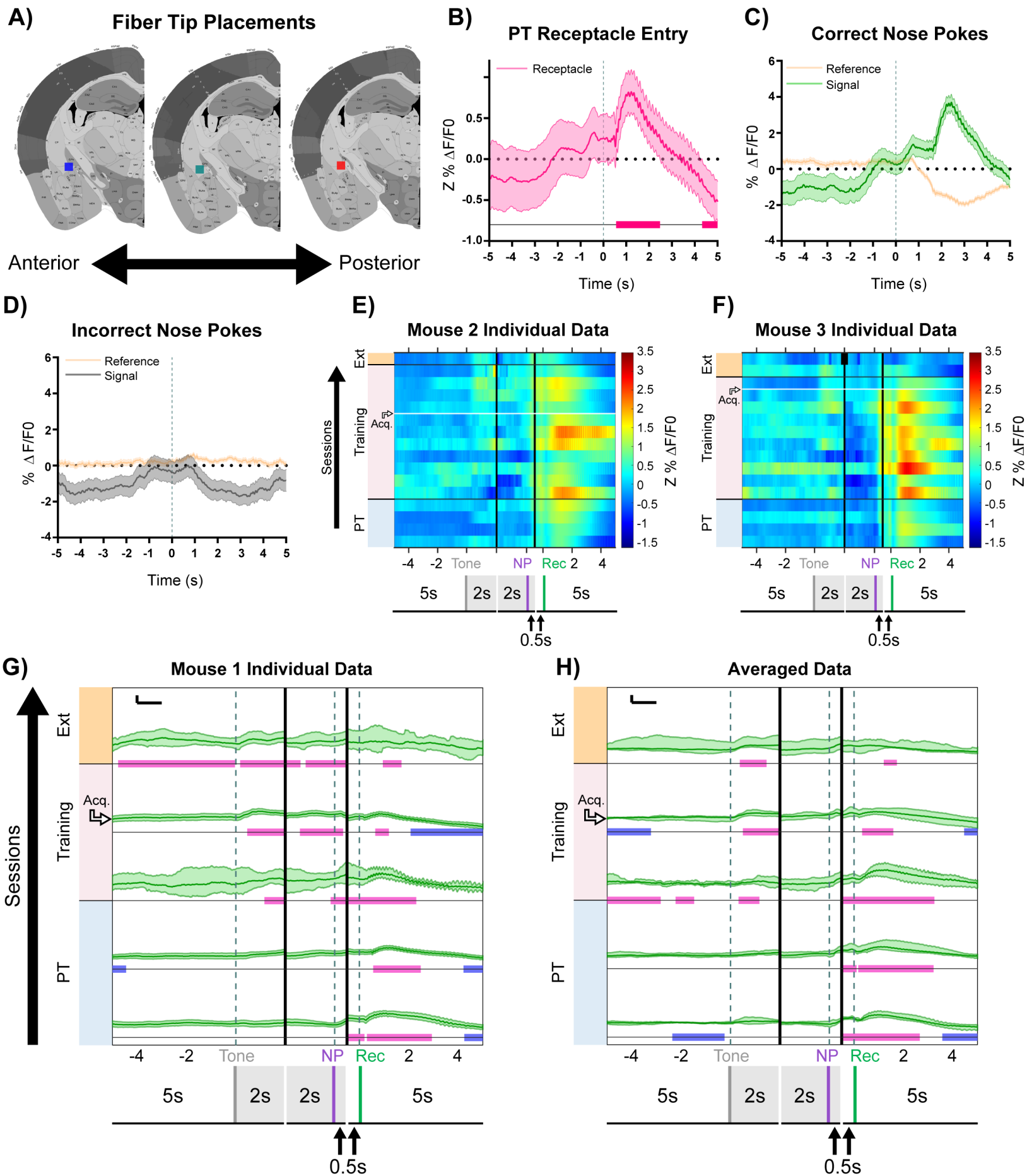


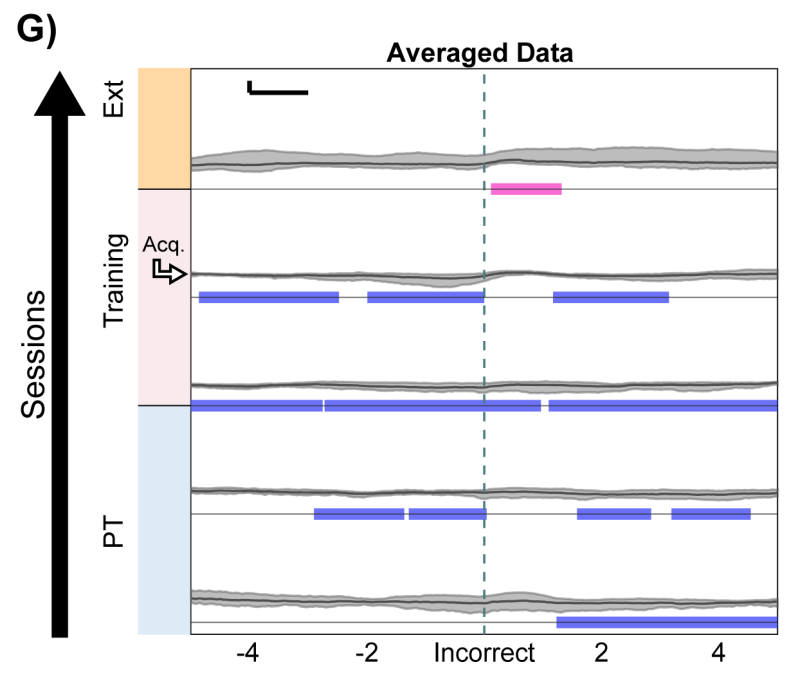
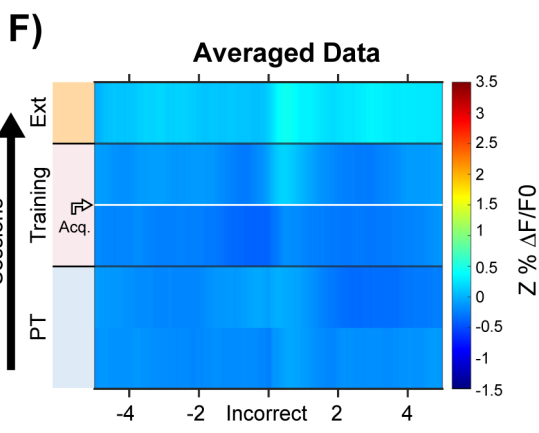
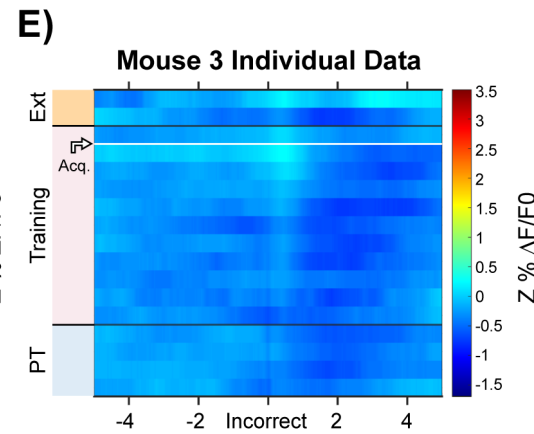
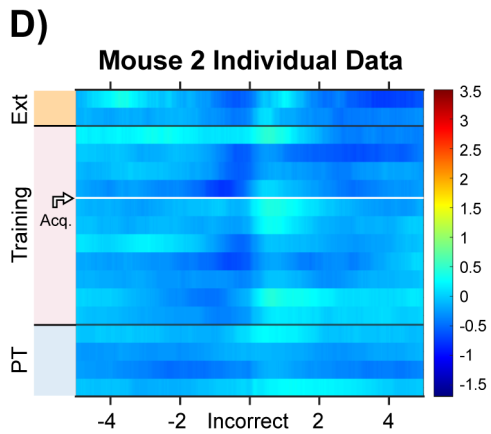
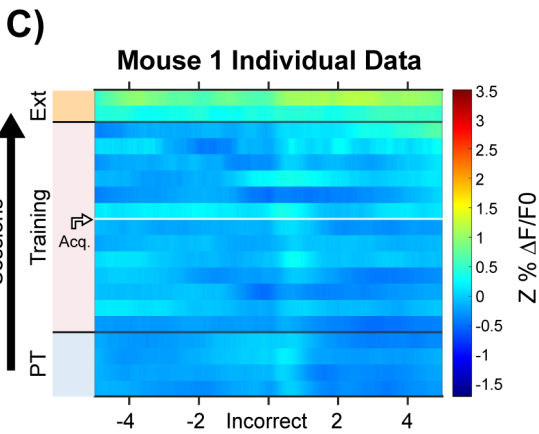
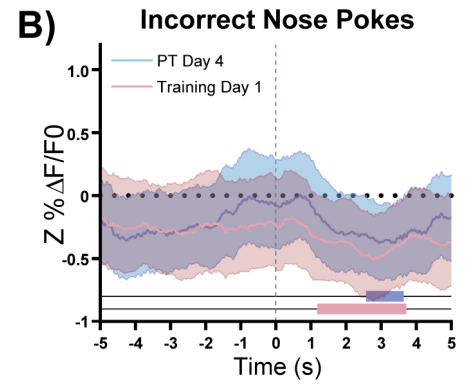
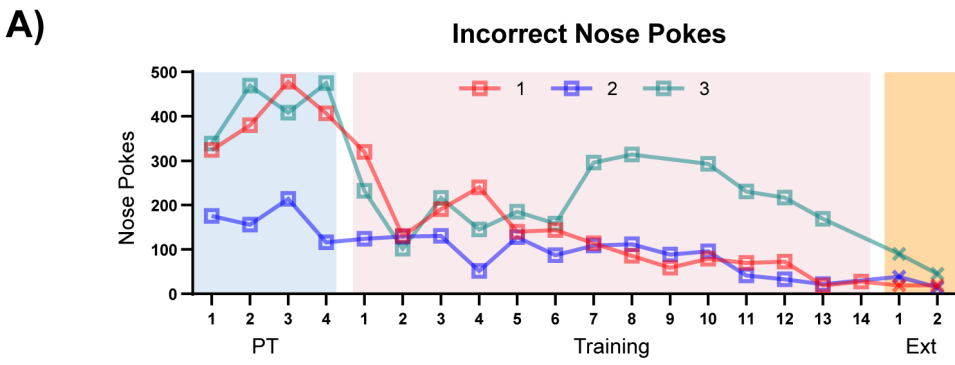
A)**Incorrect Nose Pokes****B)****Incorrect Nose Pokes****C)****Mouse 1 Individual Data****D)****Mouse 2 Individual Data****E)****NBM-BLA Averaged Data**

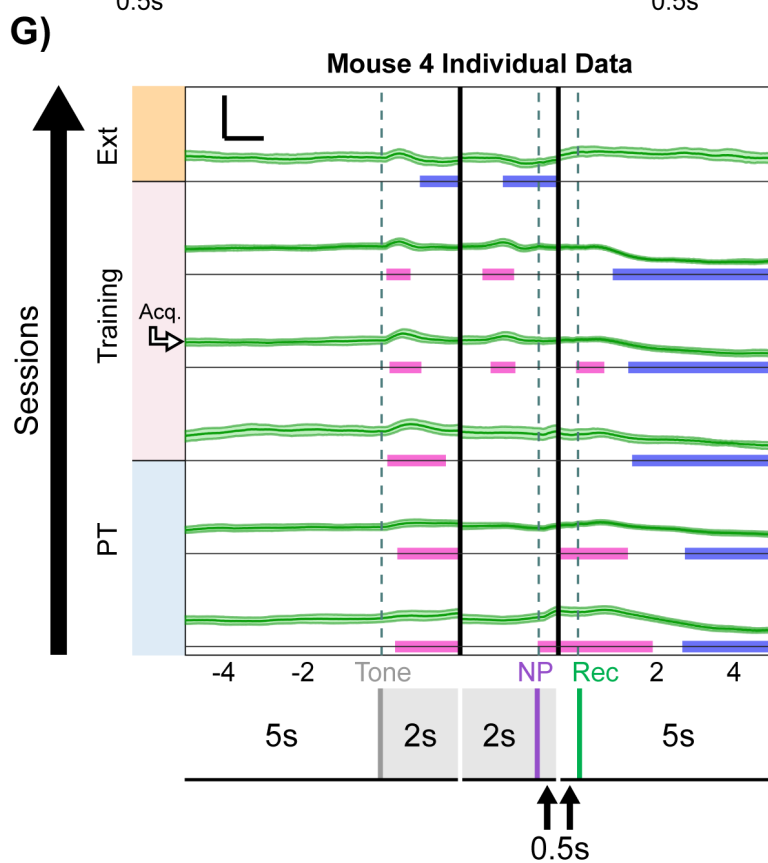
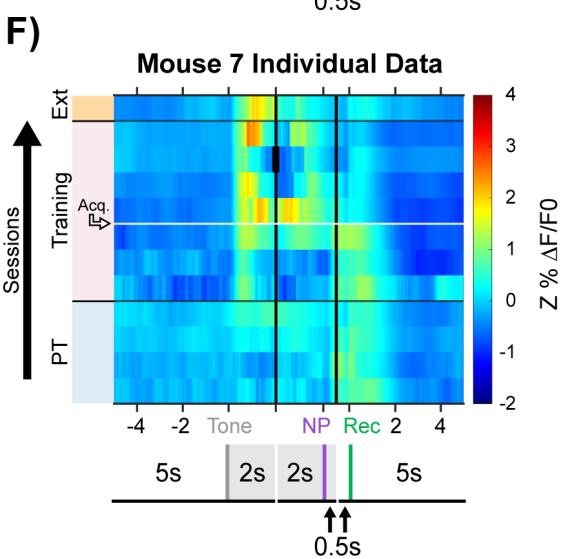
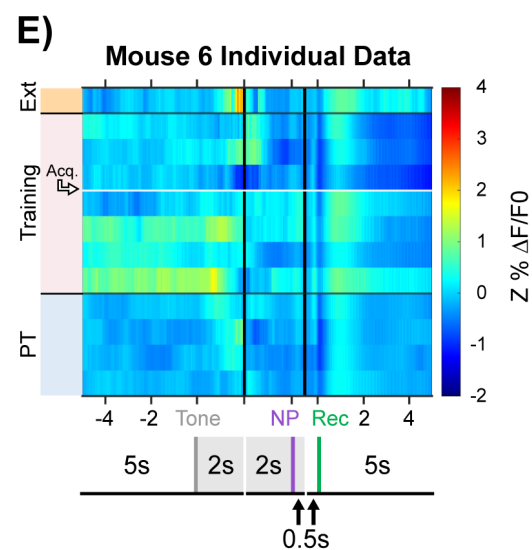
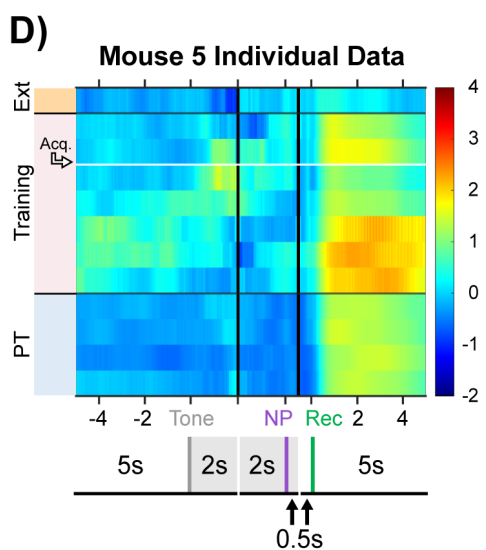
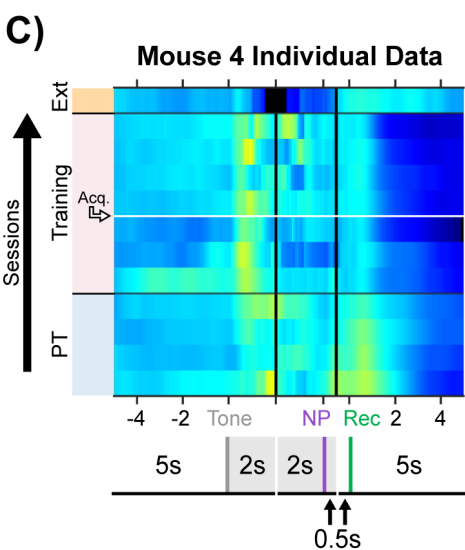
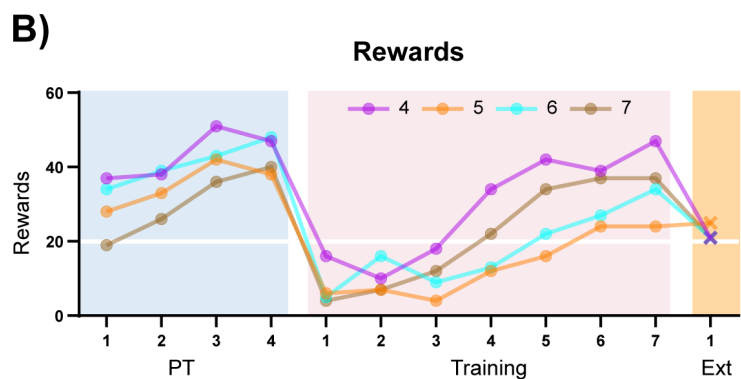
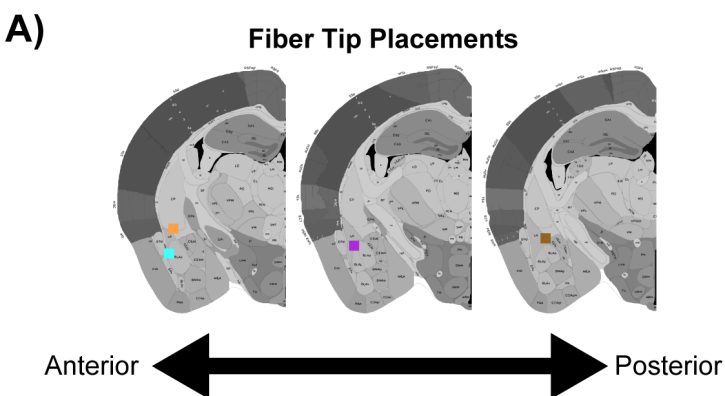


A)**B)****C)****D)****E)****Averaged Data**

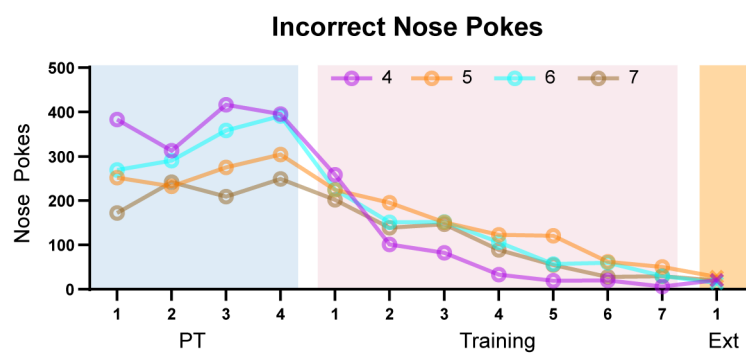
A)**DIO-jRCaMP1b****B)****C)****Injection Site****D)****ACh3.0****E) Fiber Tip Placements****ACh3.0 + RCaMP****ACh3.0 + RCaMP sham****F)****Correct Nose Pokes****G)****Incorrect Nose Pokes****H)****Correct Nose Pokes****I)****Incorrect Nose Pokes**



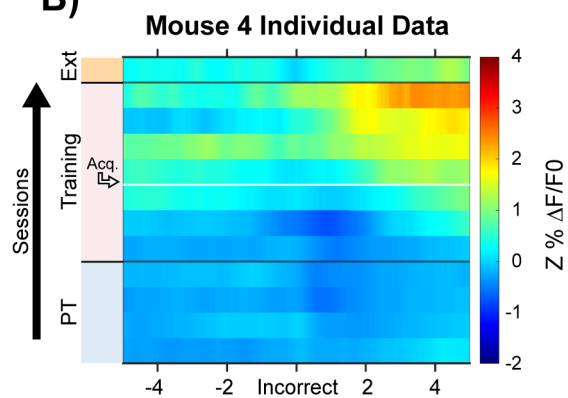




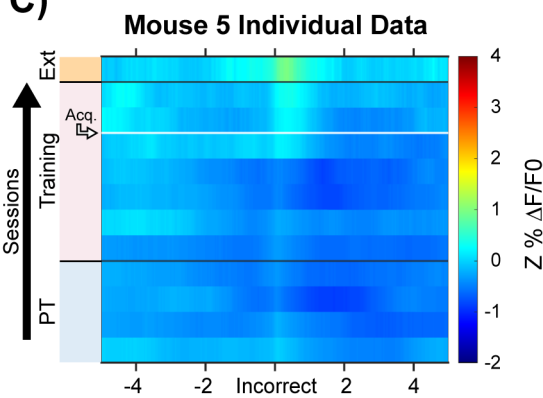
A)



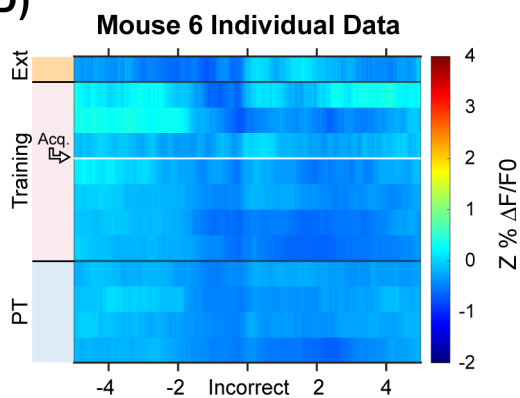
B)



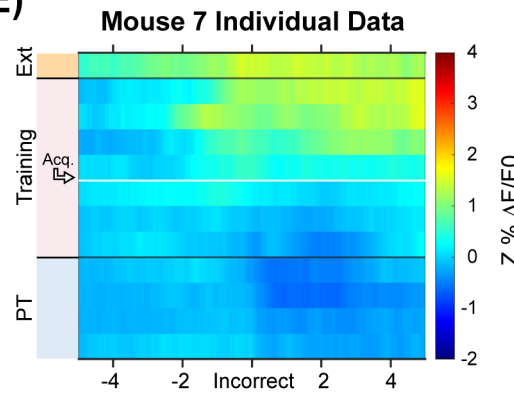
C)

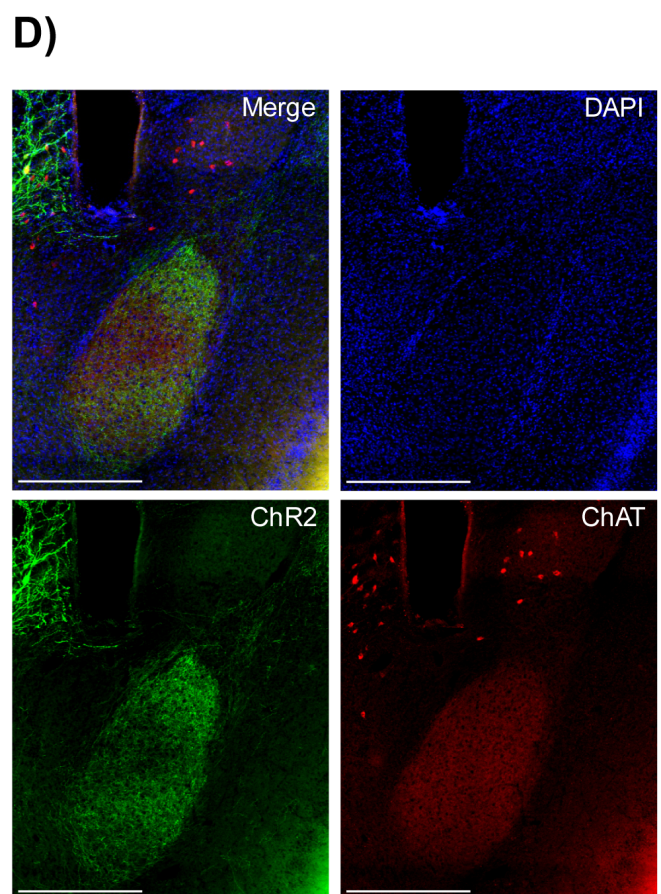
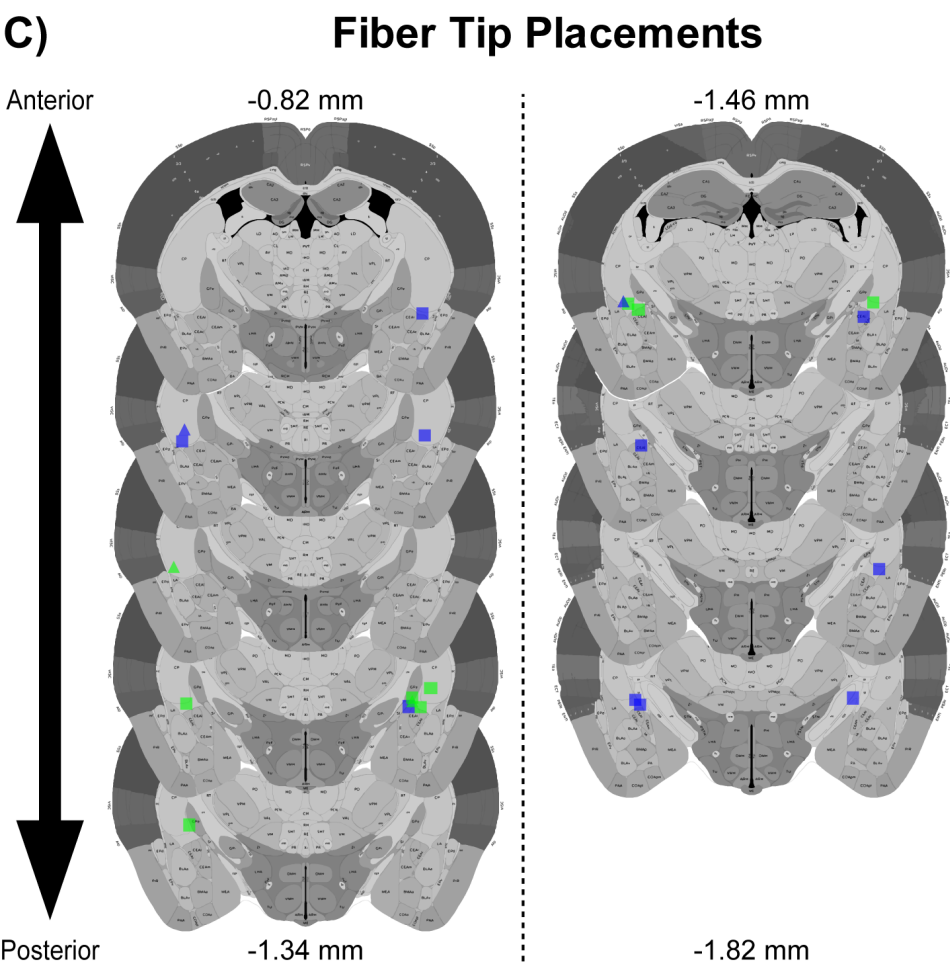
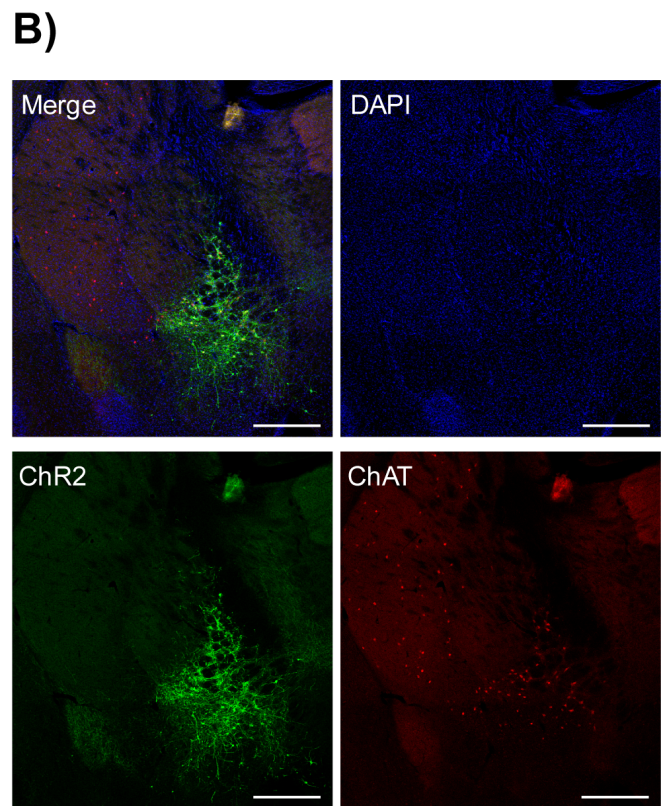
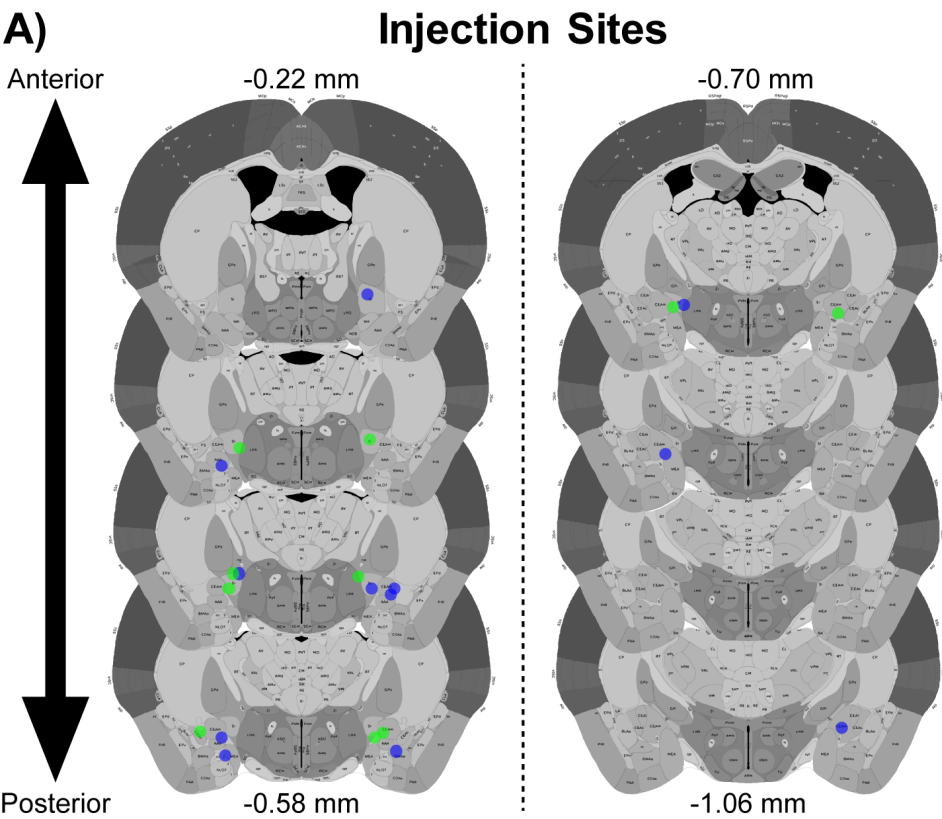


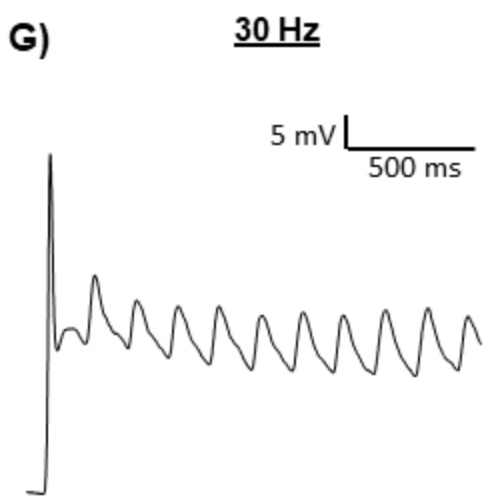
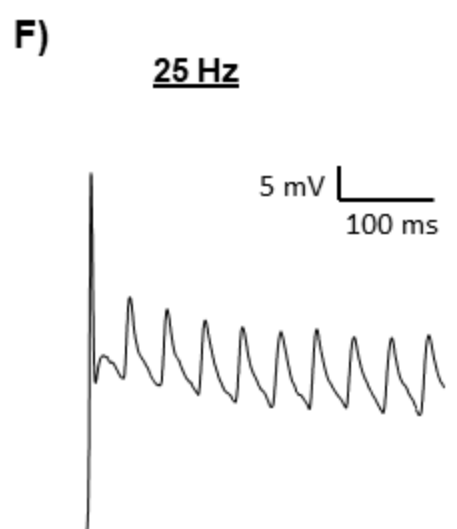
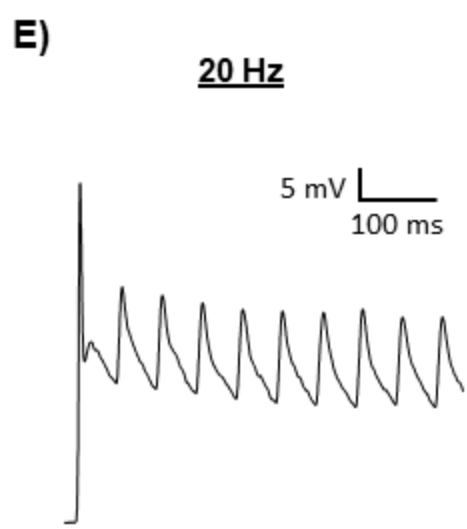
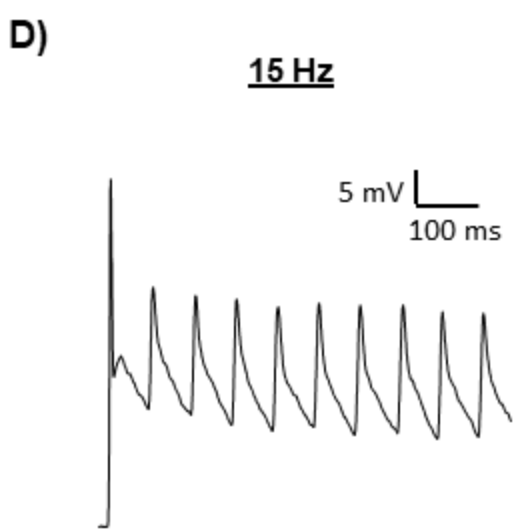
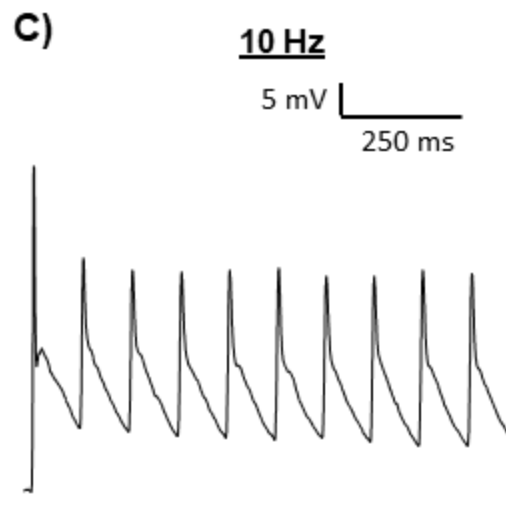
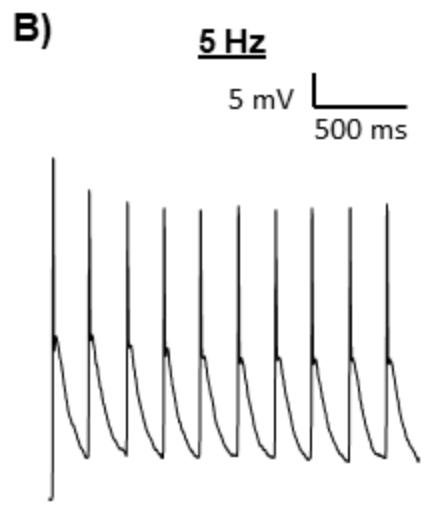
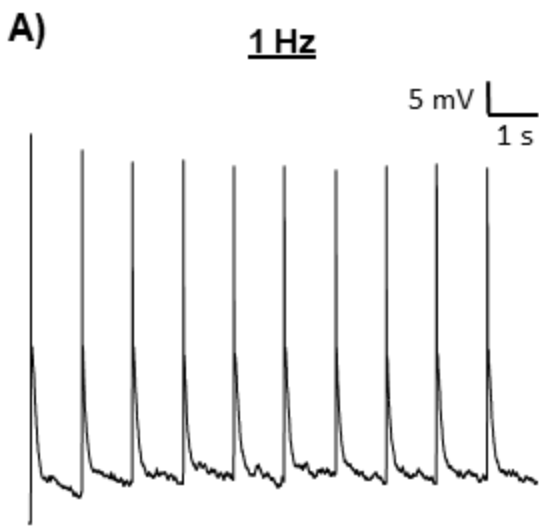
D)

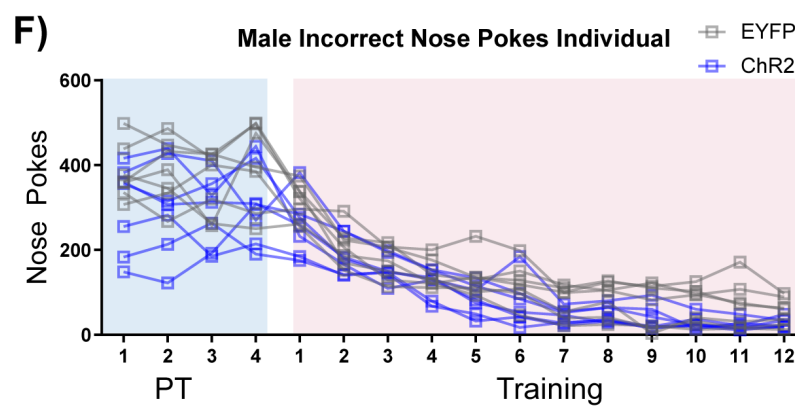
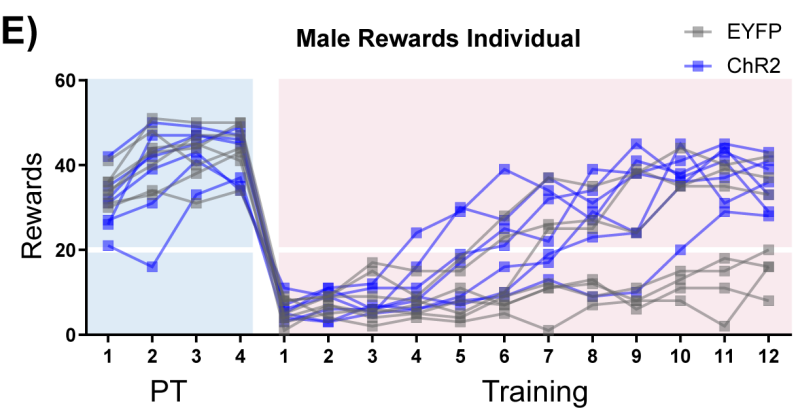
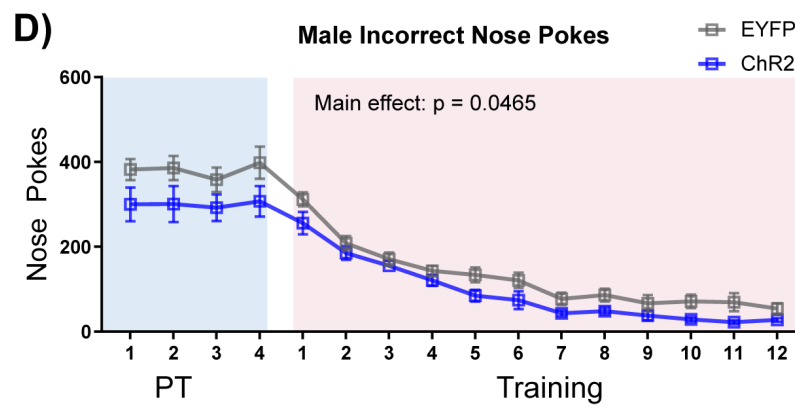
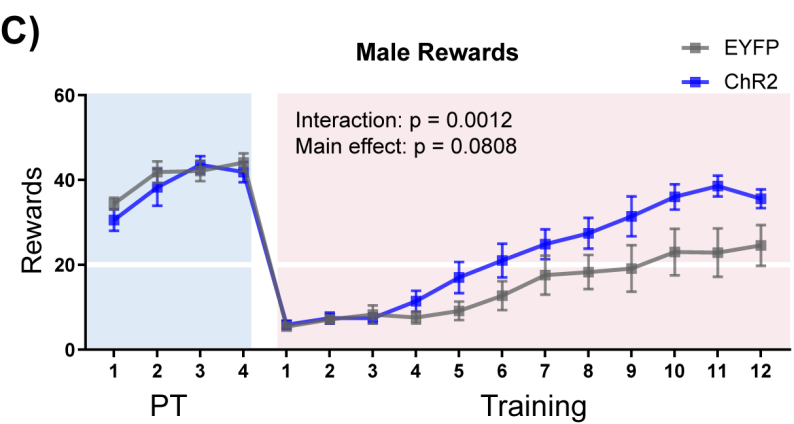
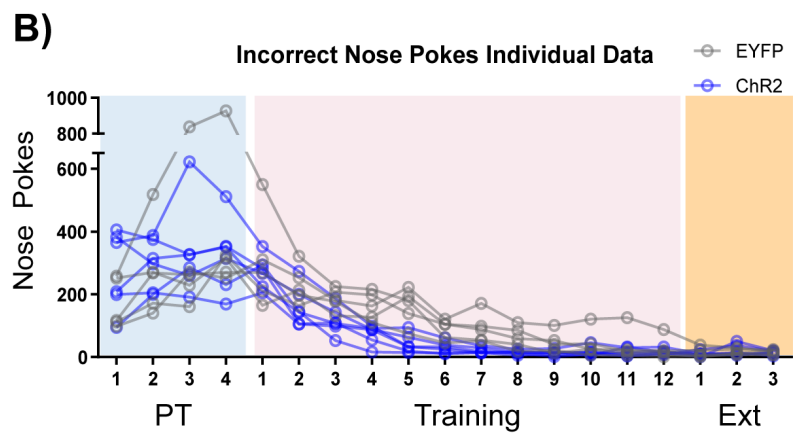
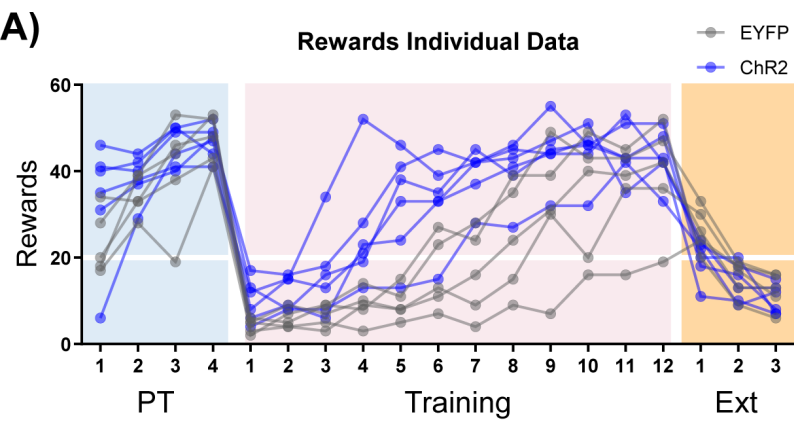


E)





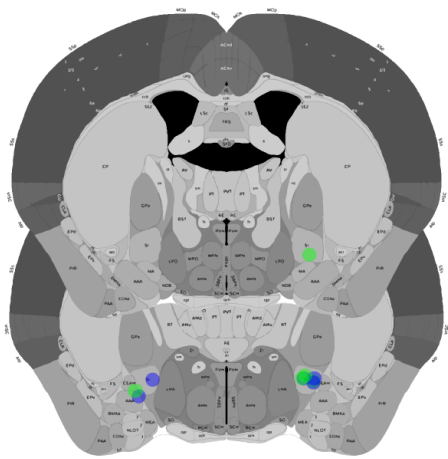




A)

Anterior

-0.22 mm

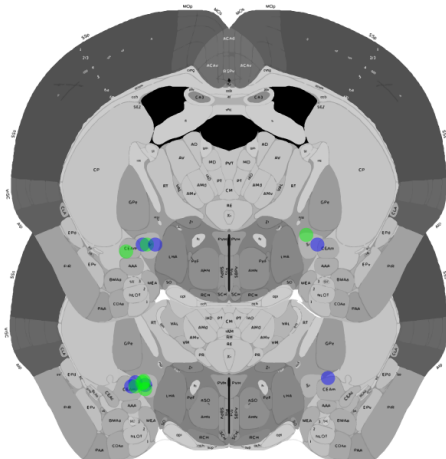


Posterior

-0.34 mm

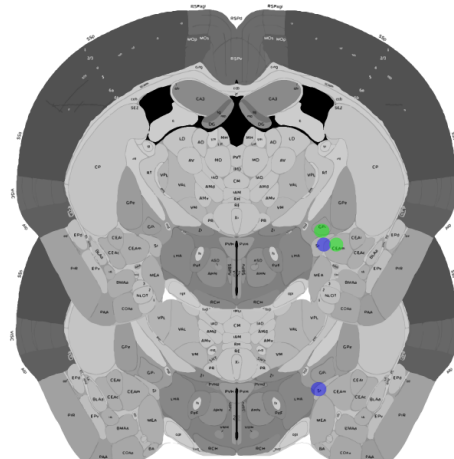
Injection Sites

-0.46 mm



-0.58 mm

-0.70 mm

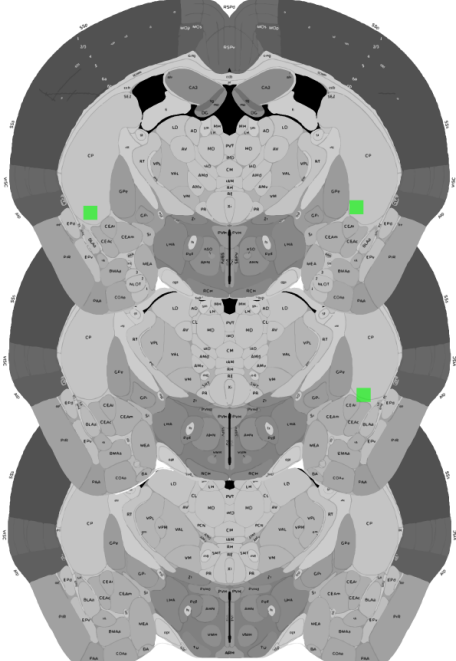


-0.82 mm

B)

Anterior

-0.70 mm

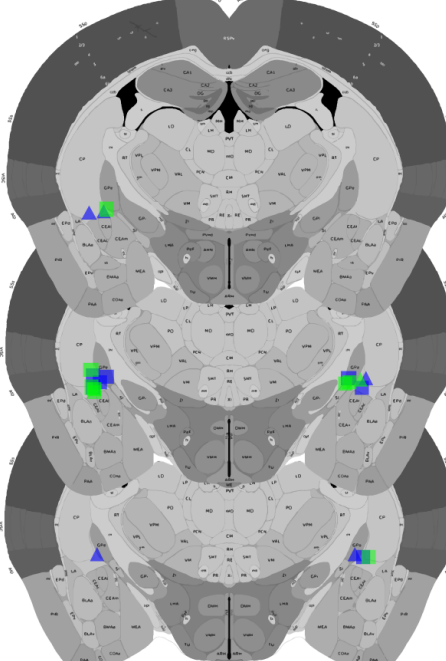


Posterior

-0.94 mm

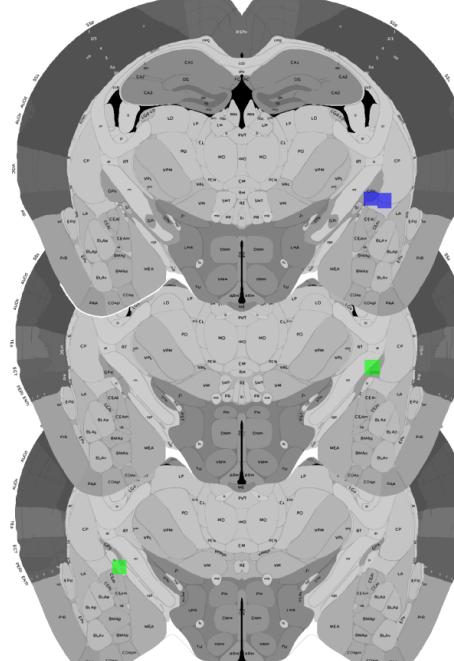
Fiber Tip Placements

-1.06 mm

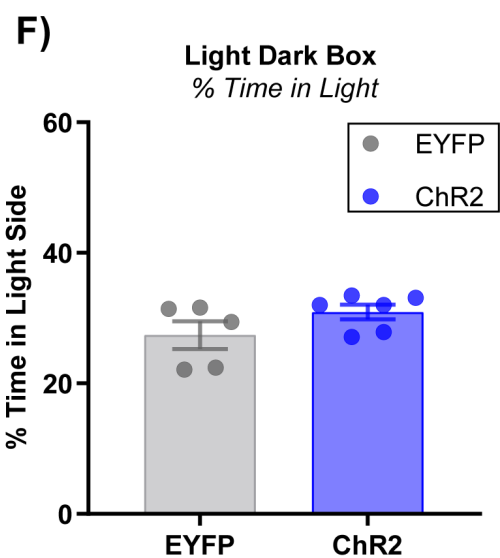
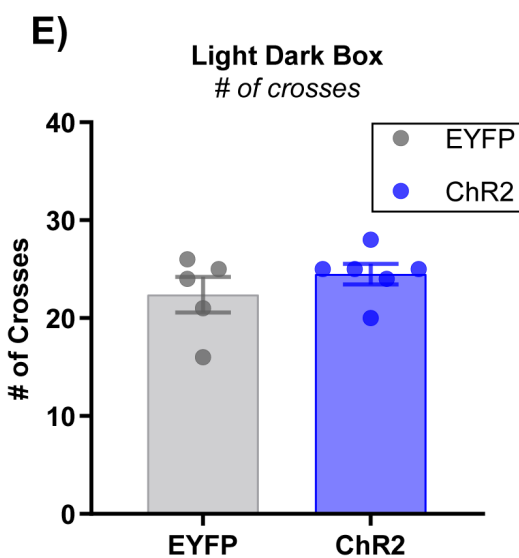
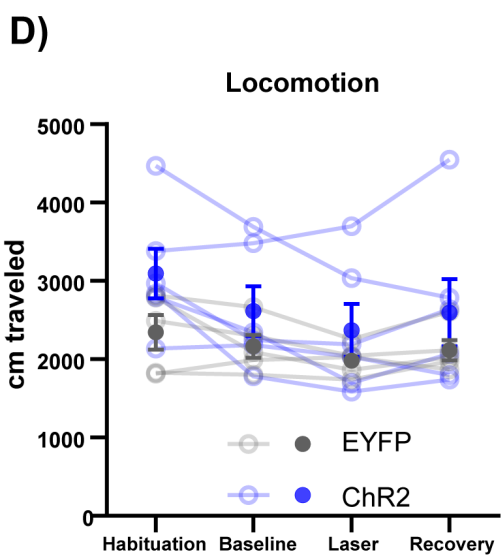
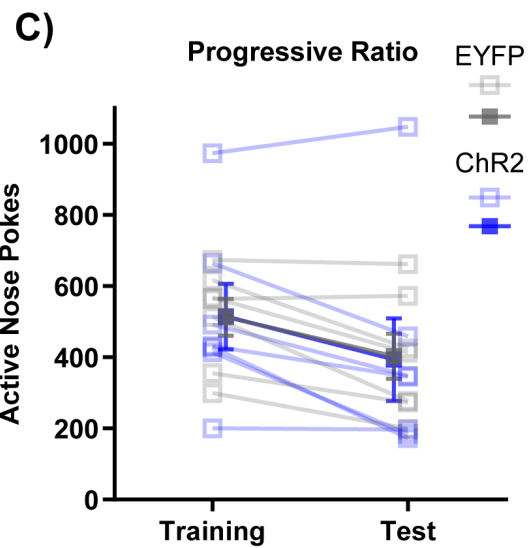
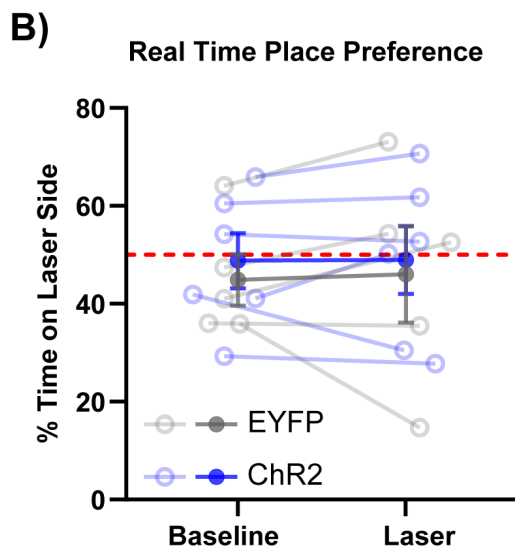
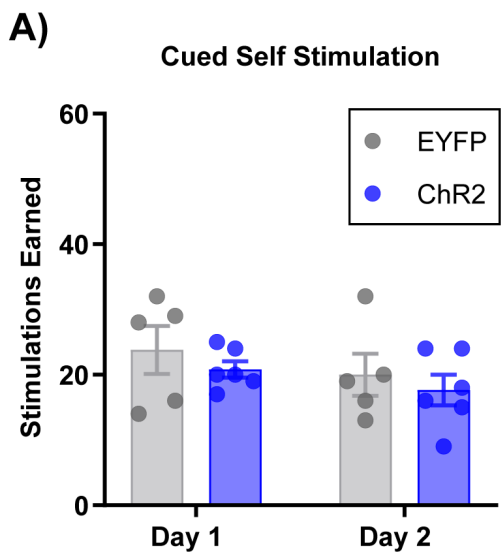


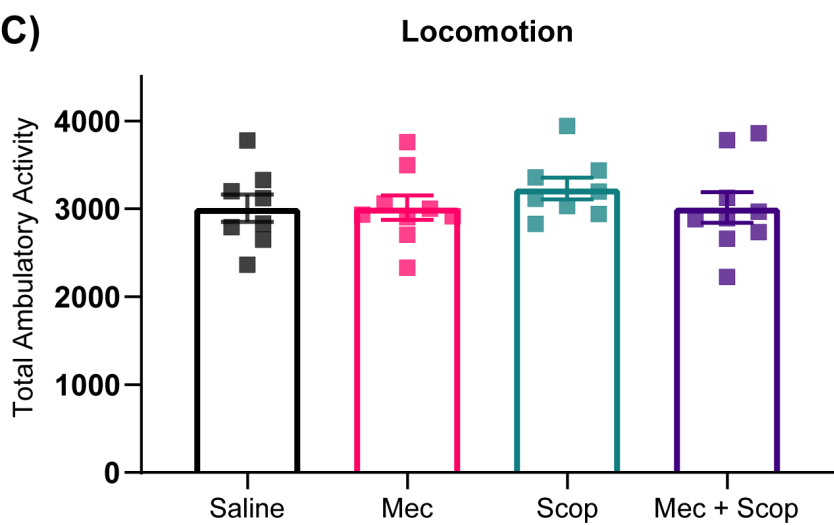
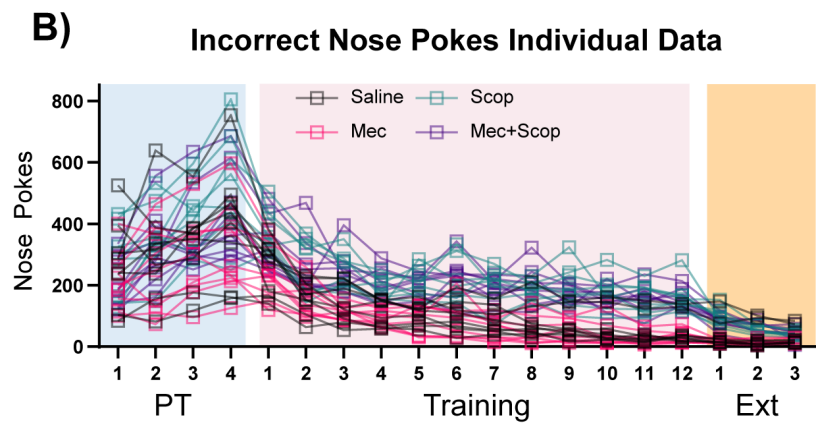
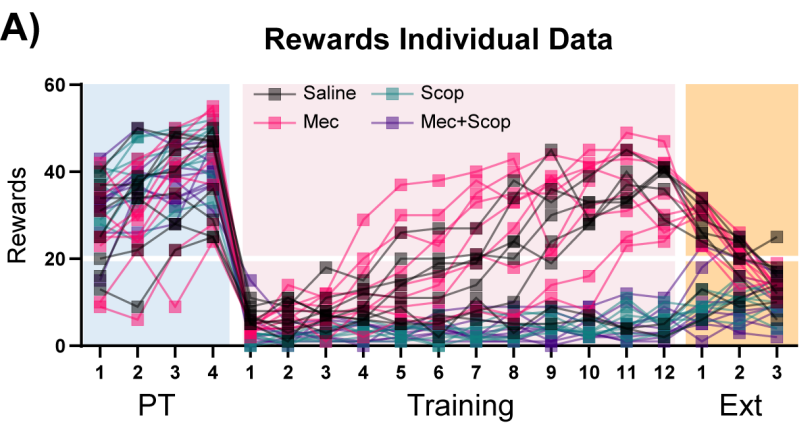
-1.34 mm

-1.46 mm



-1.70 mm





A)

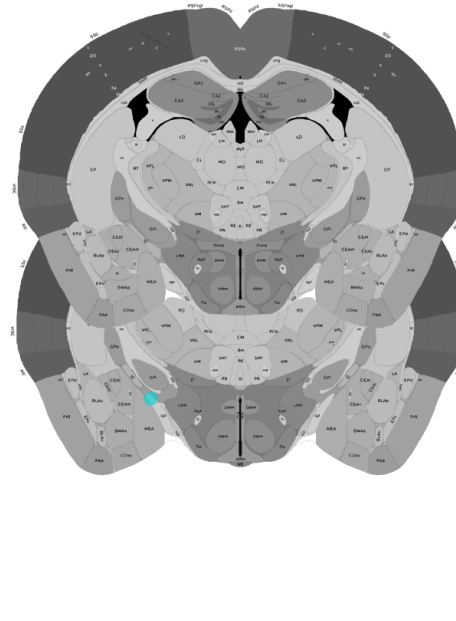
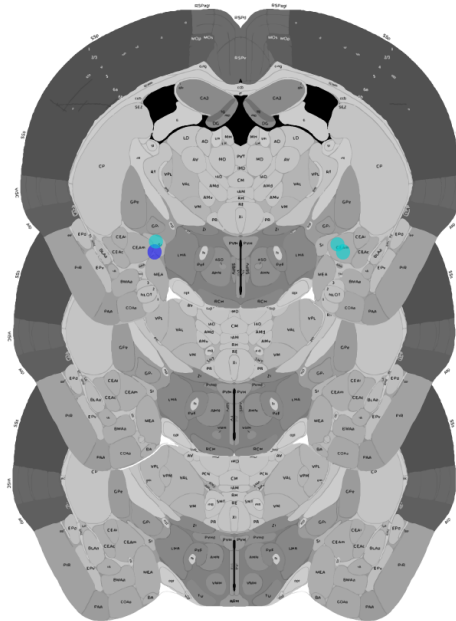
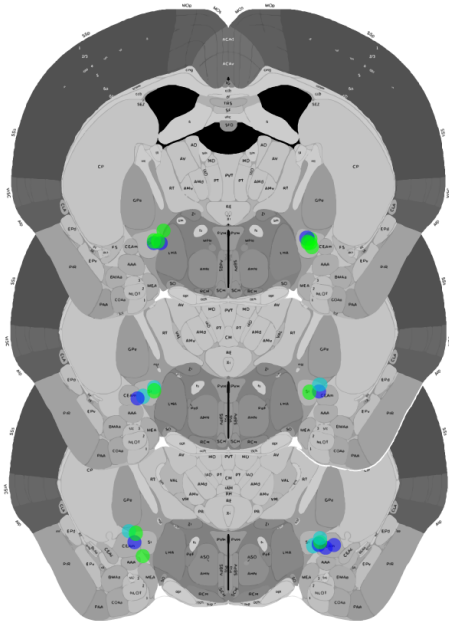
Anterior

-0.34 mm

Injection Sites

-0.70 mm

-1.06 mm



Posterior

-0.58 mm

-0.94 mm

-1.22 mm

B)

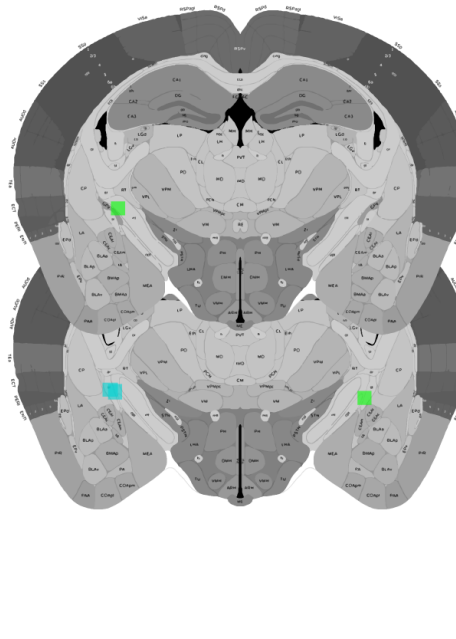
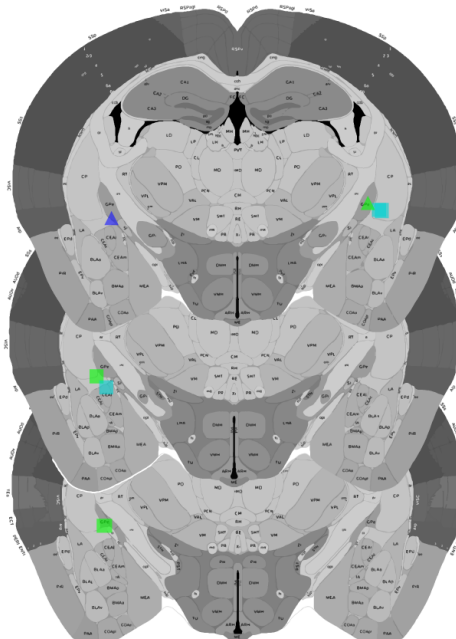
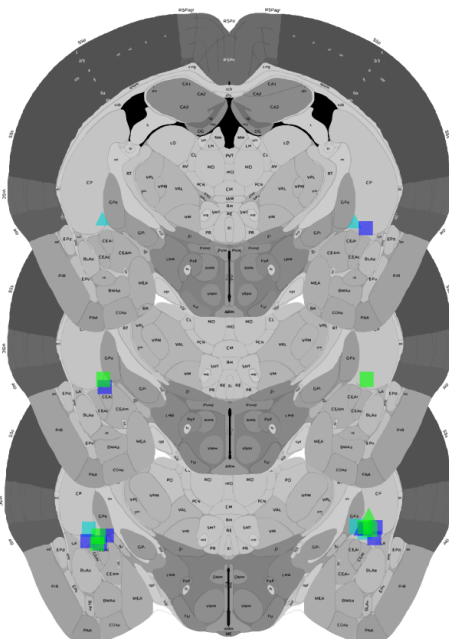
Anterior

-0.94 mm

Fiber Tip Placements

-1.34 mm

-1.70 mm



Posterior

-1.22 mm

-1.58 mm

-1.82 mm

